BIOCHEMICAL AND BIOPHYSICAL CHARACTERIZATION OF MUTANT

T. durum METALLOTHIONEIN

by

MERT AYDIN

Submitted to the Graduate School of Engineering and Natural Sciences

in partial fulfillment of

the requirements for the degree of

Master of Science

Sabancı University

August, 2011

BIOCHEMICAL AND BIOPHYSICAL CHARACTERIZATION OF MUTANT *T. durum* METALLOTHIONEIN

APPROVED BY:

Prof. Zehra Sayers

………………………………..

(Dissertation Supervisor)

Prof. Selim Çetiner

………………………………..

Assoc. Prof. Uğur Sezerman

………………………………..

Asst. Prof. Alpay Taralp

………………………………..

Assoc. Prof. Batu Erman

………………………………..

DATE OF APPROVAL: ………………………………..

BIOCHEMICAL AND BIOPHYSICAL CHARACTERIZATION OF MUTANT

T. durum METALLOTHIONEIN

Mert Aydın

Biological Sciences and Bioengineering, MSc Program, 2011

Thesis Supervisor: Prof. Zehra Sayers

Keywords: Metallothionein, cadmium, metal-thiolate cluster, reconstitution, apoprotein

ABSTRACT

Metallothionein (MT) family is characterized by low molecular weight cysteine rich proteins that bind d^{10} metals through thiolate bonds (Vasak *et al.* 2000). MTs are found in wide range of organisms and their classification was based on the phylogenetic relationships and patterns of distribution of Cys residues along the MT sequences (Kojima *et al.* 1999).

In this study, the aim was to determine structural and metal binding properties of mutant *Triticum durum* metallothionein (G65C) and to analyze differences in metal binding capacity between the mutant and the native durum metallothionein (dMT). A mutation was introduced into one of the cys motifs (C-X-C) at DNA level to mimic a mammalian motif (C-X-C-C). The 65th glycine was mutated to a cysteine and the mutated gene was expressed in *E. coli* as Glutathione S-Transferase (GST) fusion protein (GSTG65C). G65C was cleaved from GST, purified and demetallated (apo-G65C) for biochemical and biophysical characterization.

G65C mutant showed a higher level of oligomerization and polydispersity, but the cadmium content was 5 Cd^{++}/protein which is similar to that of native dMT. Homogeneous solutions of apo-G65C were used for reconstitution studies. Apoprotein was reconstituted with cadmium and zinc and changes in structure were monitored by CD and absorbance measurements. Fully cadmium loaded protein was significantly different from holo-G65C purified directly from *E.coli*. During reconstitution major changes were observed at 230 and 250 nm. The strong absorbance increase observed at

230 nm indicates that significant conformational rearrangements take place in the hinge region - connecting metal binding domains – as well as within the cys-rich domains. The folding process *in vitro* takes place in a nonlinear fashion and is different from that of native dMT with the bridging thiolates forming later. The structural model developed from SAXS measurements show that both apo- and holo- G65C have asymmetric structures, the apoprotein being more elongated (maximum dimension: ~6 nm for holo- and ~10 nm for apo-G65C). The models are consistent with two cluster structure. Results presented show that metal binding capacity is not dependent only on cys quantity, but also on cys motifs.

ÖZET

Metallotiyoneinler (MTler) düşük moleküler ağırlıklı, çok sayıda sistein içeren ve metal bağlayan proteinlerdir. Metallotiyoneinlerin keşfi yaklaşık 60 yıl once at böbreğinde kadmiyum bağlayan protein olarak gerçekleşmiştir. (margoshes vallee). MTler pek çok canlıda bulunur ve sınıflandırmaları filojenik yakınlıklarına ve sekanslarındaki sistein motiflerinin dağılımına gore olmuştur. (binz kagi 2001). MTler d^{10} elektron konfigürasyonuna sahip pek çok metali sisteinleriyle koordine edebilirler. (vasak hasler 2000).

Bu çalışmadaki amaç *Triticum durum* MTsinin (dMT) metal bağlama özelliklerinin sistein sayısı ve motifleriyle olan ilişkisini incelemektir. Bunun için dMT'nin 65. glisini sisteine mutagenez metoduyla dönüştürülmüş (G65C) ve mutant dMT *E. coli* de Glutatyon S-Transferaz (GST) füzyon protein olarak sentezlenmiştir (GSTG65C). G65C sentezlenmiş, saflaştırılmış ve boyut kromatografisi, SDS- ve doğal poliakrilamit jel eletroforezi, dairesel dikroizm, absorbans spektroskopisi, dinamik ışık saçılımı, endüktif çiftlenmiş plazma optik ışıma spektroskopisi ve düşük açılı X-Ray saçılımı ile yapısal olarak incelenmiştir. Bunun yanında G65C metallerinden arındırılarak apoprotein halindeki yapısı da incelenmiştir.

TABLE OF CONTENTS

To my family and grandmother.
Sure she's proud up there..

ACKNOWLEDGEMENTS

LIST OF FIGURES

LIST OF TABLES

ABBREVIATIONS

Apo-	Apoprotein
Ar	Argon
bp	Base pair
BSA	Bovine serum albumin
Cd	Cadmium
CD	Circular dichroism
cDNA	Complementary DNA
Co	Cobalt
Cu	Copper
Cys	Cysteine
Da	Dalton
DNA	Deoxyribonucleic acid
DLS	Dynamic light scattering
d_{max}	Maximum distance
dMT	*Triticum durum* wheat metallothionein
dNTP	Deoxyribonucleotide triphosphate
DR	Dummy residues
DTDP	4-Dithiodipyridine
DTNB	5,5'-dithiobis-(2-nitrobenzoic acid) or Ellman's reagent
DTT	Dithiothreitol
EDTA	Ethylenediaminetetraacetic acid
Fe	Iron
GST	Glutathione S-transferase
GSTdMT	Glutathione S-transferase durum wheat metallothionein

GSTG65C	Glutathione S-transferase 65th glycine mutated dMT
G65C	65th glycine mutated dMT
HCl	Hydrochloric acid
HEPES	4-(-2-hydroxyethyl)-1-piperazineethanesulfonic acid
Holo-	Holoprotein
ICP-OES	Inductively coupled plasma-optical emission spectroscopy
IPTG	Isopropyl-β-D-thiogalactoside
I(0)	Forward scattering
kDa	Kilodalton
LMCT	Ligand metal charge transfer
Me	Metal
MeP	Metalloprotein
mg	Milligram
$MgCl_2$	Magnesium chloride
ml	Milliliter
Mn	Magnesium
MT	Metallothionein
μl	Microliter
NaCl	Sodium chloride
Ni	Nickel
nm	Nanometer
PAGE	Polyacrylamide gel electrophoresis
PBS	Phosphate buffered saline
PCR	Polymerase chain reaction
PMSF	Phenylmethanesulphonylfluoride
PMW	Protein molecular weight marker

P(r)	Pair distance distribution function
R_g	Radius of gyration
R_h	Radius of hydration
SDS	Sodium dodecyl sulfate
SAXS	Small angle X-Ray scattering
TP	Thiopyridine
α	Alpha
β	Beta
$\Delta\varepsilon$	Molar ellipticity
θ	Ellipticity
Zn	Zinc

1. INTRODUCTION

As an introduction to studies on effects of mutations on *Triticum durum* metallothionein (dMT) metal binding properties a brief review is presented together with background information on biophysical techniques used for characterization of mutants.

1.1. Metalloproteins

Every third protein and half of all enzymes require a metal for proper function. Usually this is a transition metal, such as copper, zinc, iron etc (Tainer *et al.* 1991). Zn is the most abundant metal in the cell, and it is known to act as a cofactor for about 300 enzymes, most of which take part in stabilization of DNA and gene regulation (Andreini *et al.* 2006). Recently molybdenum – which is a trace element – was found in catalytic cores of nitrate reductases, sulphite oxidases and xanthine oxidoreductases with iron as FeMo –cofactors (Schwarz *et al.* 2009). Another trace metal, selenium is found as selenocysteine (SeCys) in antioxidant enzymes, and even for a trace metal like Se, there are 25 assigned enzymes that contain SeCys in humans (Kryukov *et al.* 2003).

1.1.1. Metalloproteins' Affinity to Metals

Transition metals are tightly regulated in cells to provide just the necessary amount and not more (metal homeostasis). Handling and delivery of metals in cytoplasm is done by metallochaperones, and in extracellular space of complex organisms, albumin and transferrin perform this task (Rosenzweig 2002; Rosen 2006). There are many steps between metal selection of metalloprotein and metal selection of an organism. These steps are called selectivity filters and eukarya have more complex filters. Basically what a metalloprotein provides is the last step in the process of selecting the metal. How metalloproteins choose their metals is still a question of biology, with the addition of coordination chemistry of the metalloprotein (Maret 2010).

This question can be partially answered by Irving-William series, which states that divalent metals interact with ligands with following affinity (Irving *et al.* 1948);

$$Mn^{2+} < Fe^{2+} < Co^{2+} < Ni^{2+} < Cu^{2+} > Zn^{2+}$$
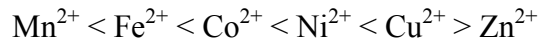
However, Irving-William series account only for isolated proteins (McCall *et al.* 2004). In addition to that, cobalt is only bio available in cells when it is coupled to vitamin B_{12}, which is a specialized handler for this metal ion, and nickel has no assigned role at all but there are deficiency symptoms in animals (Nielsen 1987).

The Irving-William series considers only relative stabilities of complexes formed by a metal ion, and in this case, the affinity is going to be very high if the protein requires the metal ion to be kept for functionality. Based on this, the equilibrium between metalloprotein (MeP) and free metal ion (Me) and the protein is going to be far to the right of below equation; (Maret 2010)

$$P+Me \rightarrow MeP$$
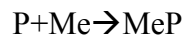
Above statement is valid only when the protein needs the metal to function properly. When the metalloprotein is only a transfer protein, dissociation is the dominant kinetic mechanism. So, Irving-Williams series is good for predicting the free metal concentration in a cell that's under equilibrium conditions (Maret 2010). Another "flaw" of Irving-Williams series is that it is based on equal total metal ion concentrations in the environment. Yet, the free metal ion concentration in a cell is very important, since sets the boundaries for other processes, such as competition between metal ions (Li *et al.* 2009).

1.1.2. Metal Concentration in Organisms

Total metal concentrations are highly variable in organisms, which are additional parameters for the selectivity process; on the other hand, while comparing concentrations, magnesium and calcium should be disregarded, since their concentrations are at least 1000 fold of second most concentrated metal ion. In *Escherichia coli*, total magnesium concentration is more than 10mM, while zinc and iron is about 100 µM each, copper and manganese 10 µM, nickel and cobalt being even

less (Finney *et al.* 2003). In humans, concentrations vary even between tissues, but they roughly follow the same trend (table 1) (Iyengar *et al.* 1978);

	Liver	Kidney	Lung	Heart	Brain	Muscle
Mn	138	79	29	27	22	<4-40
Fe	16,769	7,168	24,967	5,530	4,100	3,500
Co	<2-13	<2	<2-8	-	<2	150 (?)
Ni	<5	<5-12	<5	<5	<5	<15
Cu	882	379	220	350	401	85-305
Zn	5543	5018	1470	2772	915	4688

Table 1.1: Metal content in human organs, μg per g (Iyengar, Kollmer et al. 1978).

Metal concentrations in cell differ from those assumed by Irving-Williams series;

$$Fe, Zn > Cu > Mn > Co, Ni$$

Based solely on concentration, if not regulated, zinc can easily displace nickel or cobalt, which might cause protein dysfunction, therefore, every metal ion has to be buffered in an extremely narrow range. Right now it is difficult to determine the metal choice and coordination of a metalloprotein without purification, and isolated proteins might lose their metals completely, or may happen to bind an ion other than the native one (Maret 2010).

1.2. Characterization of Metalloproteins

1.2.1. Classification of Metalloproteins

Metalloproteins can be roughly separated into two groups, those which bind their metals tightly and do not lose them during purification, and others, which may lose their metal during purification (Vallee *et al.* 1970). If the metal is not lost during purification, direct analysis can be conducted on the metalloprotein for its biochemical and biophysical characterization. In most cases, metalloproteins contain a single type of metal ion, however, during purification process, metal ions other than the native one can be introduced into the protein, causing a heterometallic form of the protein.

3

1.2.2. Purification of Metalloproteins

While purifying, chelating agents such as ethylenediaminetetraacetic acid (EDTA) or reducing agents like dithiothreitol (DTT) have to be used, in order to avoid oxidation of thiol groups. While supplying protection, these chemicals form strong bonds with metals, and in some cases, might grab metals that are supposed to be on the protein (Krezel *et al.* 2007) and the end product might not be identical to native one.

Cells that are grown in artificial media are not the same as those that grow in nature. Under laboratory conditions many selection filters are absent. It was shown that if yeast cells are supplied with cobalt instead of zinc during growth, cobalt replaces the Zn in alcohol dehydrogenase enzyme (Curdel *et al.* 1968), which compromises the function of the enzyme. Also metal ions may be more abundant in the laboratory conditions compared to the conditions where their concentrations are limited by the "selectivity" filters in natural environment (Maret 2010).

1.2.3. Replacing the Metals

Replacement of metal ions of metalloproteins can be done *in vitro*, which is demonstrated also in this study. Hence, it is not definitive that metalloproteins are highly selective of metals, even toxic or function-impairing metals can be bound (Vallee *et al.* 1958), (Maret *et al.* 1986), and it is not possible to say that increased efficiency of a metalloprotein is an indicator of native form. Supermetallation – binding of more metals than native form - can also be observed by spectrometric measurements, however, that also does not indicate that more metals increase functionality. Excess metals can even induce loss of fold, and eventually function (Stillman *et al.* 1994).

If metal is the limiting agent in the growth medium, expression host (bacteria, yeast etc.) can be forced to incorporate non-native metals to proteins. Expression of *Pseudomonas aeruginosa* azurin in *E. coli* results in the production of zinc protein, in addition to the native copper azurin (Nar *et al.* 1992).

1.3. Metallothioneins

1.3.1. Metallothionein Definition

Metallothioneins (MTs) are members of a metalloprotein family, which were discovered by Vallee and co-workers (Margoshes *et al.* 1957) and characterized as low molecular weight, cysteine (cys) - rich and lacking in aromatic amino acids. Despite their high cys content, they lack disulfide bonds, because metal ions are coordinated by these cysteines (Kojima 1991).

1.3.2. Cysteine residue distribution

The characteristic feature of all MTs is the abundance of and their arrangement throughout metal binding domains; cys-cys, cys-x-cys, cys-x-y-cys, and cys-cys-x-cys-cys where x and y stands for an amino acid residue other than cys (Kagi *et al.* 1988; Romero-Isart *et al.* 2002). In mammalian MTs, cys-motifs are clustered in the N-terminal (β domain) and C-terminal (α domain) separated by a 3 residue hinge region. Metal binding to these domains are confirmed by an increasing number of studies on the three dimensional structure (Vasak 2005) Contrary to mammalian MTs, plant MTs have longer hinges, and these regions are highly sensitive to proteolytic cleavage (Tommey *et al.* 1991).

Metallothionein superfamily was divided into fifteen families in 1999, plant MTs being fifteenth. This classification was done according to cysteine quantity and distribution and phylogenetic distances (Kojima, Kagi et al. 1999). Plant MT family is further subdivided to 4 groups: type I, type II, type III and type IV. In types I to III, cys motifs are located in the N- and C-termini similar to mammalian MTs but the hinge region is much longer with 10 to 45 amino acids. In type IV, cys motifs cluster in 3 regions in the amino acid sequence (Freisinger 2009).

1.3.3. Functions of MTs

Several functions have been assigned to MTs, these include heavy metal detoxification, metal homeostasis (Andrews 2000; Brouwer *et al.* 2002), scavenging of reactive oxygen species (Ebadi *et al.* 1996), regulation of metalloenzymes (Andrews

2000) and transcription factors and recently potential involvement in apoptosis (Vallee *et al.* 1990; Freisinger 2008).

MTs have affinity against d^{10} metals and most of the isolated MTs contain Zn(II), Cd(II) and Cu(I), however Ag(I), Au(I), Bi(III), Co(II), Fe(II), Hg(II), Ni(II), Pt(II), and Tc(IV)O have also been shown to bind *in vitro*.

1.3.4. Spectroscopic features of MTs

UV-vis absorption spectra show that coordination of metals occur through terminal and bridging thiolates and this is accompanied by the appearance of ligand (thiolate) to metal charge transfer (LMCT) bands between 230 and 350 nm, which is the region of the spectrum that is completely devoid of bands due to the lack of aromatic amino acids (Chan *et al.* 2002). Metal binding is also detected by circular dichroism (CD) spectropolarimetry in the wavelength range of the LMCT bands. CD spectral properties depend on;

1) The metal ion,

2) Coordination geometry – terminal or bridging,

3) How the peptide chain wraps itself around the metals (Sutherland *et al.* 2011).

MTs have very little secondary structure, and that structure is abolished at demetallated apo-MT state. CD and absorbance spectra are also weak, and because of these properties, apo-MTs are generally described as random coils. Thus spectral intensity of MTs is directly dependant on metal to protein ratio and on the type of the metal ion.
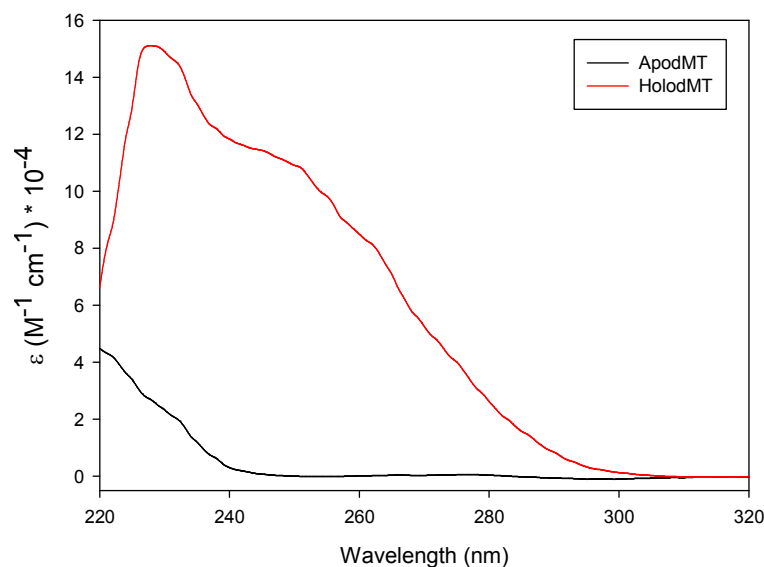
Figure 1.1: LMCT at UV-Vis absorption spectra.

1.3.5. Reconstitution of Apo-MTs

Apo-MTs have been loaded with metal ions *in vitro*, and in some cases supermetallation can be seen. Stillman and his co-workers have demonstrated that supermetallation can be seen with human MT-1, in full length peptide and α and β domains separately (Sutherland *et al.* 2010). Vasak and co-workers have demonstrated that brain specific MT-3 can also be supermetallated (Palumaa *et al.* 2002) (Meloni *et al.* 2009). Plant MTs can also be supermetallated (Peroza *et al.* 2007).

1.3.6. Coordination of metals

α and β domains usually are not seen interacting while coordinating metal ions. Beta domains of vertebrate, crustacean and echinoderm MTs have been shown to bind metals in Me_3Cys_9 fashion and α domains coordinate metals in Me_4Cys_{11} arrangement (Serra-Batiste *et al.* 2010), (Romero-Isart and Vasak 2002). Recently it was shown that histidine residues can also take part in metal coordination and form $Me_4Cys_9His_2$ at *Synechococcus* MT (Blindauer *et al.* 2001). Plants also employ His residues too coordinate metal ions, recently the NMR solution structure of a plant MT has provided evidence that a Zn(II) ion is being coordinated by two Cys and two His residues, resembling zinc fingers (Peroza *et al.* 2009; Peroza *et al.* 2009).

1.4. Determination of MT Concentration

Accurate determination of concentration of metallothioneins is essential, especially if the ApoMT is will be reconstituted with ions or native metals are going to be exchanged with others. Since MTs lack aromatic amino acids, conventional protein concentration determination using absorption at 280 nm is not possible. So far there have been three commonly used methods for MT concentration determination, (i) determination of sulfur content by inductively coupled plasma (ICP) analysis, (ii) thiol assay with Ellman's reagent (5,5′-dithio-bis(2-nitrobenzoic acid) - DTNB), (iii) thiol assay with dithiodipyridine (DTDP).

Since its introduction in 1959, Ellman's reagent has been highly popular for protein sulfhydryl determination (Ellman 1959). However, many reports indicate that Ellman's reagent may not interact with all the sulfhydryls in a protein. As an alternative, DTDP is being used, due to its small size and amphiphilic nature (Grassetti *et al.* 1967). DTDP interacts with even poorly accessible sulfhydryls, and does not require catalysts, such as cystamine, which is necessary for DTNB reaction. Reactions of DTDP and DTNB with sufhydryl groups are shown in Figure 1. One DTDP molecule interacts with one sulfhydryl, resulting in one thiopyridine (TP). Normally the breakdown of DTDP results in two unreacted TPs, however, reduction of sulfhydryl groups by TP has very small rate constant on its own, so the contribution of second TP can be neglected (Riener *et al.* 2002).
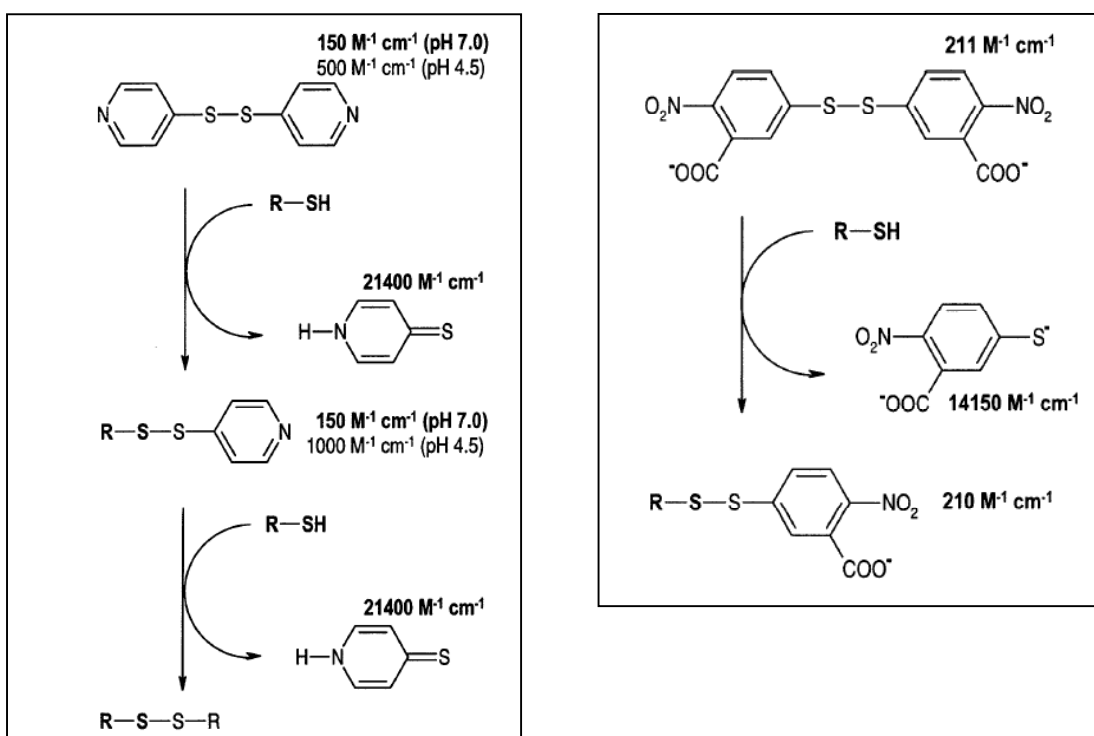
Figure 1.2: DTDP (left) and DTNB (right) reactions

TP, which DTDP yields after the reaction has a distinct absorbance maximum at 324 nm. This allows the quantification of TP due to its precise molar absorbtivity and since 1 TP is produced from reaction of 1 sulfhydryl group sulfur amount can be directly calculated from the measurements (Riener, Kada et al. 2002).

1.5. MT Structural Characterization

MTs are hard to crystallize, mainly due to their high Me:P ratio and the absence of any dominant secondary structure and so far very few crystal structures have been reported (Melis *et al.* 1983; Furey *et al.* 1987; Calderone *et al.* 2005). Lack of crystal structure has directed researchers to nuclear magnetic resonance and solution scattering applications.

1.5.1. Circular Dichroism Spectropolarimetry

Circular dichroism (CD), arising from differential absorption of left and right handed circularly polarized light by proteins and nucleic acids in a solution, is a

9

commonly used technique for spectroscopic characterization of MTs due to the techniques unique sensitivity to conformational changes. The dominating phenomenon in MT spectrum is usually the metal-thiol chromophores and even though CD provides only low resolution structural information, its extreme sensitivity to *changes* in conformation makes it a powerful tool for phenomena such as folding of MTs upon binding metal ions. Another benefit is that CD is applicable to small sample volumes in a wide range of buffer systems.

CD is generally used for;

1) Estimation of protein secondary structure,

2) Detection of conformational changes of proteins and nucleic acids, brought by changes in pH, salt concentration, solvents

3) Protein or nucleic acid unfolding,

4) Protein or nucleic acid – ligand interactions,

5) Kinetics of macromolecule interactions. (Martin *et al.* 2008)

CD spectra of secondary structure elements such as α-helix, β-sheet and random coil are shown together in figure 1.3 in the near UV-range; 180 to 260 nm (Brahms *et al.* 1980).
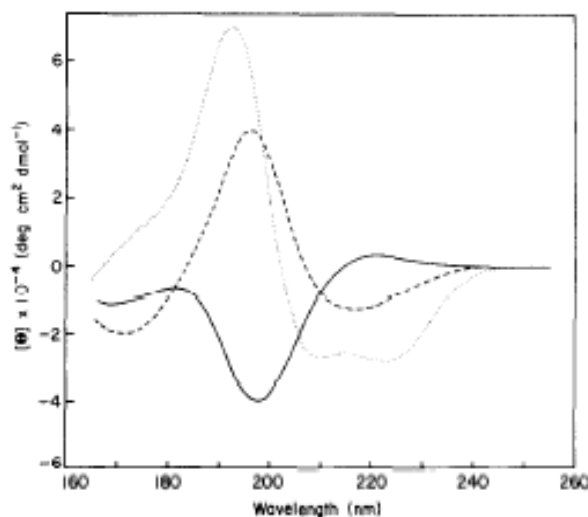
Figure 1.3: Reference CD spectra of main types of α-helix (dots), β-sheet (short dashes) and random coil (solid line). (Brahms and Brahms 1980)

1.5.2. Determination of Secondary Structure with CD

To determine secondary structure from CD spectra, ellipticity values should be converted to molar ellipticity (Δε), removing changes due to concentration. Unit conversion is done with following formula,

(1.1)
$$\Delta\varepsilon = \frac{100*\theta}{C*l*3298.2}$$

Where θ is ellipticity in milidegrees, C is concentration in molar, l is pathlength in centimeters and Δε is molar ellipticity in deg cm^2 dmol^{-1}.

As stated before, ApoMT is totally featureless above 230 nm. Although metal ions exhibit no optical features within the range of 230 to 400 nm, in the presence of a thiolate ligand LMCT occurs. Whenever there is a change in the metal-thiol chromophore, chirality is imparted and LMCT intensity is enhanced (Stillman, Presta et al. 1994).

CD intensity mechanism is sensitive to changes in the chiral thiol-metal binding sites; however same thing cannot be said for changes that occur out of the chiral center, since asymmetry allows the particle to absorb right and left hand polarized light differently.

1.5.3. Supermetallation

Under *in vitro* conditions, it is possible that the spectroscopic intensity will reach a maximum for a given Me:P ratio. This can be an indicator of a stable fold, however, may not be an indicator of metal saturation. Stillman group has proven with mass spectrometry that α and beta domains of human metallothionein are capable of binding a single extra Cd(II) above their saturation values, 4 and 3 respectively (Sutherland and Stillman 2011). Another study that was done on human MT has shown that the single addition of a Cd(II) ion causes a steep decrease in Stoke's radius, meaning that protein adapts a more compact form (Meloni, Polanski et al. 2009). Such a conformation change means that α and beta domains come together to coordinate the extra ion.

Yet, the exact metallation status is quite difficult because of the dynamic metal binding properties and structure of the protein. Taking these into account, equilibrium with that extra metal would require extreme free metal concentration in order to shift the reaction in favor of binding.

Because CD gives only low resolution results, it was thought that metallation process took place cooperatively, but recent ESI-MS data showed that metallation can progress noncooperatively through cys motifs, meaning metals will not be distributed evenly between α- and β- domains (Sutherland and Stillman 2011).

1.5.4. Small angle X-Ray scattering

Small angle X-Ray scattering (SAXS) is used to determine structures of low concentration homogeneous particles in solution. Low resolution data is the price that is paid for easy sample preparation (Svergun *et al.* 2003) and furthermore extracting three-dimensional structure information from one dimensional data poses difficulties. Due to small weak scattering from biological molecules and their relatively short half-life, reliable SAXS data which allows building structural models and systematic studies can only be collected using synchrotron radiation (Koch *et al.* 2003)

1.5.4.1. SAXS Data Processing

The small angle X-ray scattering curve (I(s)) is obtained as the difference scattering after buffer scattering is subtracted from that of the sample, I(s). It is radially symmetrical containing information from all possible orientations of the particle. The scattering is due to the electron distribution in the particle, and the pair distribution function, P(r), which shows the probability distribution of all distances between pairs of atoms in the particle, can be calculated through a Fourier transform of the scattering curve. P(r) gives information about the overall shape of the protein and its maximum dimension d_{max}. Bell-shaped symmetric P(r) indicates a spherical shape whereas asymmetric P(r) functions indicate elongated rod-like particles.
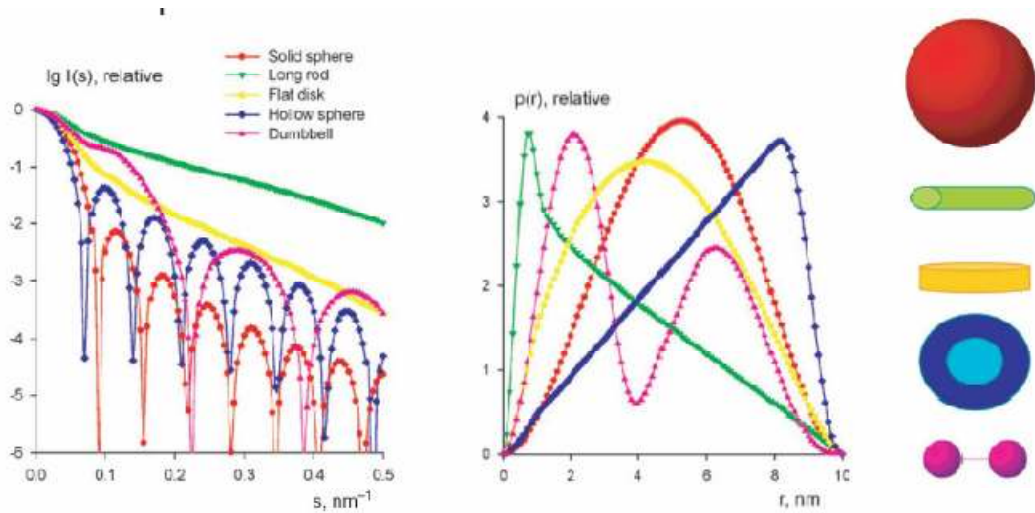
Figure 1.4: Distance distribution function from simple shapes (Dmitri *et al.* 2003).

Scattering intensity I(s) can be calculated from formula X

(1.2)
$$I(s) = \frac{e^{\mu t}}{cD(s)}\left[\frac{I_x(s)}{I_0} - \frac{I_B(s)}{I_0}\right]$$

Where $e^{\mu t}$ represents the absorbance of a solution of thickness t, $I_x(s)$ and $I_B(s)$ scattering intensities of sample and buffer respectively, c concentration and D(s) detector response.

Also P(r) function can be obtained by taking inverse Fourier transform of I(s) as shown in formula X

(1.3)
$$I(s) = 4\pi \int_0^\infty r^2 p(r)\frac{\sin(2\pi sr)}{2\pi sr}\,dr$$

Lowest resolution portion of a SAXS curve (Guinier region) is dictated by the radius of gyration (R_g) of the particle, which is calculated by taking the square root of the average squared distance of each scatterer from the particle center (Putnam *et al.* 2007). Intensity measured at zero angle, I(0), is proportional to the molecular mass of the scattering particles. This can only be determined by extrapolation since in the experimental set-up this point corresponds to the spot where beam hits the detector. A plot of log(I(s)) against q^2 in the region $0.6 < R_{gs} < 1.3$ (Guinier plot) is a straight line and is used to extract R_g and I(0). Any nonlinearity indicates polydispersity or

inhomogeneties in the sample (Guinier 1955). Another important point is that R_g is independent of protein concentration; any deviation would suggest specific oligomerization or aggregation of the sample.

1.5.4.2. Model Generation from SAXS Data

It is obvious that reconstructing three-dimensional model from one-dimensional scattering data is ill-posed problem, meaning that; there may be many three dimensional structures that can give rise to that one dimensional data (Dmitri and Michel 2003). In early attempts modeling was done in a trial and error fashion, until an envelope function was introduced for *ab initio* modeling. This allowed generation of unique models by the help of spherical harmonics (Stuhrmann 1970; Stuhrmann 1970) . On the other hand, use of envelope function was limited to simple shapes, especially particles with no holes inside.

1.5.4.2.1. DAMMIN

This was followed by modeling based on fitting rigid beads – that have very small r_0 radius – in the pre-defined shape envelope densely. According to this, the bead can either belong to the sample or the solvent, and the algorithm DAMMIN distributes random beads in a volume, calculated according to R_g, and then starts refining the interior features of the volume in a Monte Carlo-like search (Svergun 1999).

1.5.4.2.2. GASBOR

Recently more versatile *ab initio* modeling algorithms are introduced. Here the protein is represented as an assembly of dummy residues (DR), where residues correspond to the building blocks of the biological molecule; amino acids of a protein or bases of DNA. Modeling is done by fitting the scattering from DRs to the experimental data. This approach, which is implemented in GASBOR (Svergun *et al.* 2001), starts by putting all DRs into a spherical volume that is determined by d_{max} from the experimental data. As algorithm proceeds with simulated annealing method, DRs are relocated, constrained by d_{max}. Another constraint is introduced by GASBOR to avoid residue clashes and/or discontinued DRs, that being ≈0.38 nm apart from each other. With this constraint, every DR is forced to have two neighbors at about 0.38 nm.

14

1.5.4.2.3. DAMAVER

Due to the nature of ill-posed problem, there are multiple models generated with DAMMIN and GASBOR. Individual models can be superimposed and analyzed for stability by the DAMAVER algorithm (Volkov *et al.* 2003). Every individual model is aligned and the most stable model – the most probable one – is taken as a reference. All others – excluding outliers – are aligned to the reference model and a density map of beads or residues are calculated, each of them being in the envelope.

1.5.5. X33 Beamline, EMBL Hamburg

Recently the X33 SAXS beamline at European Molecular Biology Labs (EMBL) Hamburg was upgraded (figure 1.5 (a) before and (b) after). Optics, electronics, detector, sample stage and data acquisition system was upgraded for shorter measurement times and increased turnover (Round *et al.* 2008).
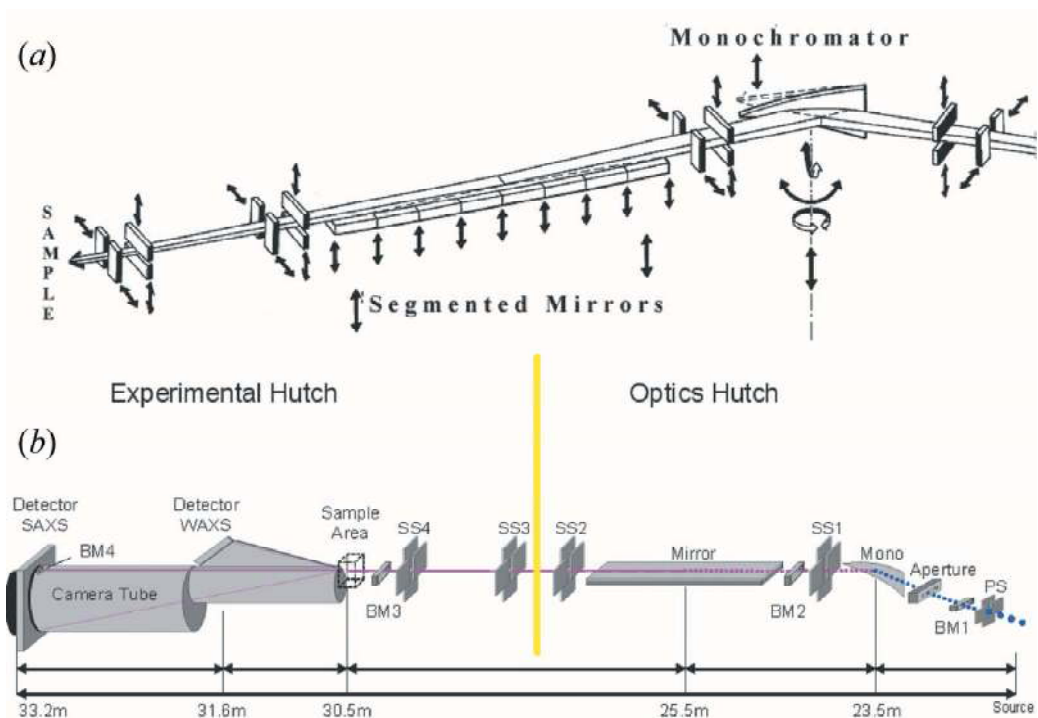
Figure 1.5: EMBL Hamburg X33 beamline sketch (Round, Franke et al. 2008).

2. MATERIALS AND METHODS

2.1. Materials

2.1.1. Chemicals

All chemicals were supplied by Stratagene, QIAGEN, Merck (Germany), Bioron, Fermentas, Riedel, Amresco, AppliChem, and SIGMA (USA).

2.1.2. Primers

Primers were designed according to the sequence of dMT (Bilecen *et al.* 2005) to mutate the Gly at position 65 to Cys and were synthesized by Iontek (Turkey). Sequences of the forward and reverse primers are shown in table 2.1 where mutations are underlined.

	Sequence
Forward	5'- GGC TGC AGC TGC TGC GAC AAC TGC AAG -3'
Reverse	5'- CTT GCA GTT GTC GCA GCA GCT GCA GCC -3'

Table 2.1: Primers used to mutate the 65th glycine of dMT to cysteine (G65C).

2.1.3. Enzymes

Restriction enzymes *Eco*RI, *Xho*I, and *Dpn*I were purchased from Stratagene and Fermentas. Pfu-Turbo DNA polymerase was supplied by Stratagene.

2.1.4. Vectors

Map of pGEX-4T2 (GE Healthcare) vector can be found in Appendix B. This is a fusion vector that allows synthesis of the target protein with GST tag. GST is attached to target protein by Leu-Val-Pro-Arg-Gly-Ser sequence, which also functions as thrombin cleavage site. Cleavage is done between Arg-Gly.

dMT was cloned into pGEX 4T-2 by *EcoRI* and *XhoI,* and same enzymes were used for diagnostic purposes at G65C at DNA level.

2.1.5. Cell Lines

E. coli strain BL21 (DE3), (provided by EMBL, Hamburg) was used.

2.1.6. Buffers and Solutions

Lysis buffer contains: 20mM HEPES pH 8, 2.5 mM $MgCl_2$, 100 mM NaCl, 1 mM DTT, 0.5 mM PMSF and for 38 ml lysis buffer 1 tablet Roche EDTA Free Protease Inhibitor Cocktail tablet was included.

Elution, wash and size exclusion column running buffer contains: 20mM HEPES pH 8, 2.5 mM $MgCl_2$, 100 mM NaCl and 1 mM DTT

Column running buffer for apo-G65C contains: 20 mM HCl pH 2.5 and 15 mM Tris.

Reconstitution buffer contains: 20 mM HCl and 42.5 mM Tris pH 8.3. Mol equivalent of metals were added to this buffer according to the protein concentration under Ar flush. Reconstitutions were carried out in a volume of 140 μl and after addition of the metal samples were incubated at room temperature for briefly 10 minutes. For 140 μl reaction, 9 μl 0.5 M Tris-Base was added.

If reconstituted buffer was to be used for pH titration experiments, buffer contained 20mM HCl and 6 mM Tris pH 8.3.

Hexaglycine was dissolved in 99% formic acid and diluted with dH_2O. pH adjustments were done with 5M NaOH.

All buffers and solutions, except those provided by commercial kits were prepared according to (Sambrook *et al.* 1989). Buffers and their compositions are given in Appendix C. All protein buffers were degassed and saturated with Ar before use.

2.1.7. Commercial Kits

Quick Change Site-Directed Mutagenesis Kit (Stratagene) and Qiaprep Spin Miniprep Kit (QIAGEN) were used in recombinant DNA manipulations.

2.1.8. Culture Media

LB (Luria-Bertani) Broth was prepared manually with following ingredients; 10 g Tryptone, 5 g Yeast extract, and 5 g NaCl for 1 liter.

LB Broth Agar was prepared by adding 15g agar-agar for 1 liter of LB Broth medium.

2.1.9. Equipment

Please see Appendix D for a complete list of all equipments that were used during this study.

2.2. Methods
2.2.1. Site-Directed Mutagenesis
2.2.1.1. PCR

Recommended reaction volumes and final concentrations of the Quick Change Site-Directed Mutagenesis Kit were used for PCR reaction mixture and primers shown in table 2.1.

Reaction was carried out in a thermal cycler following below conditions (table 2.2).

95 ^{o}C, 5 minutes	
95 ^{o}C, 1 minute	
53.5 ^{o}C, 1 minute	Total of 20 cycles
72 ^{o}C, 1 minute	
72 ^{o}C, 10 minutes	
4 ^{o}C	Until further use

Table 2.2: PCR conditions used for G65C mutation.

PCR products were analyzed by 1% agarose gel electrophoresis with TAE buffer. Samples were mixed with 6X loading buffer and gels were run at 100 mV for 30 minutes. Size of DNA fragments were estimated by using MassRuler DNA ladder mix (Fermentas) and visualized by ethidium bromide staining.

2.2.1.2. *Dpn*I Digestion

*Dpn*I restriction enzyme cleaves only methylated DNA. The template is derived from an alkaline lysis plasmid preparation and it is methylated, whereas the mutated PCR product is generated in vitro and is unmethylated. Hence, enzyme will only cleave unmutated plasmid.

1.5 µl of *Dpn*I restriction enzyme (10U/µl) was added directly to each PCR result and incubated at 37°C for 2 hours.

2.2.1.3.Ethanol (EtOH) Precipitation

PCR products were concentrated by EtOH precipitation. 1 volume of ddH$_2$O was added to each reaction to increase the initial volume, 0.1 volume of 3M ammonium acetate was added in order to increase the positive ion concentration. Then, 2 volumes 95 % EtOH was added and samples were incubated at -80 ^{o}C for o/n. Next day, the solution was centrifuged for 15 min at 16.000g to eliminate salts. Pellet was washed with 2 volumes 70 % EtOH and was centrifuged for 15 min at full speed again. Finally, they were dried and resuspended in 5 µl of ddH$_2$O.

2.2.1.4.Transformation of Bacteria

BL21 (DE3) competent cells were transformed with EtOH precipitated linear PCR products. 80 µl of *Dpn*I treated PCR product or 100 ng purified plasmid DNA was mixed with 100 µl competent cells and incubated on ice for 30 minutes, and then transformed cells were allowed to repair on pre heated 42°C rack for exactly 90 seconds which was followed by further 2 minutes on ice. Finally, transformed cells were allowed to recover in LB at 37°C for 45 – 60 minutes. Then, transformed cells and controls were spread on LB-Ampicillin (100 µg/ml) plates.

2.2.1.5.Colony Selection

Positive colonies were selected and grown on liquid LB-Ampicillin (100 µg/ml) to prepare glycerol stocks and for plasmid isolation.

2.2.1.6.Plasmid Isolation

Positive colonies were grown in 5 ml of LB-Ampicillin (100µg/ml) medium overnight at 37 ^{o}C with shaking at 280 rpm. Cells were centrifuged at 4°C at 5000 g for 3 minutes and plasmid isolation was done with Qiaprep Spin Miniprep Kit (QIAGEN). The final concentration of plasmid DNA was calculated by measuring the absorbance at 260 nm in Nanodrop spectrophotometer (Thermo) and using 0.020 (µg/ml)$^{-1}$ cm^{-1} for the extinction of DNA. DNA samples were stored at -20 ^{o}C until further use.

2.2.1.7.Restriction and Agarose Gel Electrophoretic Analysis

Presence of the gene was validated by double digestion and agarose gel electrophoretic analysis for the presence of mutant inserts. Plasmids were digested with *Eco*RI and *Xho*I restriction enzymes to verify the presence of GSTdMT gene. 0.3 µl of *Eco*RI and 0.6 µl of XhoI restriction enzymes were added to approximately 10 ng plasmid DNA. They were incubated at 37 ^{o}C for 2 hours.

2.2.1.8.Sequence Verification

Plasmids were purified with QIAGEN Plasmid Mini Kit (QIAGEN) and were DNA sequencing analysis was carried out by Iontek (Turkey).

2.2.2. Gene Expression
2.2.2.1.Monitoring the Expression of the Mutant Protein

In order to monitor the expression of the gene for the mutant protein, cells were grown in 5 ml of LB-Ampicillin (100 µg/ml) medium overnight at 37 ^{o}C with shaking at 280 rpm. Next day, cultures were 1:50 diluted in 50 ml of LB-Ampicillin (100 µg/ml) medium and induction was done with 0.7 mM IPTG when the OD$_{600}$ reached 0.8. Cells were grown continuously at 37 ^{o}C with shaking at 280 rpm. Induction was monitored by taking aliquots from the cultures before induction (t=0) and after induction at regular intervals for a maximum of about 7 hours (t=1, 2…) and pelleting the cells. Pellets were lysed with lysis buffer (150 mM NaCl, 20 mM HEPES, 2.5 mM MgCl$_2$, 10mg/ml lysozyme, pH8) and expression was monitored by 12% SDS polyacrylamide gels. Gels were first run at 80 V and voltage was increased to 120V once the samples reached

separating gel. Samples were run for around 1 hour 30 minutes. Protein bands were visualized by coomassie blue staining. Protein molecular weight markers and protein ladders (Fermentas) were used to identify the molecular weights of expressed proteins.

2.2.2.2. Culture Growth for Protein Purification

Large scale purification of G65C was carried out from 3 liter cultures. Starter culture was grown in 50 ml of LB-Ampicillin (100 µg/ml) medium overnight at 37 ^{o}C with shaking at 260 to 280 rpm. Next day, cultures were 1:50 diluted in 2.25 liter of LB-Ampicillin (100 µg/ml) medium containing 0.1 mM $CdCl_2$. Induction was done with 0.7 mM IPTG when the OD_{600} was 0.8 to 1. Cells were grown continuously at 37 ^{o}C with shaking at 260 to 280 rpm for 5.5 hours and pelleted by centrifugation at 7000 rpm for 30 minutes using a Sorvall centrifuge with SLA 3000 rotor at 10000 rpm for 20 minutes using a Sorvall ultracentrifuge. Harvested cells were kept at -80 ^{o}C until further use.

2.2.3. Protein Purification
2.2.3.1. Affinity Chromatography by Glutathione Sepharose Matrix

Purification experiments were performed under argon flush with argon saturated buffer solutions. Pellets were resuspended in lysis buffer. Cells were lysed by two rounds of 10 minutes sonication at 4 ^{o}C with 5 second of pulse and 5 second rest period. 20 % Triton X-100 was added, a final concentration of 1%, and the mixture was shaken gently at 4°C for 45 minutes. Lysate was centrifuged at 19000 g, 4 ^{o}C for 1 hour. Supernatant was incubated with 50% Glutathione Sepharose affinity beads (GE Healthcare) in purification buffer for 6 hours at 4°C. Afterwards G65C was cleaved from GST tag by 130 to 180 units of Thrombin (GE Healthcare) for 18 hours at 4°C with gentle agitation.

Cleaved protein was then eluted with 25 to 30 ml elution buffer in two successive steps and the eluate was concentrated with 10kDa molecular weight cutoff Amicon Ultra Centrifugal filter unit by centrifuging at 3000g for about 20 minutes. Depending on protein yield, samples were concentrated between 2 to 4 ml.

If precipitation occurred, sample was transferred to an eppendorf tube and centrifuged at 13.000 g for 15 minutes at 4 ^{o}C.

2.2.3.2. Size Exclusion Chromatography

Concentrated protein was loaded on a HiLoad 16/60 Superdex 75pg (GE Healthcare) size exclusion column. Column was calibrated using Vitamin B12, Ribonuclease A, Aprotinin, Ovalbumin and Conalbumin. The calibration curve (not shown) was used for molecular weight determination of mutant proteins. Column was equilibrated and run with the elution buffer. Fractions, 0.7 ml, were collected at a speed of 1 ml/min and protein was monitored by absorbance at 280 nm using the AKTA-FPLC system (GE Healthcare).

2.2.3.3. Apoprotein Preparation

Protein concentration determination was based on cysteine reactivity. In order for all C residues to be available for the reaction the protein was demetallated. ApoG65C can be obtained in two ways,

2.2.3.3.1. Via Dialysis

500 µl protein solution is dialysed against 0.02M HCl overnight, changing the buffer at least once. After dialysis, sample is taken into an eppendorf tube from dialysis membrane for direct concentration determination.

2.2.3.3.2. Via Size Exclusion Chromatography

1M DTT is added to the sample to bring total DTT concentration up to 5mM and the sample is incubated for 45 minutes on ice. Then 6M HCl is added to bring the pH down to 2 and the solution is incubated for 30 minutes at room temperature. Finally, the sample is loaded on a HiLoad 16/60 Superdex 75pg (GE Healthcare) size exclusion column and eluted with 0.02M pH2.5 Tris-HCl. Eluent was collected at a speed of 1ml/min in 0.5 ml fractions using AKTA-FPLC system (GE Healthcare). 2-4 ml of ~1 mg/ml apo-G65C can be loaded on column. Protein was monitored by absorbance at 280 nm.

2.2.4. Analyses

2.2.4.1.Protein Concentration Determination

Due to the lack of aromatic residues in the amino acid sequence of dMT-G65C protein concentration measurements cannot be conducted by absorbance measurements at 280 nm. Instead two alternative methods are used for this purpose; (1) spectrophotometric measurement of sulfhydryls in the protein and (2) determination of total sulfur content by ICP-OES.

The sulfhydryl measurement procedure is based on the reactivity of the SH groups of the residues in the protein with 4,4'-dithiodipyridine (4-DTDP or 4-Aldrithiol, Sigma, 2645-22-9 catalogue number) and was carried out as described in (Riener, Kada et al. 2002). DTDP is a small molecule that reacts readily with thiol groups and causes a change in absorbance at 324 nm with an extinction coefficient of 21 400 M^{-1} cm^{-1} at pH 8.

4mM DTDP stock was prepared by dissolving 0.22 mg in 25 ml 0.012 M HCl. DTDP is stable in acidic conditions, however, the solvent has to be degassed in order to avoid oxidation of thiol groups. Aliquots of 250 µl were stored in -20 ^{o}C and thawed aliquot was not frozen again.

Prior to measurements with protein, 3 mM cysteine (Sigma, catalogue number A7250) was used for calibration. 245 mg Cysteine was dissolved in degassed 500 ml 0.01 M HCl. Dissolved cysteine is stable in acidic conditions for at least 3 hours. After stock preparation, reaction mixtures were prepared (see table 2.4) using different volumes of 3 mM cysteine and results were compared, to understand if we could get same results with different sample volumes. (Table 2.3)

µl Cysteine Added	A_{324}	Molar Cysteine Calculated
blind	0	0
3	0.881	0.003463
6	1.612	0.003168
9	2.411	0.003159
12	3.046	0.002993
15	3.789	0.002979
18	4.532	0.002969
21	5.308	0.002981
Average		0.003102
Standard Deviation		0.000181

Table 2.3: Results of calibration trial with 3mM cysteine.

Results converge to 3±0.18 mM. The low level of SD indicates that the method is applicable to protein concentration determination.

Protein concentration was determined using by 4-DTDP assay. 4-DTDP is prepared as in table 2.4. Na-citrate buffer at pH 4 is used to provide the optimum pH for the reaction.

	Blind	Sample
Sample	0 µl	X µl
4mM 4-DTDP	12.5 µl	12.5 µl
pH4 Citric Acid / Na-Citrate	22.5 µl	22.5 µl
ddH2O	90 µl	90 – X µl
Total	125 µl	125 µl

Table 2.4: 4-DTDP assay reaction mixture ingredients.

Apoprotein was incubated with 4mM 4-DTDP at pH4 at room temperature with occasional mixing for about 15 minutes. Incubation period shouldn't exceed 2 hours, since DTDP starts decaying after 2 hours.

Absorbance of both blind and sample are measured with Nanodrop spectrophotometer (Thermo) and absorbances at 324 nm are noted. Concentration is calculated according to formula below;

(2.1)
$$[G65C] = \frac{(A_{324\,sample} - A_{324\,blind}) * Reaction\,Volume}{21200 * Amount\,of\,Sample * (\#\frac{cys}{2})}$$

Extinction coefficient of DTDP was estimated to be 21200 at pH 4. 6,5 is the available sulfhydryls in the protein divided by two.

2.2.4.2. Absorbance Spectroscopy

Absorbance spectroscopy analyses were done with Nanodrop Spectrophotometer (Thermo). For this purpose, 2 µl of sample was placed in sample chamber and upper arm was closed. The program "Protein A280" was used for measurements. Values were normalized according to concentration using the formula below;

(2.2)
$$\varepsilon * 10^{-4}(M^{-1}cm^{-1}) = \frac{A}{c*l} * 10^{-4}$$

Where A is absorbance, c is concentration in molar, l is pathlength in centimetres.

2.2.4.3.CD Spectropolarimetry

(CD, is a commonly used technique during characterization of MTs. CD arises from differential absorption of left and right handed circularly polarized light by proteins, and has high sensitivity for nonchiral environments.

140 – 150 µl protein solutions were used for CD spectropolarimetry analyses. Measurements were carried out with Jasco J-815 CD Spectropolarimeter connected to a computer with Spectra Manager™II installed.

All measurements were carried out in 1mm pathlength quartz cuvettes and data analysis / processing was done with Spectra Manager™II software. The measurements were carried out on protein samples that had 50 to 120 µM concentration. To eliminate concentration factor, ellipticity values were normalized to molar ellipticity (see introduction – equation 1.1).

2.2.4.4.Dynamic Light Scattering (DLS)

DLS analyses were done by Zetasizer Nano ZS (Malvern Instruments). This system determines the size of the particles in a solution by measuring the Brownian motion of the particles by dynamic light scattering. Changes in the position of the scattered light due to Brownian motion of particles are correlated with the diffusion speed which in turn is used to calculate the size.

Small particles move more quickly while large particles move more slowly. Stokes-Einstein equation defines the relationship between the size of a particle and its speed due to Brownian motion. The velocity of Brownian motion is determined by translational diffusion coefficient. As large particles move slowly, the intensity of the speckle pattern will also fluctuate slowly. In contrast, the intensity of the speckle pattern will fluctuate quickly for small particles as they move more quickly.

First size distribution generated by DLS is an intensity distribution. It is then converted to volume and number distributions. According to the Rayleigh approximation, the intensity of scattering of a particle is proportional to the sixth power of its diameter. That's why the most reliable analysis is an intensity distribution since the difference between scattering of small and large particles are much more than their difference in number or volume distribution.

2.2.4.5.Reconstitution of Apo-G65C with Cadmium and Zinc

Loading of apo-G65C with Cd (II) or Zn (II) were done by following a slightly modified version of the procedure given by Vasak (Vasák 1991). The solutions used were rendered oxygen free by degassing and all steps were performed under argon flush. Apo-G65C which was eluted from size exclusion column was used. The pH of apo-G65C solutions was adjusted to 8.3 using 0.5M Tris-Base, in presence of 5mM DTT to minimize aggregation for 30 minutes. Right after pH adjustment, appropriate amounts of metal calculated according to protein concentration were added for stepwise and all at once reconstitution and samples were incubated for 15 minutes at room temperature for equilibration. Absorbance, CD spectropolarimetry and ICP-OES analyses were carried out on samples for characterization.

2.2.4.6. Cadmium Titration of Zn$_2$-G65C

Cd (II) has more affinity towards G65C than zinc. To monitor binding properties and structural changes due to metal ion replacement, 1 ml aliquots of apo-G65C were reconstituted with 5 mol equivalent Zn (II) and titrated with Cd (II) stepwise. 1 mol equivalent to 5 mol equivalent Cd (II) was added to ZnG65C and absorbance, CD spectropolarimetry and ICP-OES measurements were carried out.

2.2.4.7. pH Titration of Reconstituted Cd$_5$-G65C

140 µl aliquots of Cd-G65C in 10 mM Tris-HCl, pH 8.3 was titrated with increments of diluted HCl solutions (table 2.5). After each addition, absorbance and CD profiles of the protein solutions were measured. Dilution effects due to HCl addition were negligible.

pH	Amount of 0.75 mM HCl
8.3	Default
7.02	1.96 µl
6.01	2.436 µl
5.1	2.52 µl
4.1	2.576 µl
3.05	2.772 µl
2.4	3.472 µl

Table 2.5: Amount of HCl added to lower pH of 140 µl protein solution.

2.2.4.8. Chelex 100 Treatment

Protein solutions of holo-G65C and reconstituted CdG65C and ZnG65C were incubated overnight with Chelex 100 (Sigma C7901) overnight at room temperature. Supernatant was analyzed by ICP-OES.

Chelex 100 resin was first washed with ddH$_2$O and then with pH 8.3 reconstitution buffer until resins pH was 8.

2.2.4.9. SDS and Native Polyacrylamide Gel Electrophoresis (PAGE) and Staining

SDS gels were prepared according to the recipe given in Appendix C (Laemmli 1970). 10 µl protein samples were mixed with 2 µl 6x SDS gel loading buffer (125mM Tris-HCl pH 6.8, 2% SDS, 20% glycerol, 0.2% bromophenol blue, 10% (v/v) β-mercaptoethanol) and heated at 95 ^{o}C for 5 minutes. 10 µl was loaded into 12 % SDS polyacrylamide gels having 5% of stacking gel. Gels were run in 1X SDS running buffer (25 mM Tris, 192 mM glycine, 0.1 % (w/v) SDS). For the stacking part, samples were run at constant 90V and for separating, voltage was increased to 120V.

Native gels were prepared according to the recipe given in Appendix C. 10 µl protein samples were mixed with 2 µl 6X Native-PAGE sample buffer (200 mM Tris-HCl pH 7.5, 20 % glycerol, 10 %, 0.2 % bromophenol blue) and loaded into 10 % non-denaturing PAGEs. Gels were run in 1X Native running buffer (25 mM Tris, 192 mM glycine). For the stacking part, samples were run at constant 90V and for separating, voltage was increased to 100V.

For visualization, SDS- and Native- polyacrylamide gels were stained with coomassie blue solution and de-stained in distilled water. The recipe of coomassie blue solution is given in Appendix C.

2.2.4.10. Inductively Coupled Plasma Optical Emission Spectroscopy (ICP-OES)

ICP-OES (Varian, Australia) was used to determine the metal content of a given protein solution. Also it was used to determine protein concentration from S content. Concentration of protein in the solution was determined experimentally by 4-DTDP assay and Cd(II) in solution was measured by ICP-OES to determine the ratio of Cd(II) per G65C. Since the volumes we worked on were small, we had to do dilutions before giving samples for acid dissolution. Usually 100 µl sample was topped to 500 µl and 400 µl was used for dissolution.

2.2.4.11. SAXS and A*b Initio* Low Resolution Molecular Envelope Modelling

Small angle X-ray scattering measurements were carried out on the EMBL X-33 beamline (Koch *et al.* 1983) at the DORIS storage ring, DESY, Hamburg. This beamline, optimised for low background data collection from macromolecular solutions (Roessle *et al.* 2007), is equipped with a photon counting Pilatus 1M pixel detector (67 x 420 mm^2) with a sample-detector distance of 2.7 m. During measurements samples are kept in a vacuum cell with polycarbonate windows at 18 °C and data are collected as 3 one minute frames. Scattering patterns from different frames are compared for monitoring possible radiation damage occurring during the measurements. Data were collected from G65C in the concentration range 0.3 to 1.4 mg/ml in 20 mM HEPES pH 8.0, 100 mM NaCl.

The data is presented as logarithm of the scattered intensity (I(s)) against momentum transfer s (s = 4πsinθ/λ, where 2θ is the scattering angle and λ is the wavelength: 0.15 nm). Preliminary data analysis involving correction for beam intensity, background correction, buffer subtraction and concentration normalization were carried out using the PRIMUS (Konarev *et al.* 2003) software in the ATSAS suit of programs (Petoukhov *et al.* 2007) at EMBL Hamburg. Following the initial data reduction further analyses are carried out to determine the forward scattering I(0) and the radius of gyration Rg of the protein. Additionally Porod plot is calculated to obtain information about the structural flexibility of the macromolecule (Porod 1982).

Calculations of Rg and molecular mass of the protein in solution can be be carried out according to the Guinier approximation (Guinier 1955). Guinier approximation states that for a monodisperse solution the scattered intensity at small angles I(s) is a linear function of s^2 and the scattered intensity extrapolated to s= 0, I(0), is proportional to the molecular mass of the protein in solution. The slope of the linear fit yields the radius of gyration and for globular particles at s values where sRg <1.3;

$$(2.3) \qquad I(s) \cong I(0)\exp\left(-\frac{1}{3}R_g^2 s^2\right)$$

For molecular mass (MM) determinations the scattering form a reference protein (e.g. BSA) can be used and the unknown molecular mass calculated as:

(2.4)
$$MM_S = \frac{I(0)_S}{c_S} * \frac{c_{BSA} * MM_{BSA}}{I(0)_{BSA}}$$

where MM_S, $I(0)_S$, c_S, MM_{BSA}, $I(0)_{BSA}$, c_{BSA} stand for molecular mass of the sample, scattering intensity at zero degrees, concentration of the sample, molecular mass of BSA, scattering intensity at zero degrees for BSA and concentration of BSA respectively. For the measurements BSA was prepared fresh in 20 mM HEPES, pH 8.0, 150 mM NaCl and 1 mM DTT at a concentration of ~5 mg/ml.

The pair distribution function which is proportional to the probability of observing a given distance inside the particle can be calculated using the indirect transform package GNOM (Svergun 1992). The output of GNOM analysis is used in molecular shape modelling calculations. *Ab initio* calculations were carried out using the algorithms DAMMIN (Svergun 1999) and GASBOR (Svergun, Petoukhov et al. 2001). The models are calculated using dummy residues or beads by a simulated annealing procedure and the difference between the scattering from the model and the experimental scattering intensity are minimized. Fifteen different models were calculated with each algorithm and convergence of the models calculated by the two algorithms to a similar shape was observed. The final average model was obtained using DAMAVER (Volkov and Svergun 2003)

3. RESULTS

In the following section, experimental data on biochemical and biophysical characterization of a mutant (G65C) of durum wheat metallothionein (dMT) will be presented. These results include purification of the protein, on holo- and apo-G65C, structural modelling based on SAXS data and comparison with native dMT.

G65C is a mutant obtained from dMT with site directed mutagenesis; 65th glycine of dMT was mutated to cysteine.

```
MSCNCGSGCS  CGSDCKCGKM  YPDLTEQGSA  AAQVAAVVVL  GVAPENKAGQ  FEVAAGQSGE
1           11          21          31          41          51

GCSCCDNCKC  NPCNC
61          71
```

Table 3.1: Amino acid sequence of G65C. The cysteine that was introduced in dMT sequence is marked with red.

3.1. Confirmation of G65C Expression at Protein Level
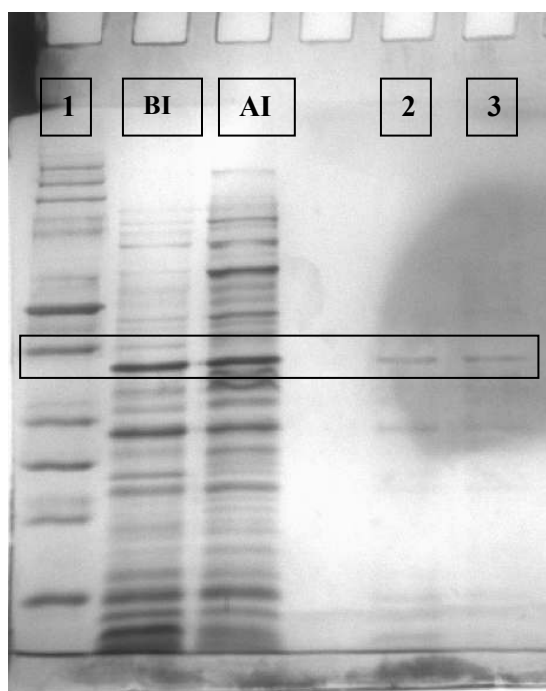
Figure 3.1: 12% SDS-PAGE analysis of mutant dMT expression in *E. coli.*

Lane 1: Fermentas Unstained Protein Ladder, BI: lysate before induction, AI: lysate after induction, Lanes 2 and 3 1/5 dilution of BI and AI respectively. Position of GSTG65C (~35kDa) is indicated with a box.

Figure 3.1 shows SDS-PAGE analyses of total cell lysate from *E. coli* expressing the GSTdMT gene with G65C mutation. Lanes BI and AI show samples from cells before and after induction of this gene respectively. In lanes 2 and 3, BI and AI samples are run after 1/10 dilution. In the diluted samples, recombinant protein is easier to detect. The fact that G65C is observed also in the lysate of non-induced cells shows that the strong promoter of pGEX4T-2 leads to a high level of background expression. These results confirmed synthesis of the GSTG65C fusion protein.

3.2. Purification of G65C from *E. coli*

The purification scheme for G65C can be summarized as follows:

Growth
BL21 (DE3) cells containing G65C DNA were grown in 3L LB medium in presence of 0.1 mM $CdCl_2$ and 1 mM ampicillin at 37 ^{o}C and 280 rpm.

Induction
Cells were induced at when their OD_{600} was 0.8 to 1 with 0.7 mM IPTG

Harvesting of cells
Cells were harvested by centrifuging at 17.000g for 15 minutes.

Lysis
Cells were lysed in lysis buffer, in presence of $CdCl_2$

Binding of GSTG65C to GST Affinity Matrix
Cleared cell lysate was incubated with 50% GST beads for 4 to 6 hours and GST tag was cleaved (with Thrombin) while GSTG65C was bound.

Size Exclusion Chromatography (SEC)
G65C was eluted from affinity matrix, concentrated and loaded on HiLoad 16/60 or 26/60 Superdex 75 pg size exclusion column.

3.2.1. GST Affinity Matrix Purification

The recombinant GSTG65C was first purified using a Glutathione Sepharose matrix. Elution of G65C from Glutathione Sepharose beads were done in two parts, each with 15ml elution buffer and absorbance of eluates were measured separately. If the protein content of the second eluate was at least half of first both eluates were mixed – otherwise discarded - and the absorbance of the combined eluate were measured

again. Then protein solution was concentrated to 2 to 4 ml before loading on size exclusion column.

Characterization of the protein at this stage of the purification are shown below. In figure 3.2, the SDS PAGE analysis of cell lysate is shown together with samples taken from matrix wash and cleaved G65C eluted from the GST matrix. G65C band, indicated with an arrow, is seen together with unbound GST (~25 kDa) and other nonspecific proteins. On this figure a sample taken from concentrated eluate is also shown after 1/10 dilution for convenience. In figure 3.3, UV-vis absorbance curves for eluates of GST matrix, combined sample and as well as the concentrated sample are shown. Features of these spectra are in agreement with those that are expected from G65C (see below).
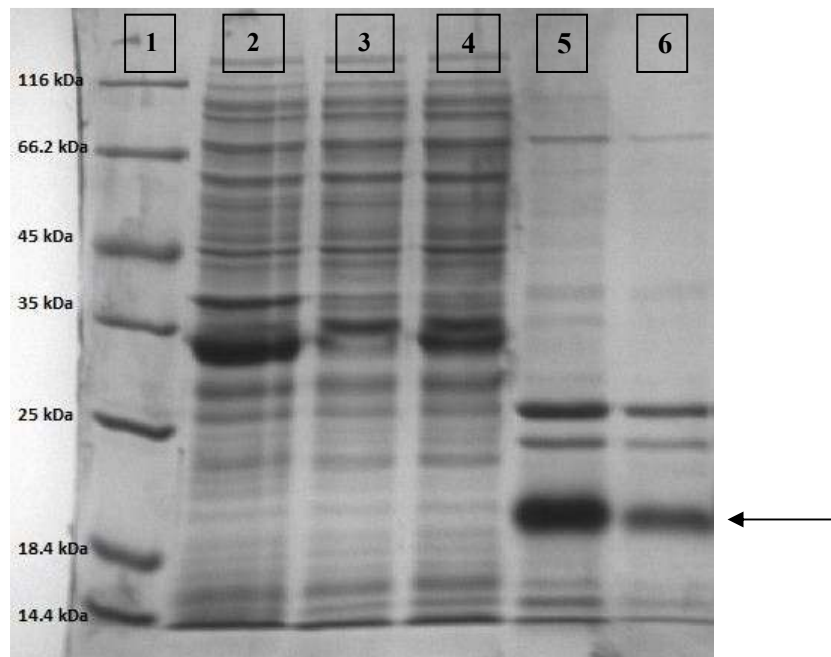
Figure 3.2: 12% SDS PAGE analysis of batch purification results and eluate before size exclusion chromatography.

Lane 1 contains Fermentas Unstained Protein Molecular Weight Marker (PMW), Lane 2 is cell lysate, Lanes 3 and 4 are proteins that are not bound to GST affinity matrix, Lanes 5 and 6 are G65C that was eluted after thrombin cleavage, before and after concentration respectively. Lysate and G65C after concentration samples were diluted 1/10 for convenience.

Other proteins than G65C were eliminated by SEC.
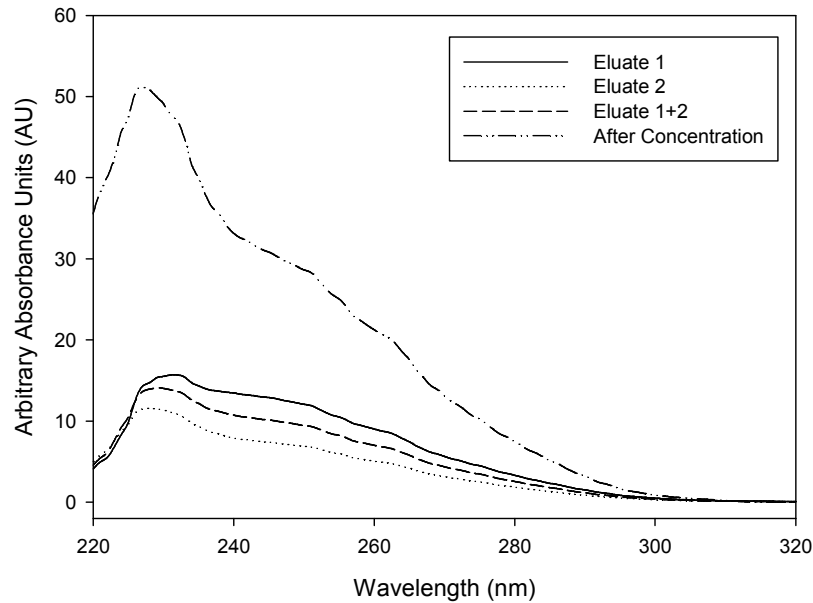
Figure 3.3: UV-vis absorbance curves for eluted G65C, before and after concentration. Y axis shows arbitrary absorbance units (AU).

3.2.2. Size Exclusion Chromatography (SEC)

Concentrated G65C was loaded on HiLoad 16/60 Superdex 75pg Size Exclusion Column (GE Healthcare). The reason sample is concentrated before loading on the column is; large volume samples usually do not get separated well during chromatography. If protein yield is high (~10 mg) and / or concentration is above 2 mg/ml, one might need to do more than one run. 4 mg protein was loaded on HiLoad 16/60 and 8 mg was loaded on 26/60 size exclusion column in 2 and 4 ml respectively. If recommended sample amount is exceeded in either volume or concentration-wise, resolution decreases, resulting in bad separation of proteins.
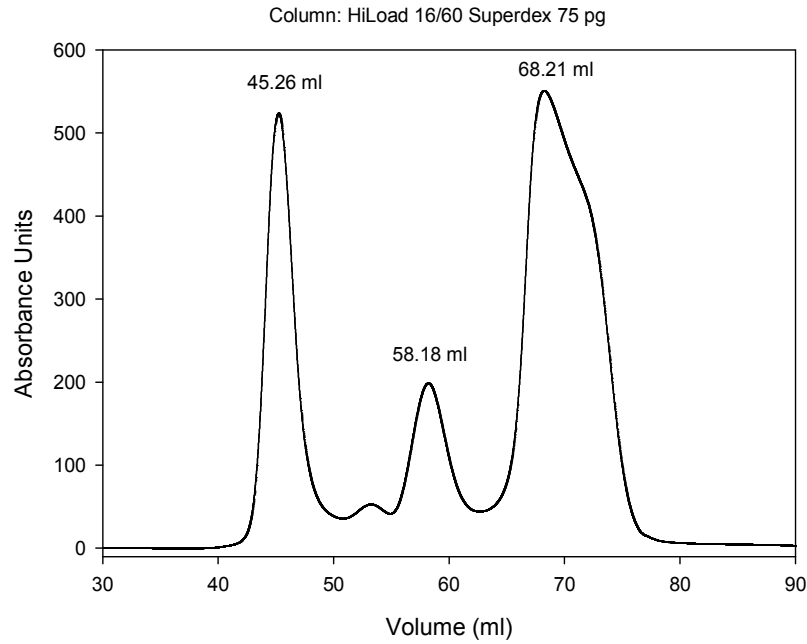
Figure 3.4: Size exclusion chromatogram for holo-G65C. Elution volumes for the peaks are indicated.

The first two peaks of the chromatogram in figure 3.4 at 45.26 ml and 58.18 ml correspond to be unbound and aggregated forms of GST. Protein band in SDS-PAGE result in figure 3.4 show that third peak eluting around 68 ml only contains G65C. The width and asymmetric shape of the peak indicates polydispersity in the eluted G65C. The range of molecular mass within the elution volume of this peak 31.6 to 14.2 kDa, which confirms that a range of oligomeric states from dimeric to tetrameric state, elute in this volume. Top of the peak contains the most concentrated sample and corresponds to 23.5 kDa.

For further analyses, fractions of this peak were pooled. In general top and right side of peak (after 68 ml) was used because these correspond to lower oligomeric forms. Left side (between 65 and 68 ml) was included in the pool only when the amount of protein pool was not sufficient for overall analyses. Fractions and pools of the third peak were analyzed with SDS PAGE for purity, and single bands were obtained both in individual fractions and pooled fractions, which means there is only one protein specie in the solution and our sample is pure.
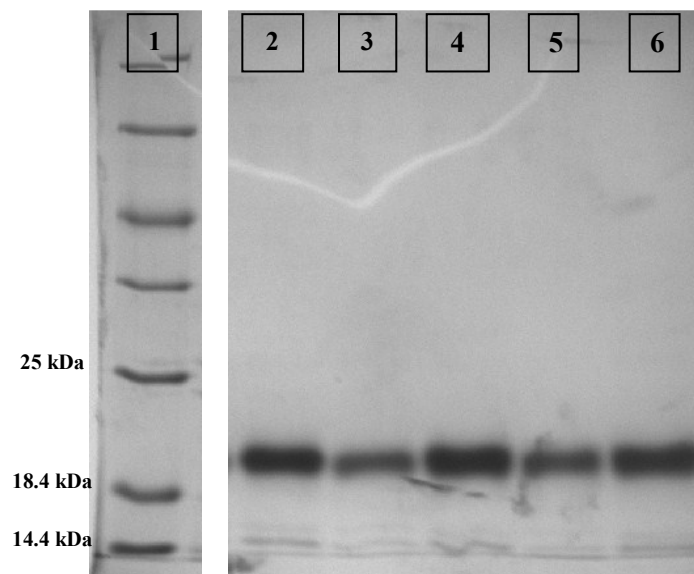
Figure 3.5: 12% SDS PAGE analysis of samples eluted from size exclusion column. Lane 1 is Fermentas Unstained PMW, Lanes 2 to 5 are samples from third peak (G65C) and Lane 6 is pooled fractions.

As shown in SDS PAGE results in figure 3.5, G65C migrates above 18.4 kDa marker band, which is more than dimer mass. This can be explained by presence of bound cadmium ions (see discussion).

3.3. Biophysical and Biochemical Characterization of Holo-G65C

3.3.1. UV-Vis Absorbance Spectroscopy

Absorbance spectra were measured in order to see if mutant protein displayed spectroscopic features unique to dMT.

As can be seen in figure 3.6 absorbance spectra of G65C have two distinctive features; one is the peak at 230 nm, caused by protein backbone absorption and other is the shoulder at 250 nm. The latter is the characteristic LMCT band due to Cd-S interactions. There is no band at 280 nm because of the paucity of aromatic amino acids in MTs.
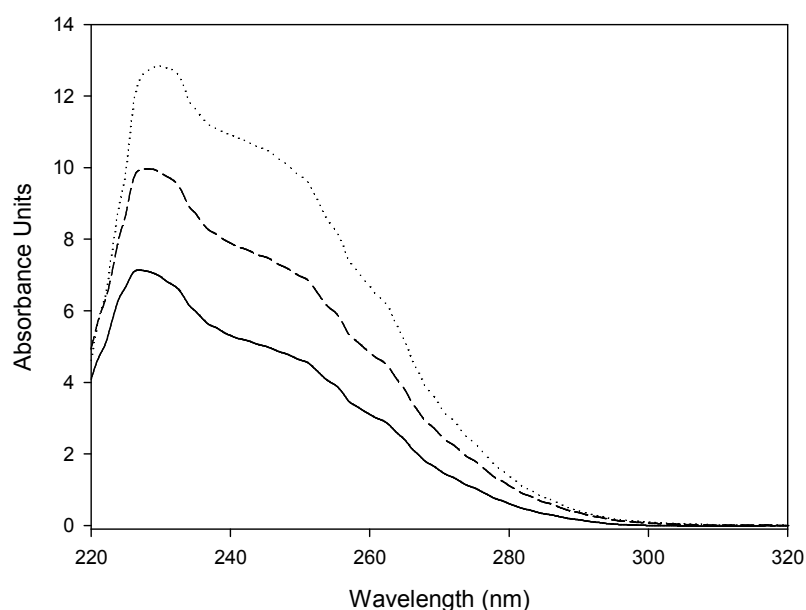
Figure 3.6: Absorbance curves of three fractions from the size exclusion column.

Shifts among spectra in figure 3.6 are caused by the concentration differences. Absorbance measurements help to obtain a quick rough estimate of the concentration of the fractions from the size exclusion column using formula derived from standard proteins used in calibration (not shown). Depending on the analysis that will be done – for example SAXS requires small sample volume (60-70 µl) but as high concentration as possible, on the other hand apoprotein preparation requires higher sample volume (5-6 ml) – fractions can be pooled or used individually.

3.3.2. CD Spectropolarimetry

CD spectropolarimetry was used to obtain information on secondary structure of G65C. As G65C has only 2 aromatic amino acids – one phenylalanine and one tyrosine at the hinge region – CD features originate mainly from Cd-S LMCT. CD spectra of protein solutions containing G65C, e.g. figure 3.7, have a global maximum at around 240 nm, which is an envelope caused by Cd-S interactions. Far UV region (210-230 nm) of CD spectrum is dominated by random coil secondary structure, which is seen as a global minimum around 210 nm.
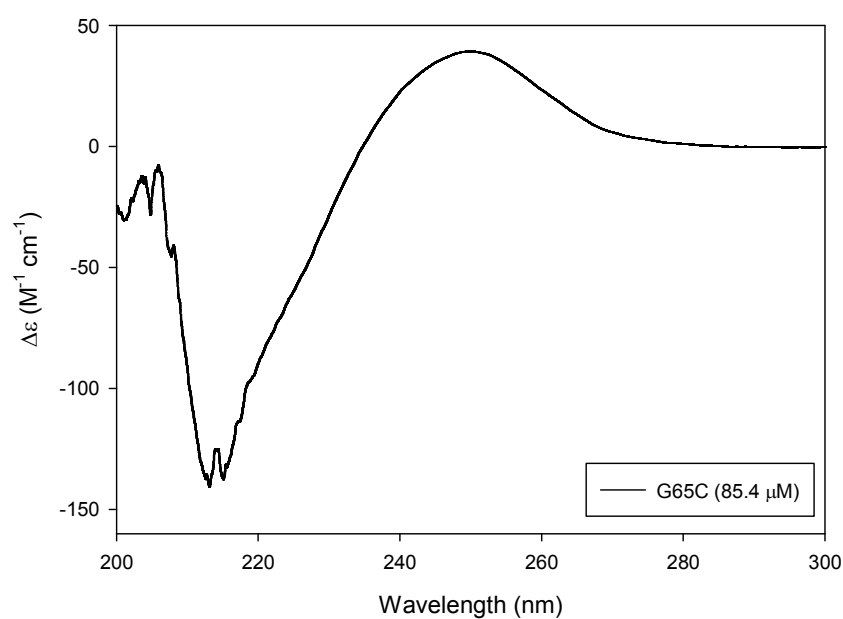
Figure 3.7: Molar ellipticity of G65C pool at 85.4 µM.

Protein concentrations were optimized for CD measurements because some of the features, e.g. the minimum at 210 nm, is not easily discernable at low concentrations.

3.3.3. Dynamic Light Scattering

G65C fractions that have been obtained from size exclusion chromatography have been subject to DLS analyses, to determine polydispersity and to see whether the protein is aggregated / degraded.
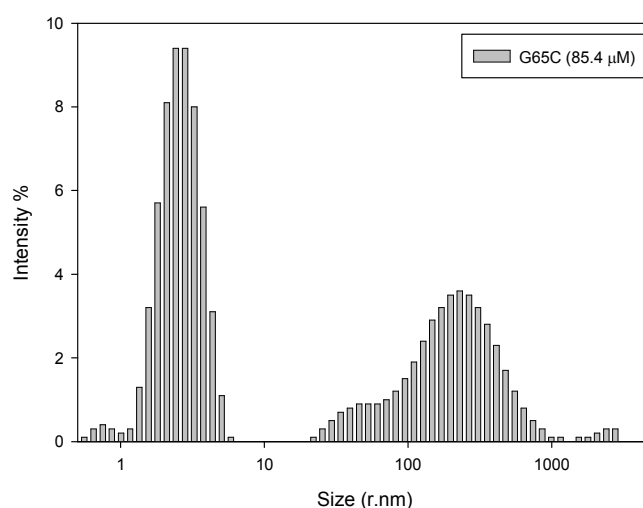
Figure 3.8: Size distribution of G65C (85.4 µM) according to scattered intensity.

The dominant peak in figure 3.8 corresponds to a hydrodynamic radius (R_h) of 2.04 nm, and the protein mass calculated according to this value is 17.9 kDa, which indicates dimer (or other oligomers) presence. These results are consistent with those of size exclusion chromatography and show that purified G65C solutions are polydisperse. Previously in figure 3.4 it was shown that purified G65C solutions contain multiple species and their mass ranges between 14.2 to 31.6 kDa, the top of the peak being 23.5 kDa. The low-intensity peak below 1 nm can be artifact due to instrument error or degradation, which cannot be seen on SDS PAGE.

Polydispersity index, calculated according to the standard deviation of the main scattering peak is 33.1%. This suggests that there is more than one oligomeric form of protein population in the peak, or aggregates. The fact that only one band is observed on SDS-PAGE (figure 3.5) shows that the numerous oligomeric forms can be reduced to a single species.

3.3.4. Metal Content Determination with ICP-OES

Metal content of protein samples were determined by ICP-OES. ICP-OES measurements were repeated on equivalent samples from different protein purifications and results were analyzed to show the reproducibility. Results shown in table 3.2 are

calculated by dividing metal content of the solution by protein concentration, which was determined by DTDP assay (see below).

	[G65C] (μM)	[Cd^{++}] (μM)	Cd^{++}/G65C
Holo-G65C	7.44E-05	0.000370217	4.98±0.74

Table 3.2: Metal content determination of holo-G65C. Metal / protein ratio (± standard deviation) calculated from 12 measurements are shown.

Unless indicated otherwise, all samples are treated with Chelex 100 resin, which is a low affinity metal binding matrix. Chelex 100 was primarily used to remove unbound metal ions in protein solution.

3.4. Apo-G65C Preparation

Apoprotein can be obtained by two methods,
- By dialyzing holo-G65C against 0.02M HCl overnight with 2-3 changes of the dialysis solution.
- Treating holo-G65C with HCl and running it through a size exclusion column at pH 2.5.

Dialysis option is not very reliable; the protein gets aggregated and/or degraded during prolonged dialysis, and at the end the apo-protein cannot be used. Running treated holoprotein through the size exclusion chromatography column, on the other hand, is faster and more reliable. The drawback is, however, that direct acid treatment can demetallate the protein fast and cause aggregation. To overcome this problem, DTT concentration is increased to 5mM in the solution before loading the protein to 16/60 HiLoad Superdex 75 pg size exclusion column.
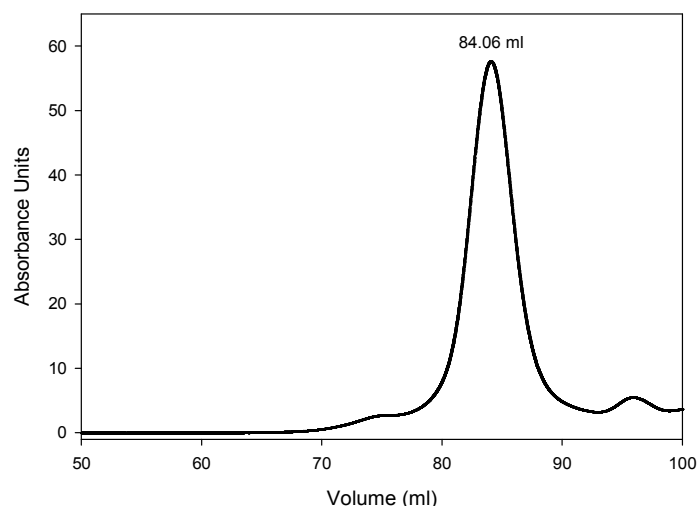
Figure 3.9: Size exclusion chromatogram of apo-G65C.

The elution profile of apo-G65C from size exclusion column is shown in figure 3.9. Apo-G65C at 84.06 ml is symmetric, however, holo-G65C at 68.21 ml is asymmetrical (figure 3.10). It is seen that apo-G65C elutes later, which is an indicator of smaller size. When the elution volume of apo-G65C – 84.06 ml – is used to calculate molecular mass, the result is 8.04 kDa, while mass calculated from amino acid sequence is 7.9 kDa. So basically, apo-G65C elutes from the column in monomeric form, while holo-G65C elutes in multiple forms. This shows that acid treatment and removal of cadmium ions lead to stabilization of monomeric form of G65C
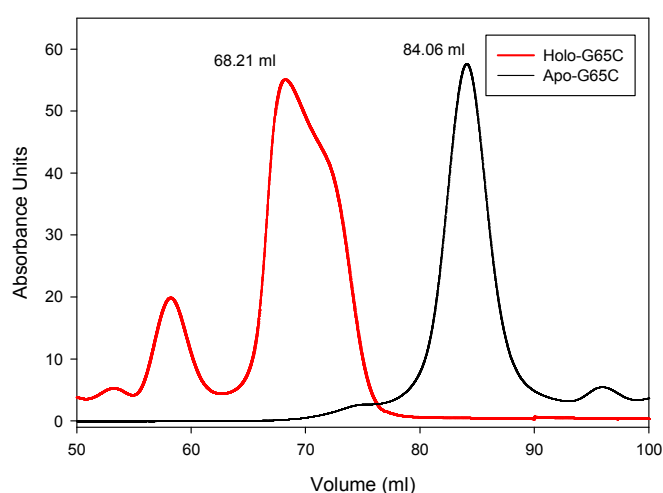
Figure 3.10: Comparison of the elution patterns of holo- and apo-G65C from the size exclusion column

3.4.1. Concentration Determination Methods

As explained in materials and methods, once apo-G65C fractions are collected, their concentrations can be directly measured with 4-DTDP since running buffer contains no sulfur, which may cause interference in DTDP assay and therefore deviate results.

When holo-G65C fractions were pooled after size exclusion, 500 µl aliquot of pool was dialyzed against acid overnight to get rid of DTT and to determine concentration. Typically, holo-G65C pools contained 120 µM and apo-G65C pools contained 70 µM protein. Depending on concentration of individual fractions, concentration of the pool may vary between 70 µM to 150 µM for holo-G65C and 50 µM to 80 µM for apo-G65C.

After the DTDP method was established for determination of the G65C concentration an empirical method for quick determination of concentration based on A250 measurements was also established.
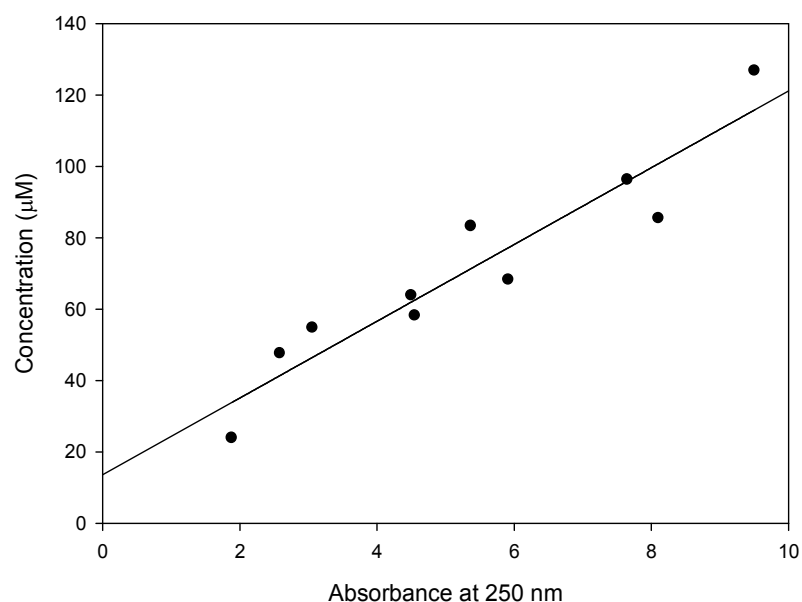
Figure 3.11: Relation between A_{250} and concentration for G65C.

The regression line of figure 3.11 yields $y = 10.7x + 13.567$, where y is concentration in µM and x is A_{250} of the sample at 1 cm pathlength. This method is

particularly useful for estimation of G65C concentration during the purification procedure, where DTDP assay cannot be applied due to presence of interfering sulfur atoms in the buffer.

Concentration can also be determined by ICP-OES, by measuring the sulfur content of the protein in solution. However, if the buffer also contains any other source for sulfur, this will inevitably have a dominating effect and will interfere with the protein concentration determination. For example sulfur absorbance that comes from 1 mM DTT can easily suppress the contribution of sulfur absorbance from 50 µM protein solution.

3.5.Effect of pH on Protein Backbone

After apo-G65C was prepared at pH 2.5 it was used in cadmium or zinc reconstitution experiments at pH 8.3. Increasing the pH caused changes in the spectroscopic features of the protein and this effect was further investigated through studies of a control peptide, hexaglycine. Hexaglycine was exposed to different pH values and changes were monitored by absorbance spectroscopy and CD. The reason why hexaglycine was chosen is that there is no side chain to interfere in spectroscopic measurements, so the features that are observed are due to protonation/deprotonation of the peptide backbone.
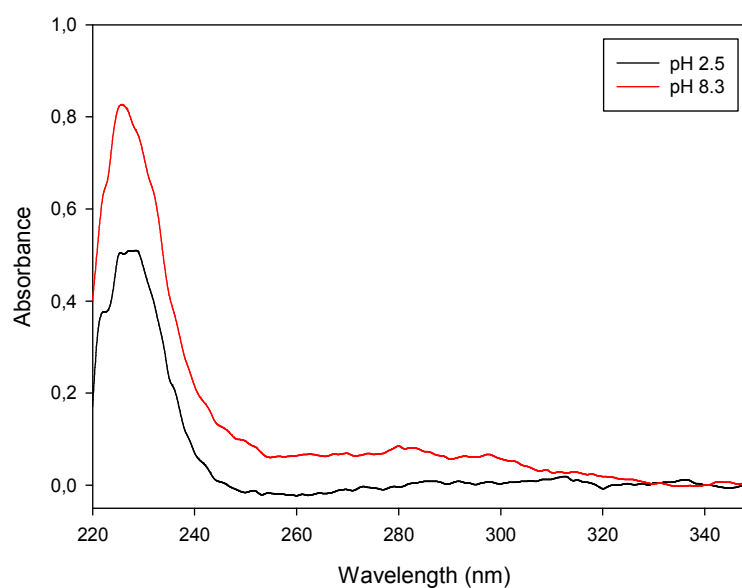
Figure 3.12: Changes in 0,2 mg/ml hexaglycine absorbance spectra due to pH.

Figure 3.12 shows changes in the absorption spectra of a 0,2 mg/ml hexaglycine solution in the range 220 to 350 nm when pH is increased to 8.3 from 2.5. It is clear that the protonation of amino groups shifts the overall spectral envelope to higher values and the peak at 230 nm becomes more prominent.
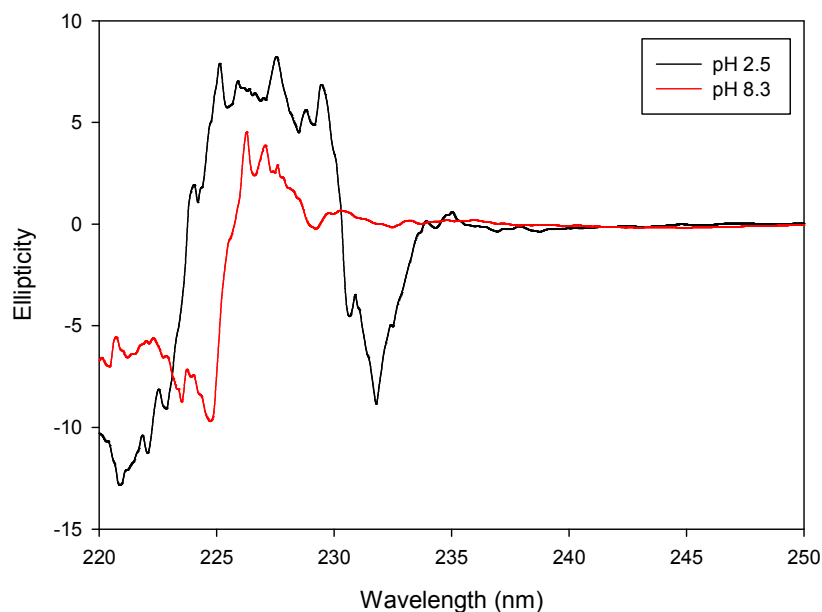
Figure 3.13: CD spectra of hexaglycine at pH 2.5 and 8.3

CD spectra of the 0,2 mg/ml mM hexaglycine solution at pH 2.5 and 8.3 show more dramatic changes. As can be seen from figure 3.13 at pH 2.5, there is a minimum around 232 nm, which disappears at pH 8.3. Also at pH 8.3 a peak is formed at 226 nm. Changes around 230 nm are critical for the peptide backbone because the peptide bond absorbs at that wavelength. When figures 3.12 and 3.13 are taken together, it is seen that at higher pH, absorbance and ellipticity increases. This information facilitates interpretation of changes that are seen at pH 2.5 and 8.3 in apo-G65C solutions.

3.6. Structural Characterization of Apo-G65C

3.6.1. UV-Vis Absorbance Spectroscopy

When G65C loses all its metals, its distinctive features, the peak at 230 nm and shoulder at 250 nm are lost. However, when the pH of solvent is increased to 8.3 from 2.5, A_{230} also increases and we've shown that this is due to rearrangement of protein backbone.
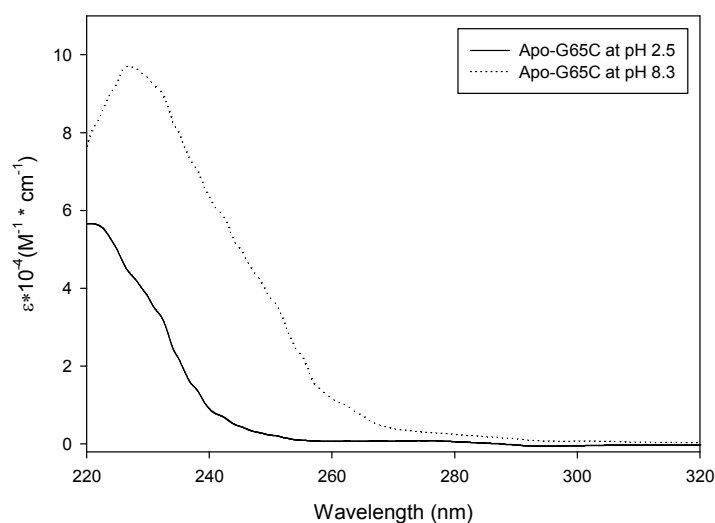
Figure 3.14: Absorbance spectra of apo-G65C at pH 2.5 (77.8 µM) and 8.3 (73.4 µM) compared.

The increase of absorbance seen in figure 3.14 at 230 nm indicates that protein backbone is changing conformation; and the increase at 250 nm is not due to LMCT caused by Cd-S interaction. ICP-OES results of both pH 2.5 and pH 8.3 samples show no cadmium present in the environment. What is observed is a general red shift of the whole spectrum.

3.6.2. Circular Dichroism Spectropolarimetry

Similar to results obtained with UV-vis absorbance measurements, features are lost in the CD spectra of demetallated G65C. Only the minimum at 210 nm is retained indicating that the protein is still a random coil. In agreement with figure 3.14, once pH is increased to 8.3, CD spectra changes, especially at 230 nm as shown in figure 3.15.
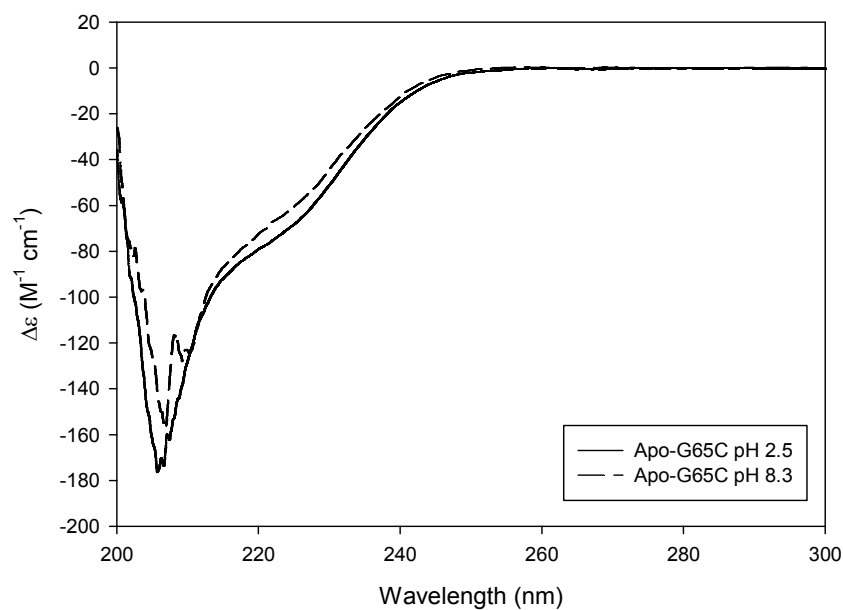
Figure 3.15: CD spectra of apo-G65C at pH 2.5 (77.8 μM) and at pH 8.3 (73.4 μM) compared.

Once pH is increased, the protein backbone rearranges itself, which in return causes the increase of intensity at around 230 nm and a blue shift of envelope at 230 nm. Above spectra is another confirmation that there is no LMCT involved, since there is no change at 250 nm.

3.6.3. Dynamic Light Scattering

Apo-G65C fractions that have been obtained from size exclusion chromatography were analyzed with DLS, to determine polydispersity index and to see whether the protein is aggregated / degraded or not.
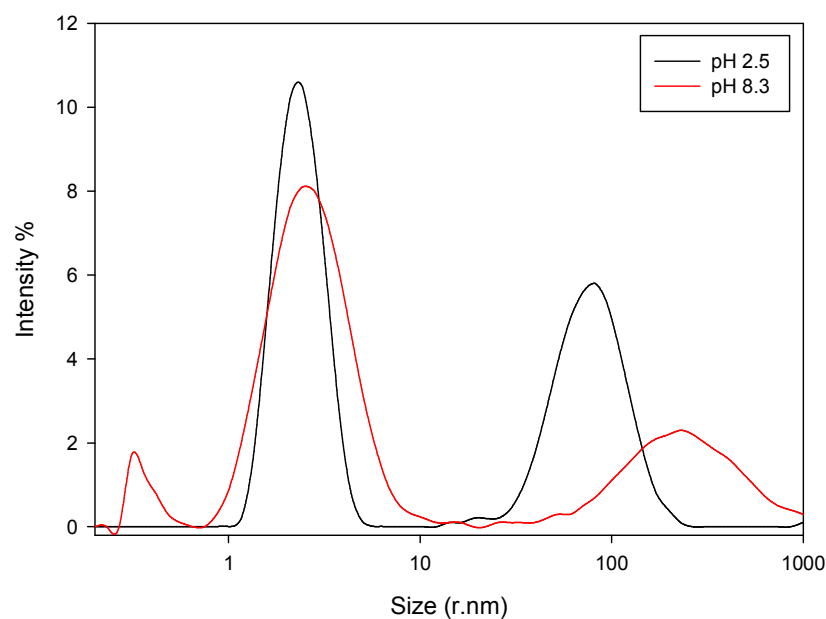
Figure 3.16: DLS analysis of apo-G65C at pH 2.5 and 8.3.

Comparison of DLS measurements of apo-G65C at pH 2.5 and 8.3 are shown in figure 3.16. Although the major size distribution peaks overlap at both pHs, the width of the peaks and the distributions are different. The peaks of apo-G65C at pH 2.5 are narrower and the peak positions are shifted towards smaller values.

3.6.4. Metal Content Determination with ICP-OES

	[G65C] (μM)	[Cd^{++}] (μM)	Cd^{++}/G65C
Apo-G65C at pH 2.5	5.70E-05	3.27435E-07	0.00574±0.001
Apo-G65C at pH 8.3	0.000052	1.78571E-08	0.000343407

Table 3.3: Metal content determination of holo- and apo-G65C. Standard deviations are shown for metal / protein ratio by ± values.

Taken together with absorbance spectroscopy and CD spectropolarimetry results, it is proven that apo-G65C fractions collected from size exclusion chromatography have no bound cadmium ions (table 3.3). The spectral shift that is seen

47

when the pH is raised to 8.3 from 2.5 is not due to incorporation of metal ions, rather it is due to backbone rearrangements.

3.7. Cadmium Reconstitution of Apo-G65C

Once apo-G65C is obtained, it is possible to load it with metals, in other words reconstitute the holo-protein. For this purpose, pH of the protein solution should be at optimum – an acidic environment would protonate the cysteine residues, which will inhibit metal binding. *E. coli* synthesized G65C is purified at pH 8 and after consideration of conditions mentioned above it was decided to conduct reconstitution experiments at pH 8.3.

In reconstitution studies, cadmium was added stepwise, 1 mol to 10 mol equivalents per mol protein; absorbance and ellipticity profiles were monitored. The effect of cadmium reconstitution on electrophoretic migration behaviour of G65C was monitored with SDS and Native PAGE analyses.

3.7.1. Changes of G65C Absorption Spectra During Cadmium Reconstitution

While apo-G65C loses all characteristic spectroscopic features, as the metal is added, some of the features gradually come back. (However, it was seen that holo-G65C – which is shown to bind 5 cadmium ions – is not the same with 5 mol equivalent reconstituted G65C – which binds 3.5 ± 1 cadmium ions. The difference in cadmium amount reflects on spectroscopic features as well.)
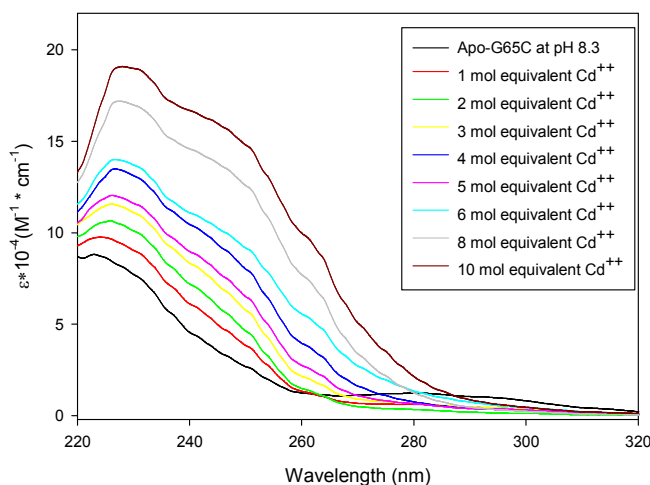
Figure 3.17: Cadmium reconstitution of apo-G65C (52μM).

48

The absorbance spectra shown in figure 3.17, intensity at 230 nm increases and the LMCT shoulder at 250 nm becomes more prominent as mol equivalents of cadmium is increased.

Figure 3.18 confirms that increase in absorbance is not linear; there are two increments that disrupt the linearity, these are at 3 to 4 mol and 6 to 8 mol equivalents. It is possible to speculate that bridging thiolates are formed and therefore the increase does not follow a linear fashion.
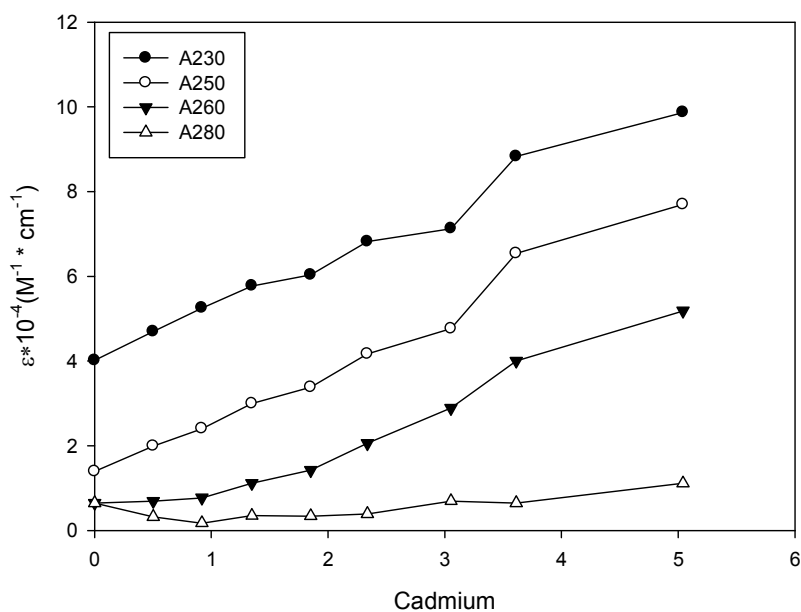
Figure 3.18: Changes in absorbance due to cadmium binding to G65C (1 mol equivalent increments). Y axis is molar absorbance and X axis is cadmium per protein, which was determined by ICP-OES after chelex treatment.
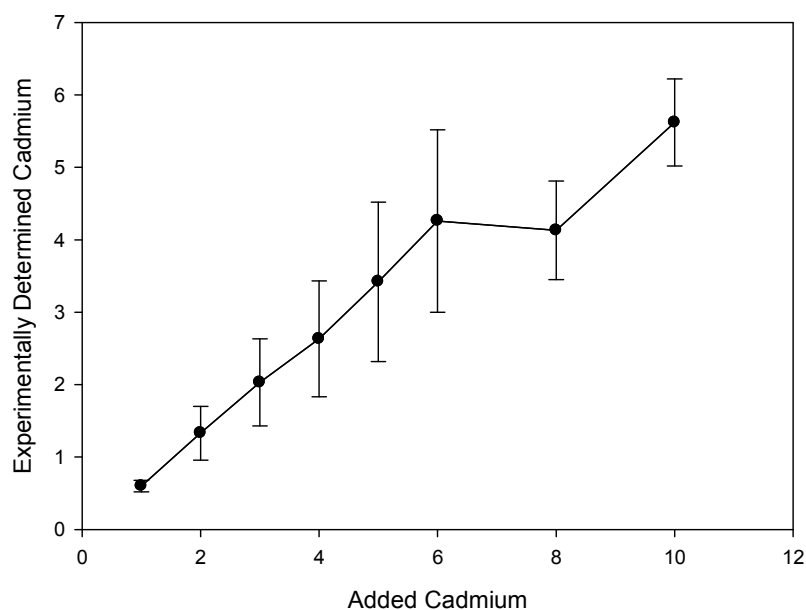
Figure 3.19: Theoretically added cadmium against experimentally determined metal content (with ICP-OES). Experimental results were obtained from samples treated with Chelex 100.

Figure 3.19 shows that the added amount of cadmium is twice the experimentally determined bound cadmium. It should be noted that experimentally measured cadmium was obtained from protein solutions treated with Chelex 100, so the values indicate only tightly bound metals.

3.7.2. Changes in Ellipticity of G65C During Cadmium Reconstitution

As in absorbance spectra, reconstituted G65C was shown to regain characteristic features in CD spectra. The fold of the protein changes when the first metal is added, and changes continue until 10 mol equivalents are added.
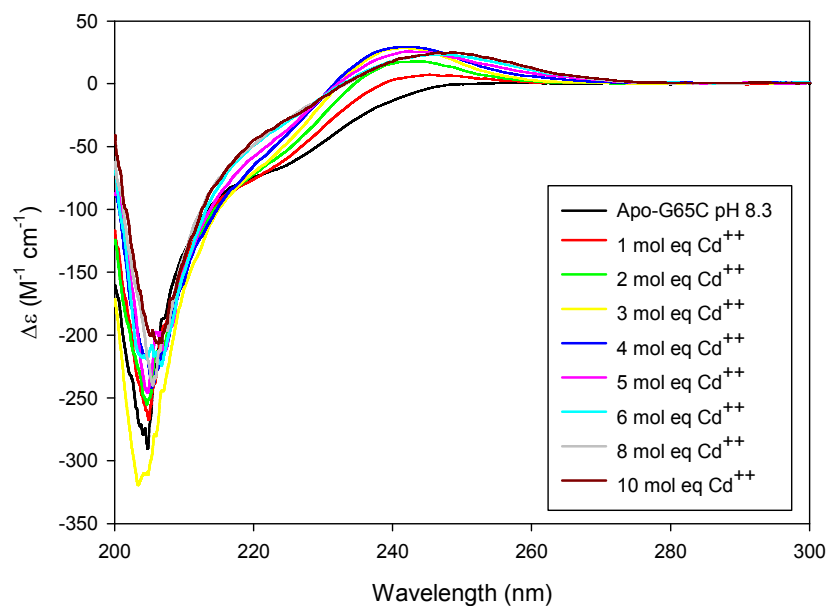
Figure 3.20: Changes in molar ellipticity during cadmium reconstitution of apo-G65C (52 μM).

Molar ellipticity give in figure 3.20 show that the band at 240 nm increases when metal is added - forming a shoulder-like envelope - as the one seen in holo-G65C spectra. The biggest change occurs between 1 and 2 mol equivalents. Also, as metal concentration is increased, molar ellipticity at around 230 nm changes, which is an indicator of fold change due to protein backbone wrapping itself around metals, forming a cluster.
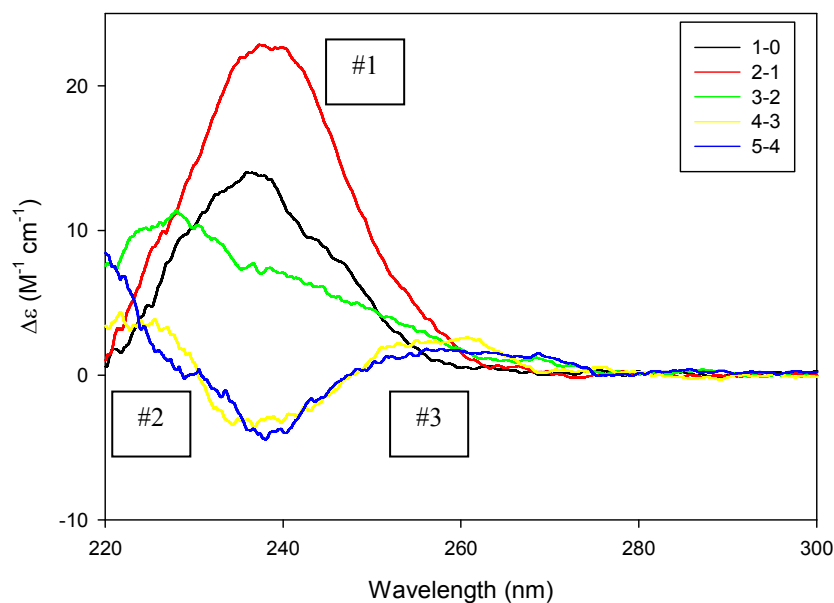
Figure 3.21: Difference CD spectra for consecutive cadmium reconstitution measurements.

Changes in features can be better visualized via difference CD spectra for reconstitution studies. Difference spectra in figure 3.21 shows that, until 4 mol equivalent addition, a single peak is dominant at 250 nm (peak # 1). After that point, peak #1 shifts to blue - to 220 nm - (peak #2), a minimum that occurs at 240 nm and a second peak forms at 260 nm (peak #3).

To elaborate these results, cadmium increments were dropped to 0.5 mol equivalents (figure 3.22), and same results were obtained, major change being between 2 and 1.5 mol equivalents.
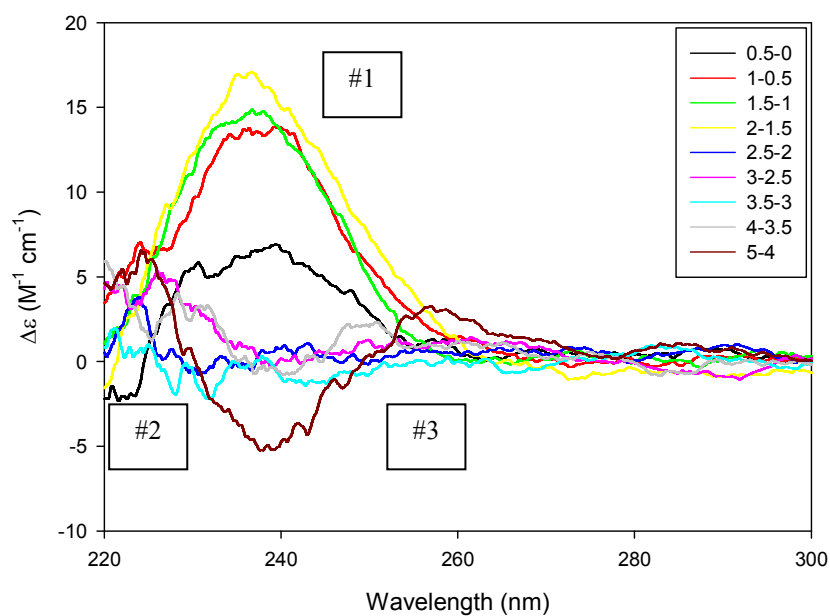
Figure 3.22: Difference CD spectra for consecutive cadmium reconstitution measurements with 0.5 mol cadmium increments.
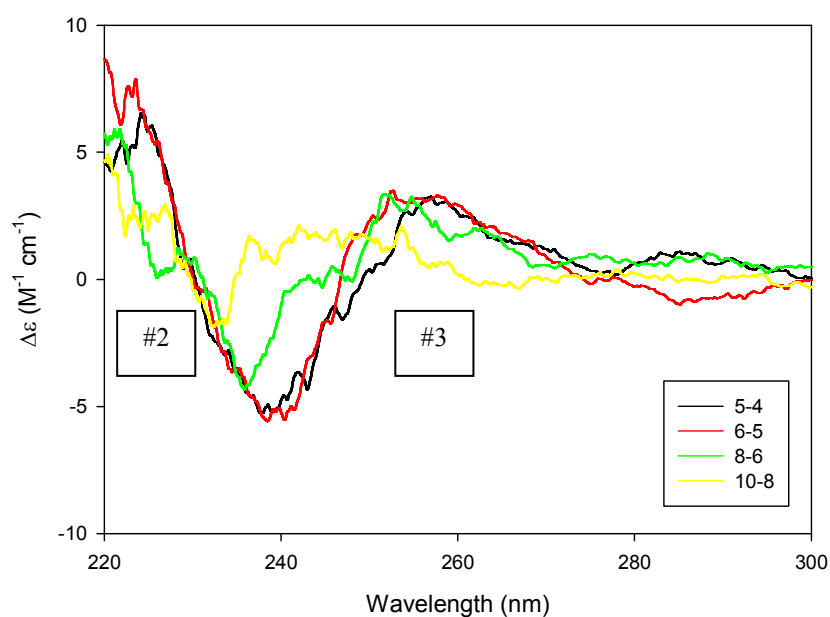
Figure 3.23: Difference CD spectra for consecutive cadmium reconstitution measurements at excess cadmium addition.

Difference CD spectra, shown in figure 3.23, for above 5 mol equivalent samples show complete loss of peak #1, yet peaks #2 and #3 are present until 10 mol equivalent. At 10 mol equivalent, the plot becomes rather flat, which means there is not much of a structural change between 8 and 10 mol equivalent additions.

3.7.3. Metal Content Determination with ICP-OES

Metal content of reconstituted samples were determined by ICP-OES and those values were divided by concentration to obtain metal / protein ratio. It should be noted that the samples were treated with Chelex 100 resin before metal determination. Chelex 100 is a matrix that has low affinity for metal ions and loosely bound cadmium ions; they are going to be removed by the resin.

	[G65C] (µM)	[Cd^{++}] (µM)	Cd^{++}/G65C
1 mol eq Cd^{++}	5.99E-05	3.58784E-05	0.599±0.079
2 mol eq Cd^{++}	5.99E-05	7.98949E-05	1.33±0.37
3 mol eq Cd^{++}	5.99E-05	0.000121432	2.03±0.6
4 mol eq Cd^{++}	5.99E-05	0.000157264	2.63±0.8
5 mol eq Cd^{++}	5.99E-05	0.000205013	3.42±1.1
6 mol eq Cd^{++}	5.99E-05	0.000255016	4.26±1.26
8 mol eq Cd^{++}	5.99E-05	0.00024764	4.13±0.68
10 mol eq Cd^{++}	5.99E-05	0.000336493	5.62±0.6

Table 3.4: Cadmium content determination by ICP-OES and cadmium per protein calculation.

Results given in table 3.4, (which are obtained from same samples that are shown in figure 3.20) show that that apo-G65C can be loaded with cadmium. However, it appears that not all metal ions are bound with same affinity. It was seen that after 10

mol equivalent addition, there is no more change in terms of metal binding, so 10 mol equivalent is the maximum metal concentration used for reconstitution.

3.8. Zinc Reconstitution of Apo-G65C

Same protocol as cadmium reconstitution was used during zinc reconstitution. Unlike Cd-S LMCT band at 250 nm, Zn-S bond is spectroscopically silent due to zinc atom having no unpaired electrons at its outer shell. Major changes occur only at 230 nm, which is caused by backbone rearrangement and metal-thiol cluster formation.

3.8.1. Changes of G65C Absorption Spectra During Zinc Reconstitution

Absorbance changes during zinc reconstitution, as shown in figure 3.23, displaying an increase at 230 nm and an overall increase in the spectra.
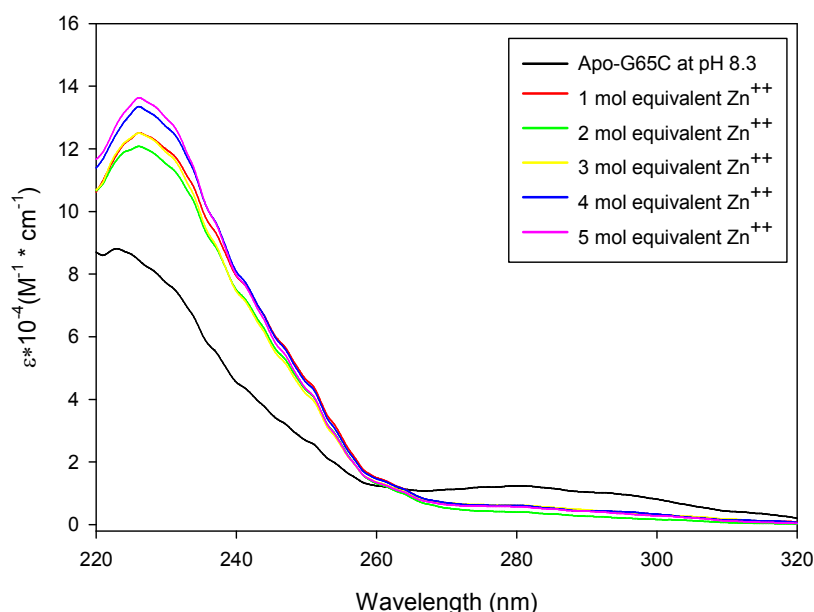
Figure 3.24: Zinc reconstitution of apo-G65C (52 μM).

Differences between curves are less in zinc reconstitution. The main reason for this is that Zn-S interactions are colorless, so the most prominent change is seen at 230 nm, which is caused by peptide backbone changes. In addition to this; thiols have less affinity for zinc ions, and when compared with cadmium reconstitution, changes in absorbance spectra are less pronounced.

3.8.2. Changes in Ellipticity of G65C During Zinc Reconstitution

Changes are more pronounced in CD spectra, due to its sensitivity to smallest conformation changes. Zn-S interactions – though not dominant – can be seen between 225 nm and 240 nm as shown in figure 3.25.
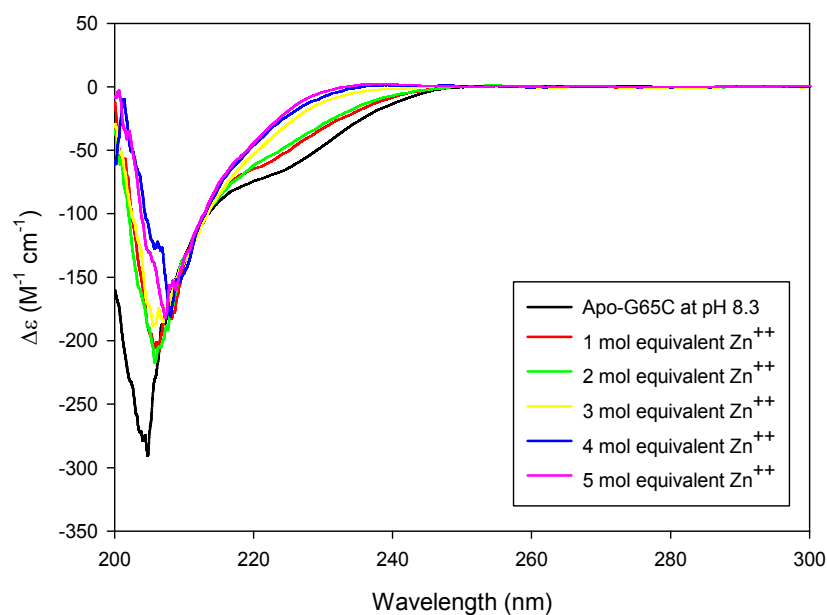
Figure 3.25: Zinc reconstitution of apo-G65C (52 μM).

The increase of molar ellipticity between 220 nm and 240 nm indicates that zinc is being coordinated by thiols. Another notable change occurs between 200 and 220 nm, which gradually shifts to red (230 nm), indicating that random coil structure is altering to a more ordered structure, by forming a thiol – metal cluster.

3.8.3. Metal Content Determination with ICP-OES

Protein solutions containing Zn reconstituted G65C were treated with Chelex 100 resin and analyzed with ICP-OES as shown in table 3.5.

	[G65C] (μM)	[Zn^{++}] (μM)	Zn^{++}/G65C
1 mol Zn^{++}	0.000052	2.84E-05	0.5466
2 mol Zn^{++}	0.000052	3.65E-05	0.7019
3 mol Zn^{++}	0.000052	6.24E-05	1.1998
4 mol Zn^{++}	0.000052	6.47E-05	1.2434
5 mol Zn^{++}	0.000052	0.000107	1.1718

Table 3.5: Zinc content determination by ICP-OES and zinc per protein calculation.

G65C has low affinity for zinc, and the reconstitution process reaches a plateau after addition of 3 mol equivalents. The results in table 3.5 show that even at this level of saturation only ~1.2 zinc ions are bound with high affinity. These results are also consistent with CD spectra shown in figure 3.25, where the change in the envelope reaches a saturation point at the same level.

3.9.Titration of Zn$_2$-G65C with Cadmium

Thiols have more affinity for cadmium than zinc and it is possible to titrate Zn-G65C with cadmium ions. Titration of Zn-G65C with cadmium allowed reproduction of spectroscopic features of Cd-G65C.

3.9.1. Changes in Absorbance Spectra During Cadmium Titration of Zn$_2$-G65C

During cadmium titration of Zn-G65C, as shown in figure 3.26, absorbance at 250 nm increases and gradually resembles purified CdG65C, which indicates that

cadmium and thiols are interacting, cadmium is either binding to unoccupied cysteine residues or replacing zinc ions that are bound to G65C.
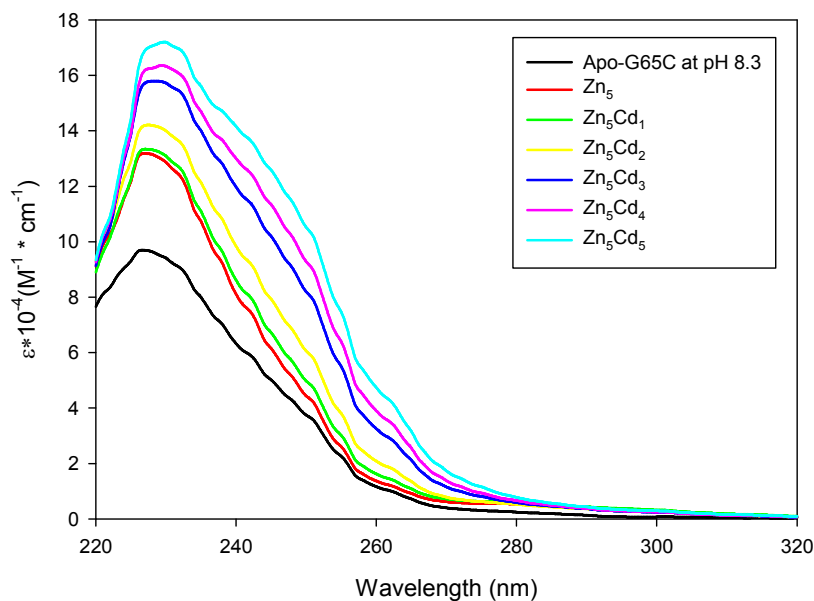
Figure 3.26: Changes in absorbance during cadmium titration of Zn_2-G65C (73.4 µM)

ICP-OES measurements showed that starting sample contained Zn_2G65C. The absorbance spectra of the first two cadmium increments do not show significant changes. After 3 mol equivalent cadmium addition, the shoulder at 250 nm becomes the dominant spectroscopic feature. Absorbance at 230 nm increases steadily with cadmium addition. These results are consistent with absorbance results from cadmium reconstitution experiments, as shown in figure 3.27.
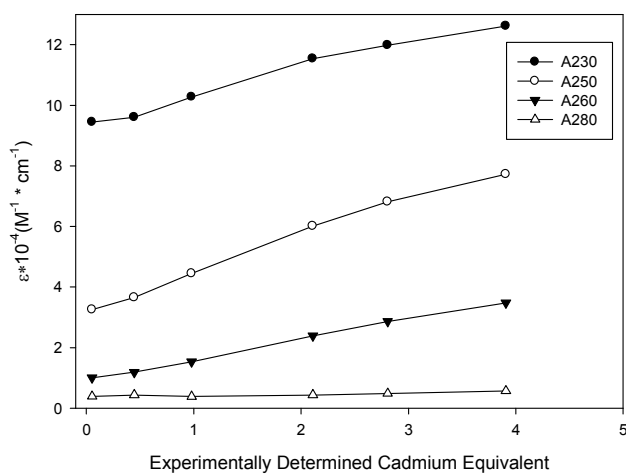
Figure 3.27: Absorbance changes due to cadmium titration. X axis represents experimentally determined cadmium content (with ICP-OES).

Figure 3.27 shows the increase in absorbance values at given wavelengths with respect to increased cadmium concentration. Starting point was Zn_2G65C and it was seen that as cadmium concentration was increased, absorbance profile shifts to higher values.

3.9.2. Changes in Ellipticity During Cadmium Titration of ZnG65C

CD spectra confirm the incorporation of cadmium ions, as shown in figure 3.28, which shows a red shift of the envelope between 210 nm and 230 nm. Molar ellipticity at 240 nm gradually increases, which is in alignment with cadmium reconstitution data.
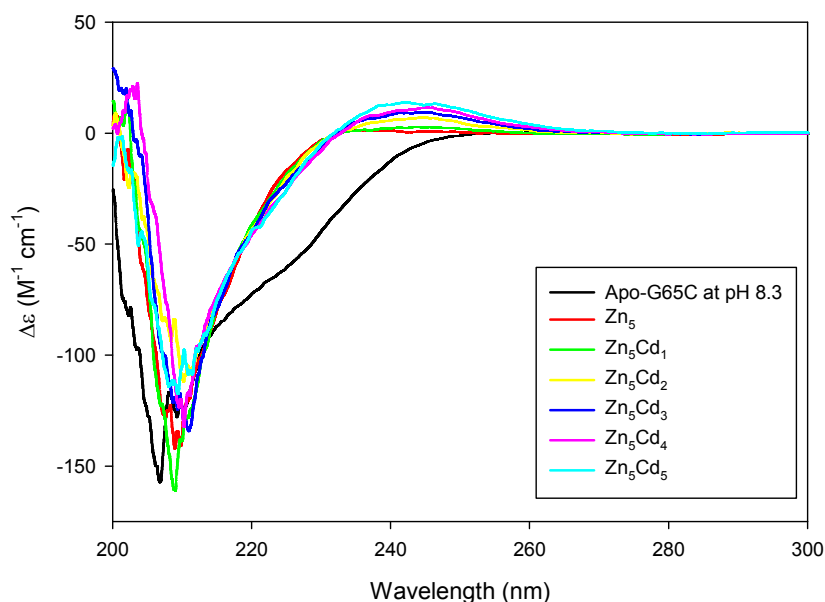
Figure 3.28: Changes in CD spectra during cadmium titration of Zn-G65C (73.4 µM).

CD results are concurrent with absorbance spectroscopy results. Titration of Zn_2G65C with cadmium allowed reproduction of spectropolarimetric features of reconstituted CdG65C. Addition of 3 mol equivalent cadmium shifts the ellipticity envelope between 210 and 230 nm to red, which is a feature also seen at cadmium titration of apo-G65C. Molar ellipticity at 250 nm gradually increases, due to LMCT between Cd and thiols.
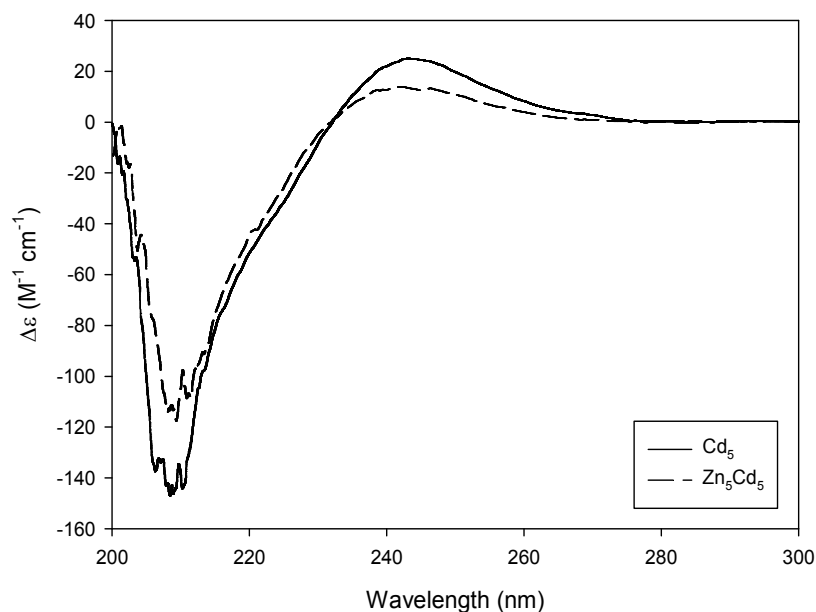
Figure 3.29: Comparison of 5 mol equivalent reconstituted G65C and cadmium titrated Zn-G65C.

Retention of one zinc ion can be detected by CD, especially when compared to cadmium reconstituted G65C. Figure 3.29 shows the comparison of 5 mol equivalent cadmium reconstituted G65C and Zn-G65C titrated with 5 mol equivalent cadmium. There are two differences amongst these spectra, one being blue shift of Zn_1Cd_3 between 210 and 230 nm, and the other being more intense envelope of $Cd_{3.5}G65C$ at 240 nm.

3.9.3. Metal Content Determination with ICP-OES

	[G65C] (µM)	[Zn^{++}] (µM)	Zn^{++}/G65C	[Cd^{++}] (µM)	Cd^{++}/G65C
Zn$_5$Cd$_1$	6.27E-05	0.000109	1.74E+00	2.62E-05	0.417±0.05
Zn$_5$Cd$_2$	6.27E-05	7.84E-05	1.25E+00	5.43E-05	0.866±0.2
Zn$_5$Cd$_3$	6.27E-05	7.14E-05	1.14E+00	9.93E-05	1.58±0.9
Zn$_5$Cd$_4$	6.27E-05	5.94E-05	9.47E-01	0.000131	2.09±1.2
Zn$_5$Cd$_5$	6.27E-05	5.72E-05	9.13E-01	0.000194	3.09±1.4

Table 3.6: Metal content determination and metal / protein ratio calculation of cadmium titration of Zn-G65C by cadmium.

As shown in table 3.6 it was confirmed that binding of cadmium occurs even in presence of zinc ions bound to G65C. Cadmium per protein ratio is consistent with cadmium reconstitution results (table 3.4) where 5 mol equivalent cadmium reconstituted G65C was found to bind 3.42±1.1 cadmium ions. It is possible to speculate that the remaining zinc ion does not hamper cadmium incorporation into G65C. Yet, even 5 mol equivalent cadmium addition was not sufficient to displace the last zinc ion.

3.10. pH Titration of Cadmium Reconstituted G65C

It is possible to titrate G65C with HCl in order to observe the release of metal ions by monitoring the changes in A$_{250}$ and ellipticity. These experiments were done on 5 mol equivalent cadmium reconstituted G65C, since purified G65C is shown to coordinate 5 cadmium ions by ICP-OES.

In order to facilitate adjustment of pH without significant change in protein concentration, G65C was in 6 mM Tris-HCl pH 8.3, instead of 30 mM Tris-HCl pH 8.3. Small increments of concentrated HCl were added and measurements were done. (See materials and methods section, table 2.5)

3.10.1. Changes in Absorbance Spectra During pH Titration of Cd-G65C

Metal binding capabilities of G65C are dependent on pH, and as pH was lowered as shown in figure 3.30, metal ions were released and the intensity of absorbance spectra decreased.
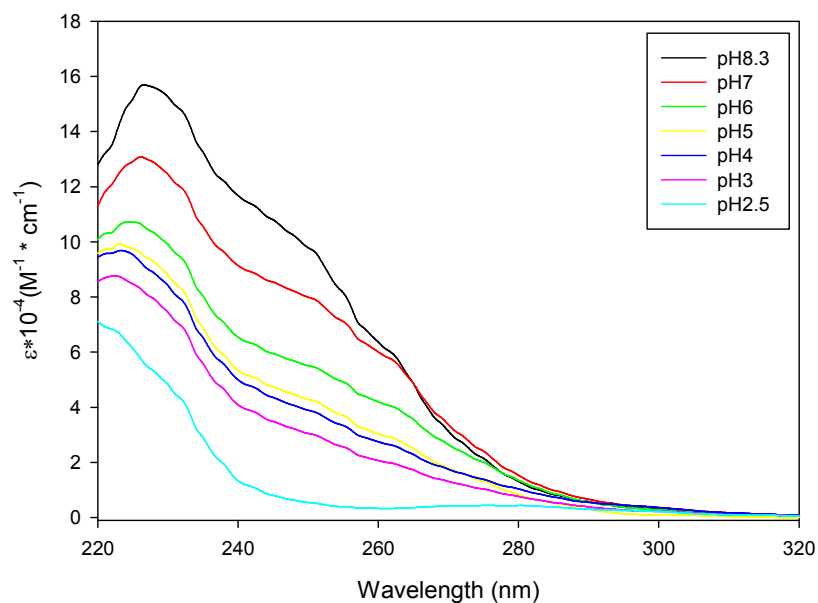
Figure 3.30: pH dependent metal ion release of 5 mol equivalent cadmium reconstituted G65C (samples were not treated with Chelex 100 resin).

It is not possible to determine how many cadmium ions are released by one unit drop in pH (see discussion). However, as shown in figure 3.31, at pH 2.5, all metal ions are released and A_{250} is reduced to 0, which is concurrent with apo-G65C absorbance.
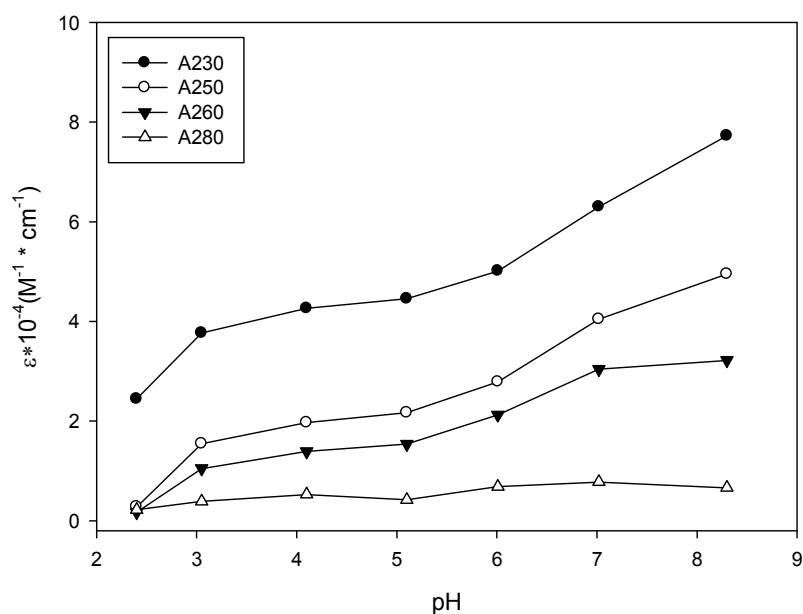
Figure 3.31: Changes in absorbance during pH titration.

Figure 3.31 confirms gradual decrease of absorbance in response to pH changes. It is seen that the biggest decreases occur in pH range of 8.3 to 5.1, which can be interpreted as major changes in backbone as well as loss of metal ions. Between pH 5.1 and 3, the rate of decrease is smaller. At pH 2.4, all metal ions are released and apo-G65C is obtained, which is confirmed by A_{250} values. Decrease in A_{250} shows depletion of Cd-S bonds. (See figure 3.33 for apo-G65C from column against apo-G65C obtained with titration.)

3.10.2. Changes in Ellipticity During pH Titration of Cd-G65C

Loss of metals was confirmed with CD measurements, once pH was dropped to 2.5, apo-G65C was obtained (figure 3.32). Most drastic change was seen between pH 7 and pH 6, which might be the indicator of protonation multiple cysteine residues, and loss of more than one cadmium ion.
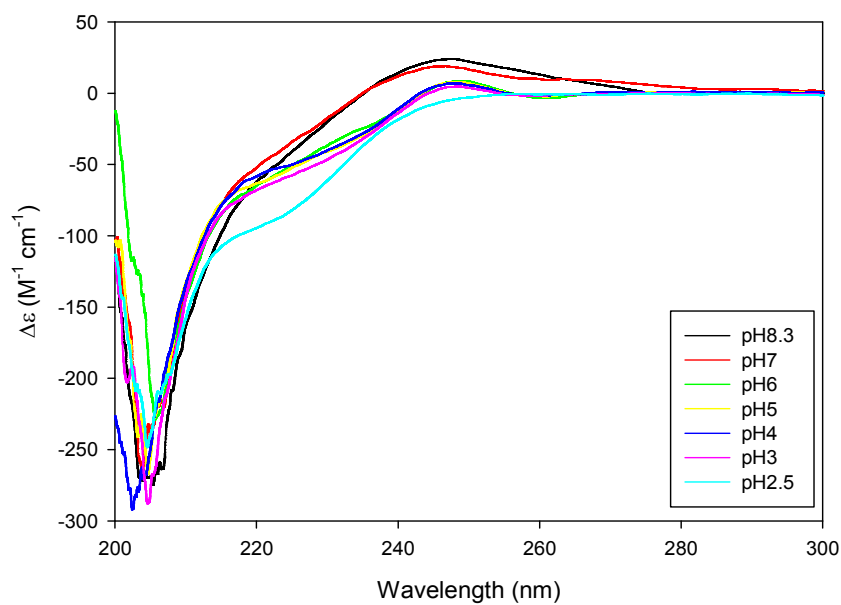
Figure 3.32: CD spectra showing changes in ellipticity during pH titration of 5 mol equivalent cadmium reconstituted G65C (50.6 µM).
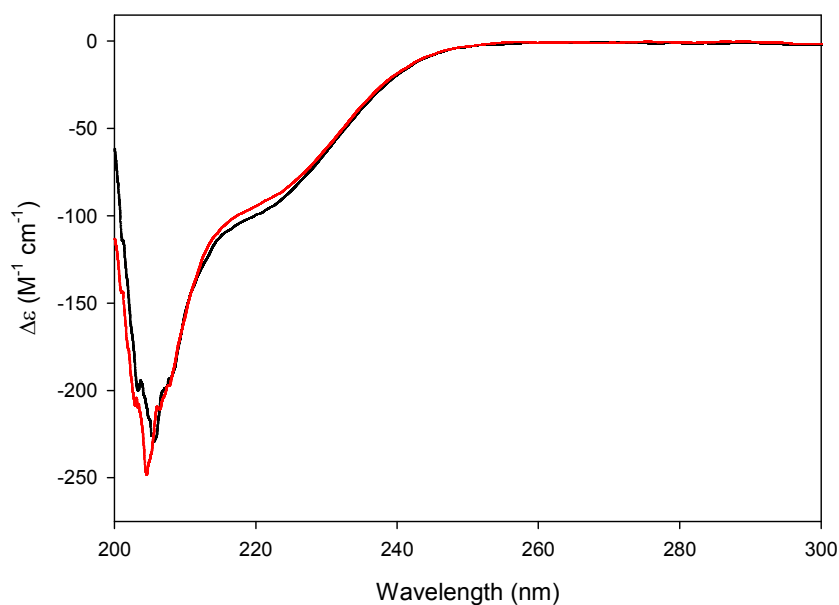
Figure 3.33: Comparison of CD spectra of apo-G65C obtained from size exclusion column (black line) and apo-G65C obtained by pH titration of reconstituted G65C (red line).

Figure 3.33 shows that apo-G65C that was eluted from SEC and apo-G65C obtained by pH titration are the same, only with a small difference at 220 nm, which is most likely caused by ~5mM Tris that is present in titrated sample.

Two points should be considered here, the difference between pH 7 and pH 6 in terms of ellipticity at 250 nm and the change of CD envelope at 230 nm. Changes are consistent with previous observations mentioned above on reconstitution experiments.

3.11. SDS and Native Polyacrylamide Gel Electrophoresis
3.11.1. SDS PAGE analysis

G65C samples were also analyzed with 12% SDS-PAGE to detect differences during reconstitution. As mentioned above holo-G65C migrates on SDS gels to a position which is approximately a dimer, above 18.4 kDa marker.
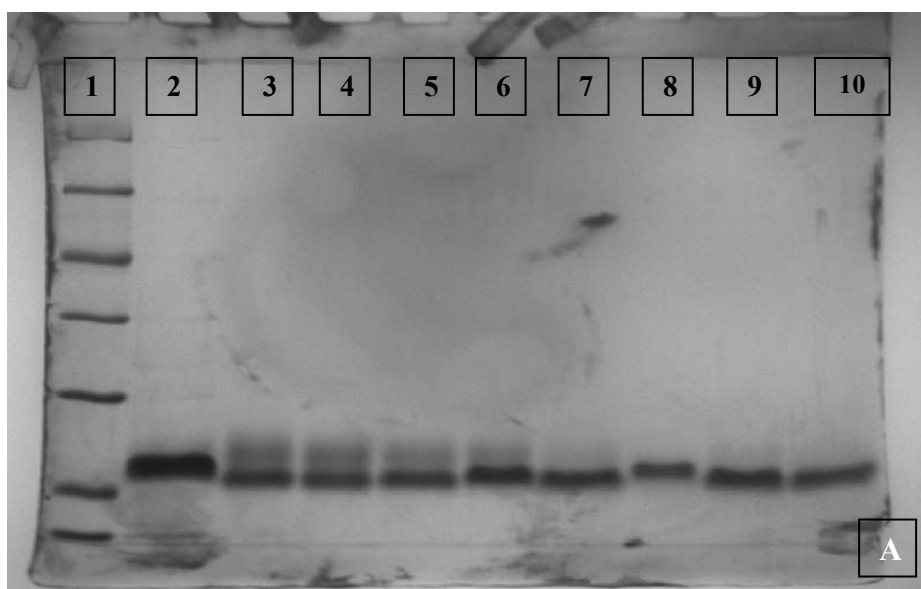
Figure 3.34 (A): 12% SDS PAGE analysis of holo- and apo-G65C with reconstituted samples.
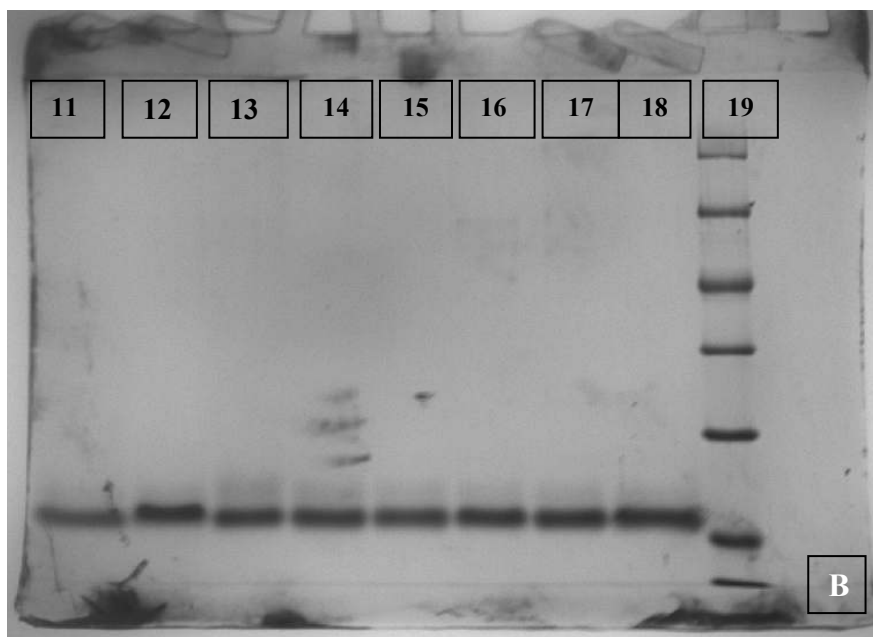
Figure 3.34 (B): 12% SDS PAGE analysis of reconstituted samples.

Lanes 1 and 19: Fermentas Unstained PMW Marker, Lane 2: Holo-G65C, Lane 3: Apo-G65C at pH 2.5, Lane 4: Apo-G65C at pH 8.3, Lane 5-12: 1 mol to 10 mol equivalent cadmium reconstituted G65C, Lane 13 5 mol equivalent zinc reconstituted G65C, Lane 14-18 titration of Zn-G65C with 1-5 mol equivalent cadmium.

Apo-G65C fractions migrate as two bands; one slightly above and other slightly below holo-G65C. The lower band is still above 14.4 kDa marker. During the reconstitution process, the top band disappears at 4 mol equivalent reconstituted G65C.

3.11.2. Native PAGE Analysis

To obtain further information about the conformation of the protein PAGE analyses were carried out under non-denaturing conditions. Figure 3.35 shows native PAGE analyses of holo- and apo-G65C at pH 2.5 and 8.3. Holo-G65C migrates faster than apo-G65C. Apo-G65C at pH 8.3 on the other hand, migrates slower than apo-G65C at pH 2.5. These results confirm the findings that there is a significant conformational difference between apo-G65C at the two pH values.
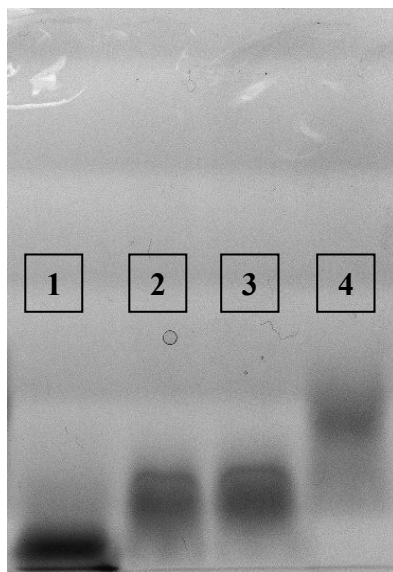
Figure 3.35: 8% Native PAGE analysis of holo- and apo-G65C.

Lane 1: holo-G65C, Lanes 2 and 3: two apo-G65C samples with different concentrations at pH 2.5, Lane 4: apo-G65C at pH 8.3.

It is seen that holo- and apo-G65C have different migration behaviour on native PAGE, which is caused most likely by changes in conformation.
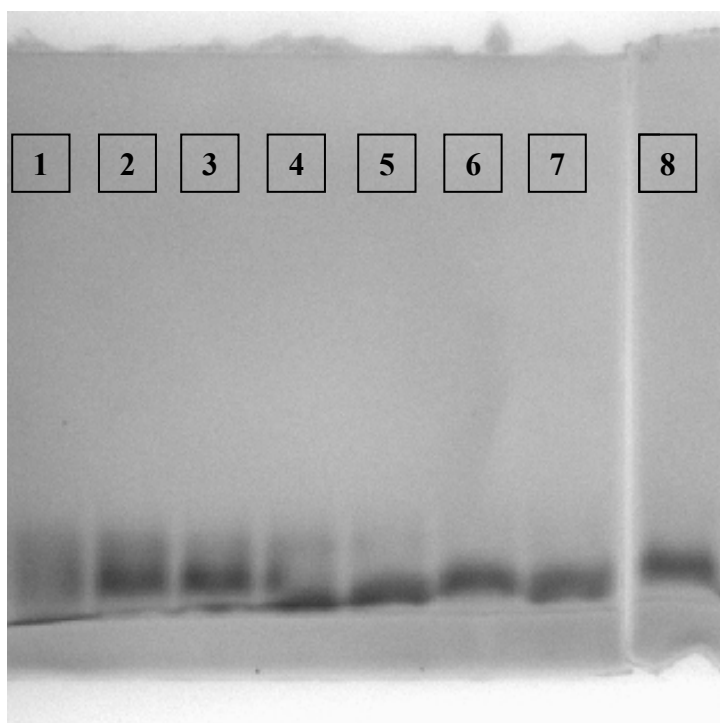
Figure 3.36: 8% Native PAGE results for cadmium reconstituted G65C.

Lanes 1 to 8 are 1 to 10 mol equivalent cadmium reconstituted G65C.

Figure 3.36 shows native PAGE analyses of cadmium reconstituted G65C, which has unusual migration behaviour, at least until 5 mol equivalent reconstituted sample. Before that point, the protein is visualized a broad band, which is likely to indicate dynamic state of protein conformation.

3.12. Small Angle X-Ray Scattering of G65C

SAXS analyses on holo- and apo-G65C were carried at EMBL Hamburg, X33 SAXS Beamline. The aim was to detect structural differences between holo- and apo-forms of G65C and develop structural models. Scattering profiles of holo- and apo-G65C are shown in figures 3.38 and 3.42. For correct evaluation of SAXS data, right concentration input is required and precise measurements with DTDP assays, helped avoid this problem. Structural parameters obtained from SAXS, given in table 3.7, reveal that apo-G65C is indeed more elongated than holo-G65C. Experimental molecular mass calculated from SAXS data for holo-G65C is 18 kDa, which closer to the dimeric molecular mass. On the other hand, calculated molecular mass for apo-G65C is 14 kDa, this value, lower than that of holo protein, is still larger than expected monomer molecular mass.

	Concentration (mg/ml)	R_g (nm)	I(0)	sR_g	d_{max} (nm)	Mass (kDa)
Holo-G65C	0.9	1.84±4%	15.62	0.519 – 1.272	6.5	18
Apo-G65C	0.6	2.84±19%	12.5	0.58 – 1.185	9	14

Table 3.7: Experimental data obtained from SAXS measurements. Standard deviation for radius of gyration is shown with ±. R_g: radius of gyration, I(0): intensity at s=0

Differences between compactness of proteins can be seen by comparing d_{max} values; which is 50% longer in apo-G65C, this also reflects on R_g values.

Since G65C is a rather small protein (~8 kDa) it is natural to have noisy data. Data quality is based on two criteria, one being the size of the particle and second is

concentration of measured sample. Since larger particles and dense solutions will scatter with higher intensity, they would have less noisy scattering patterns. For holo-G65C, better quality data were collected due to cadmium clusters at α and β domains and low-resolution models confirmed the presence of cadmium clusters. Data for apo-G65C on the other hand, is noisier as shown in figure 3.37
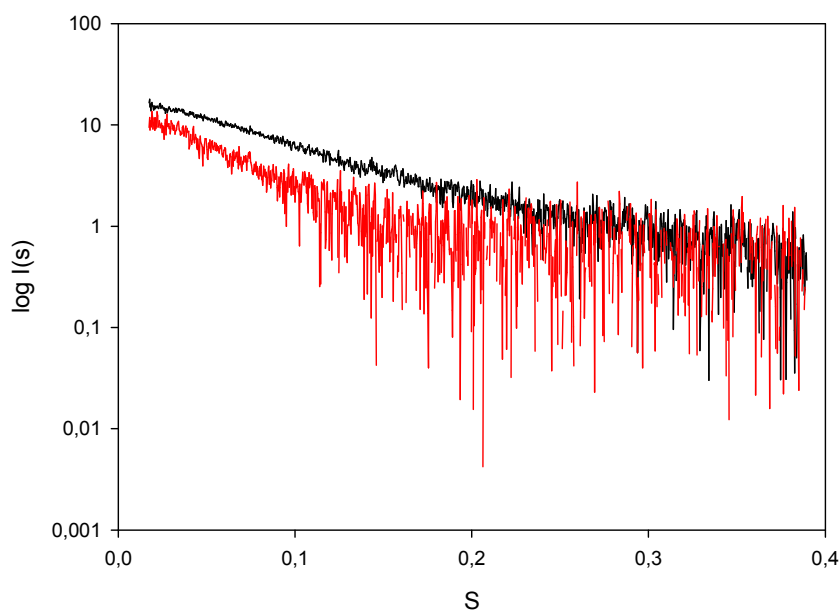
Figure 3.37: Scattering profiles of holo- (black) and apo-G65C (red) compared.

In addition to SEC results, SAXS data confirm that holo-G65C at 0.9 mg/ml concentration is in dimeric form in solution. Although this dimeric structure is disrupted when protein loses its metals, its structure becomes more extended and yields larger d_{max} and R_g.

3.12.1. *Ab initio* Modelling of Holo-G65C

Low resolution molecular shape envelopes were generated using GNOM output files in DAMMIN and GASBOR algorithms. GNOM algorithm produces inverse Fourier transform of the scattering data to obtain basic information about the shape envelope. Results of GNOM analyses for holo-G65C are shown in figures 3.38 and 3.39. In figure 3.38 the agreement between experimental data and the scattering from the shape model are compared and in figure 3.39 pair distribution function which yields the maximum distance (d_{max}), R_g and the asymmetry of the molecular shape is shown.

Holo-G65C was modelled using GASBOR and DAMMIN algorithms. 15 models were generated using GASBOR and 10 models were generated with DAMMIN. Convergence of the models was verified by DAMAVER algorithm and the minimum shape envelope that these models converged to was determined through a filtering process.
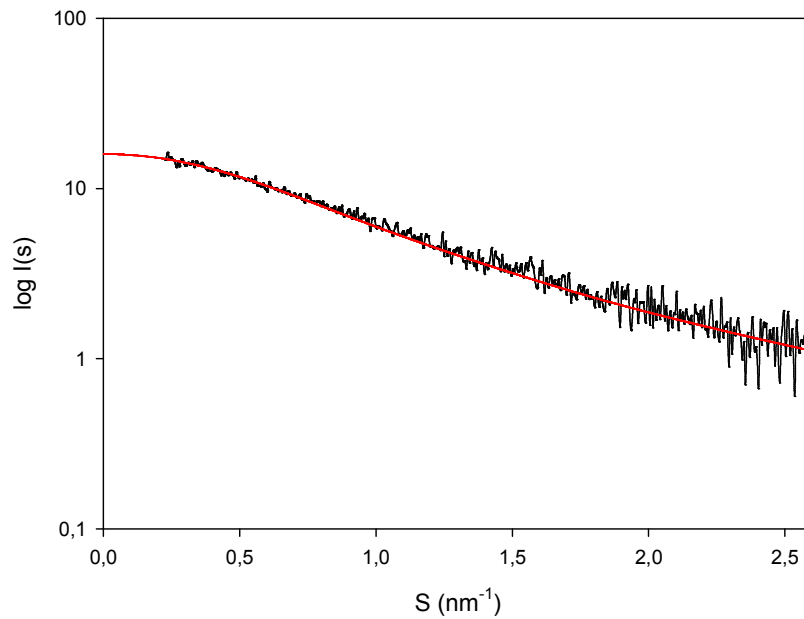
Figure 3.38: Comparison of holo-G65C SAXS data (black line) with theoretical scattering curve (red line).
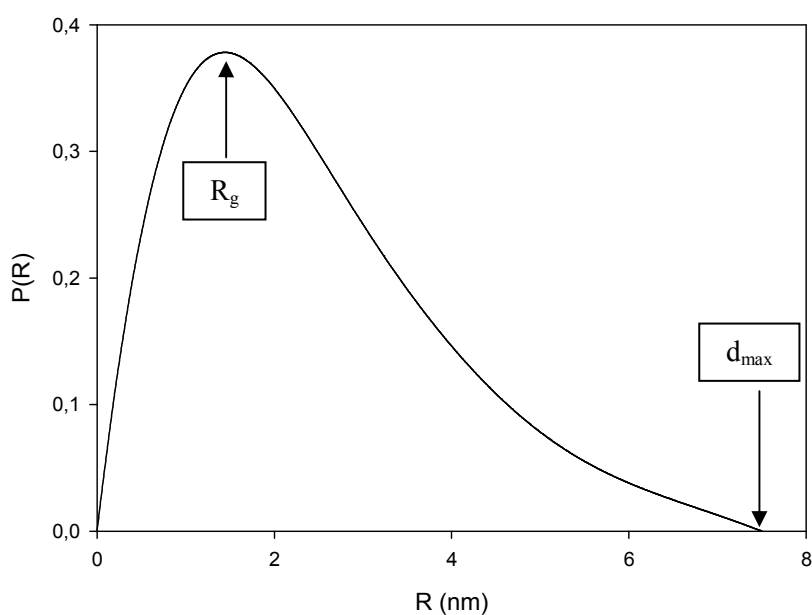
Figure 3.39: Pair distribution function of holo-G65C calculated by inverse Fourier transform by GNOM algorithm.

Pair distribution function (P(R)) was calculated by GNOM algorithm and the best agreement with experimental data was obtained when maximum distance (d_{max}) was set to be 8,5 nm. The shape of the P(R) curve indicates that the protein is elongated. Parameters obtained from GNOM are shown in table 3.8.

	Data Limits	d_{max} (nm)	R_g (nm)	I(0)
Holo-G65C (0.9 mg/ml)	55-955	7.5	1.85 ± 0.01	15.62

Table 3.8: Structural parameters used obtained from GNOM analysis for holo-G65C.

Intensity at 0 degrees (I(0)) is proportional to molecular mass. Interestingly, I(0) shows a mass of 15.62 kDa, which is almost the mass of a dimer (~16 kDa). This is yet another proof that G65C – if not totally dimeric – is in multimeric forms.

As explained above, scattering data is noisy, due to small size of protein and the complete range of data cannot be used for modelling. Data points 55 to 955 were chosen for calculation of P(R).
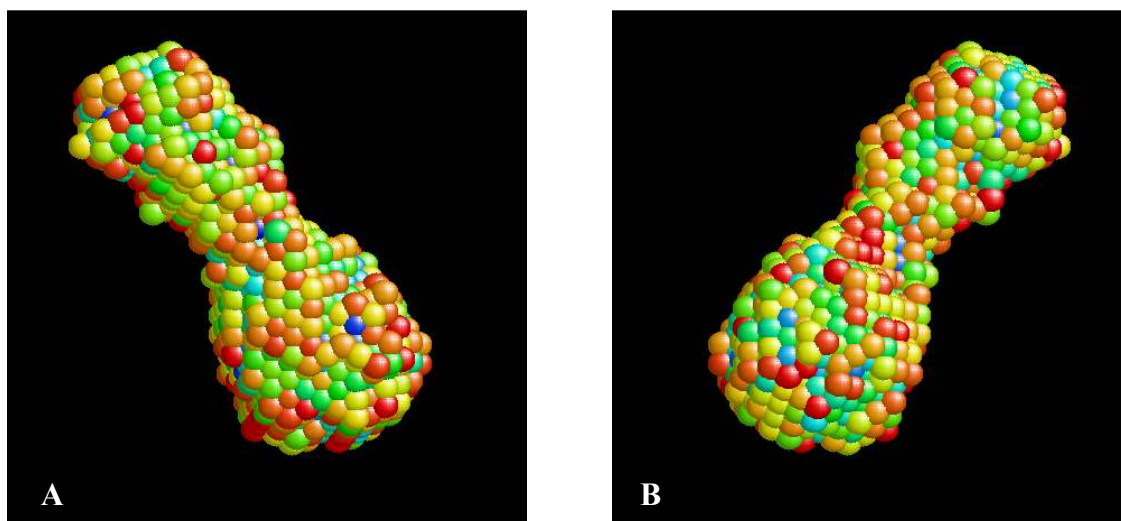
Figure 3.40: Low resolution molecular shape envelope models of holo-G65C generated via GASBOR algorithm. (B) was obtained by 180° rotating (A) around Y axis.
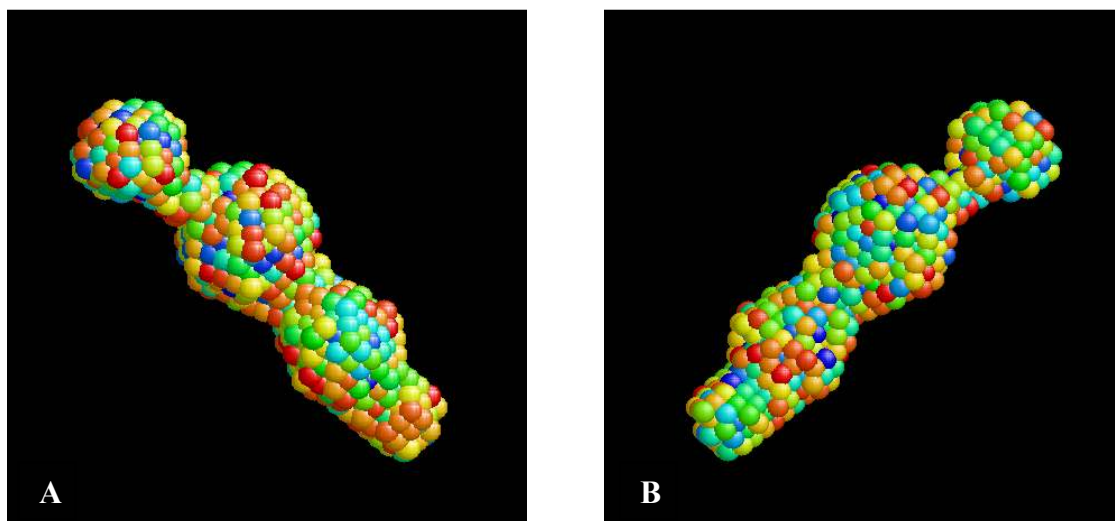
Figure 3.41: Low resolution molecular shape envelope models of holo-G65C generated via DAMMIN algorithm. (B) was obtained by 180° rotating (A) around Y axis.

Molecular shape envelope models shown in figures 3.40 and 3.41 have been generated by using P(R) function in figure 3.39. Length of the molecule is 5.8 nm according to GASBOR and 7.3 nm according to DAMMIN model. Cadmium clusters can be seen especially in GASBOR model, and one side of the model being bigger may mean unequal distribution of cadmium ions along cysteine motifs.

3.12.2. *Ab initio* Modelling of Apo-G65C

Holo-G65C is hard to model, mainly because of small size, but apo-G65C is even harder to model, due to lack of additional scattering from cadmium ions. Figure 3.37 shows the comparison of holo- and apo-G65C scattering data. Even though the curves are normalized according to concentration, the difference in the s range 0.05 to 2 nm^{-1} due to lack of cadmium at apo-G65C is obvious.

As can be seen from figure 3.42 apo-G65C has a noisier scattering curve. However, there are valid data points up to s=2.8 nm^{-1}, and this range was used to model apo-G65C. Not surprisingly, the value of R_g indicated a longer molecule when compared to holo-G65C (table 3.9). Based on this, P(R) function was calculated (figure 3.43) by setting d_{max} to 10 nm, while it was 8.5 for holo-G65C.
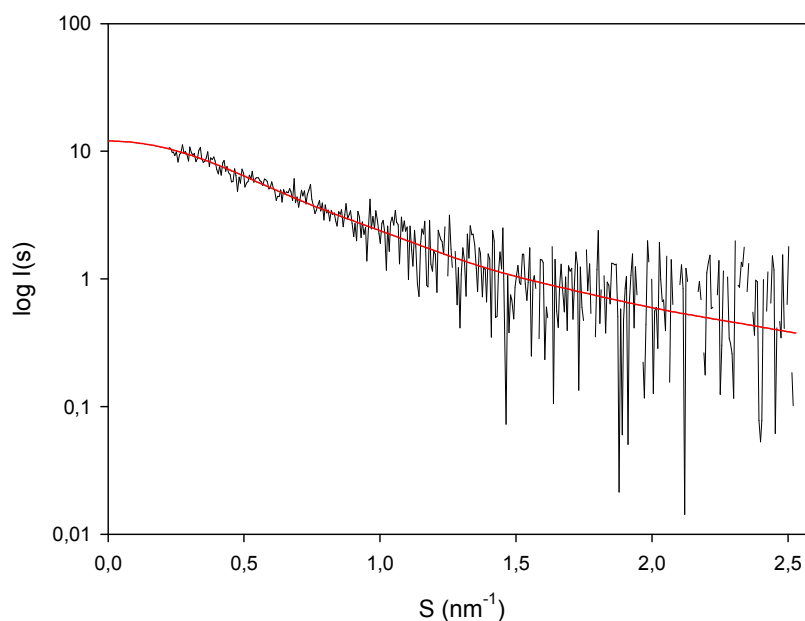
Figure 3.42: Comparison of apo-G65C SAXS data (black line) with theoretical scattering curve (red line).
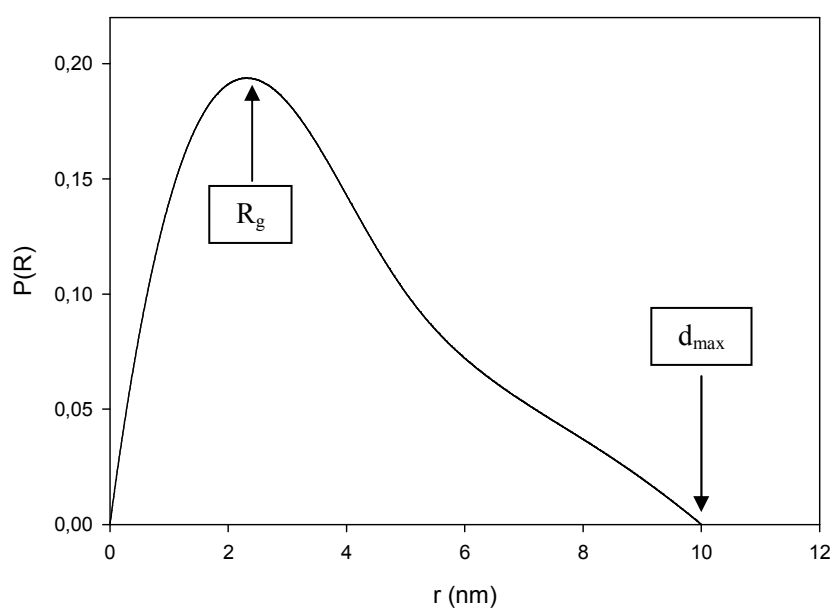
Figure 3.43: Pair distribution function of apo-G65C calculated by inverse Fourier transform by GNOM algorithm.

Pair distribution function (P(R)) was calculated by GNOM algorithm and the best agreement with experimental data was obtained when maximum distance (d_{max}) was set to be 10 nm. The shape of the P(R) curve indicates that the protein is elongated. Parameters obtained from GNOM are shown in table 3.9.

	Data Limits	d_{max} (nm)	R_g (nm)	I(0)
Apo-G65C (0.6 mg/ml)	50-1100	10	2.7 ± 0.05	12.2

Table 3.9: Structural parameters used obtained from GNOM analysis for apo-G65C.

One interesting point here is that apo-G65C is more elongated than holo-G65C (1.85 nm for holo- and 2.7 nm for apo-G65C) and in addition to that, mass calculated from scattering curve shows lower mass. Even though this is not a clear implication of monomerization, yet shows that apo-G65C is a smaller molecule in terms of mass. These values obtained from inverse Fourier transform analysis are in agreement with those obtained from scattering curves.
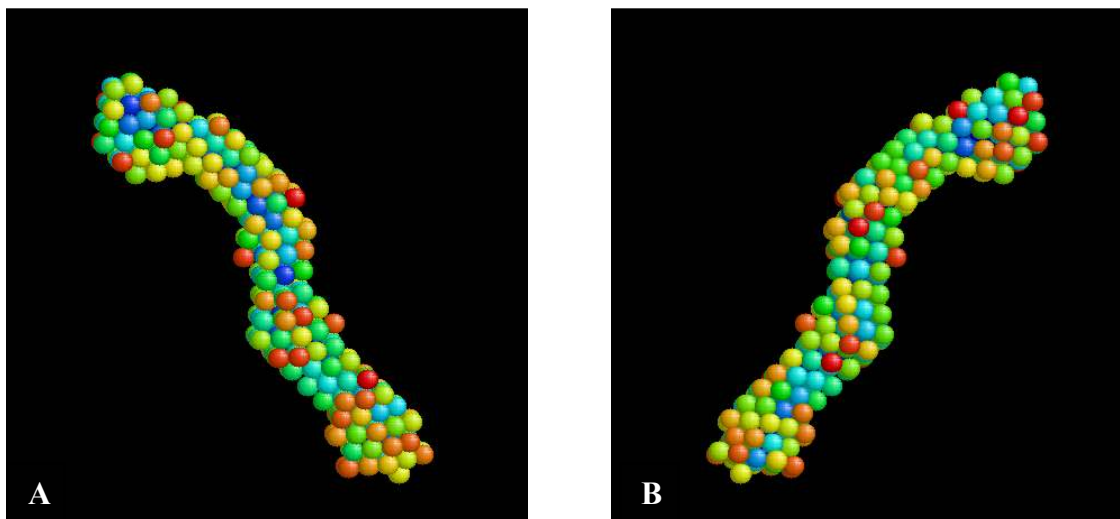
Figure 3.44: Low resolution molecular shape envelope models of apo-G65C generated via GASBOR algorithm. (B) was obtained by 180° rotating (A) around Y axis.
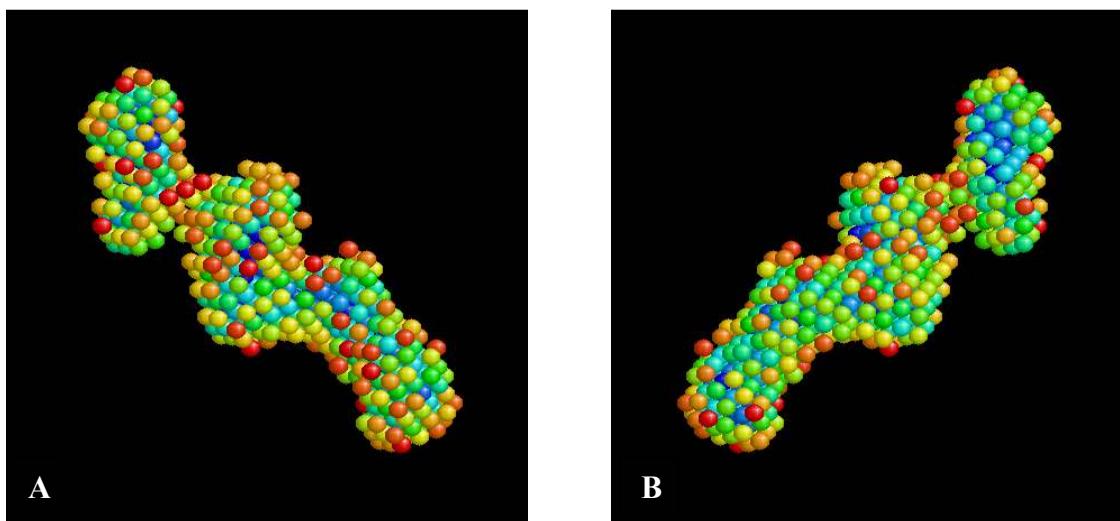
Figure 3.45: Low resolution molecular shape envelope models of apo-G65C generated via DAMMIN algorithm. (B) was obtained by 180° rotating (A) around Y axis.

Molecular shape envelope models shown in figures 3.44 and 3.45 have been generated using GASBOR and DAMMIN algorithms by P(R) function displayed in figure 3.43. Not surprisingly, the intense cadmium scattering is not present in apo-G65C models. Another notable fact is that 8.4 nm length is seen with the model obtained from GASBOR and 10.3 nm is seen from DAMMIN model, which confirms the theory that apo-G65C is a more elongated molecule than holo-G65C

3.13. Comparison of G65C with dMT

The aim of this project was to introduce a mammalian cysteine motif (C-X-C-C) to dMT and investigate the differences caused by this introduction.

3.13.1. Comparison of SEC Elution Profiles
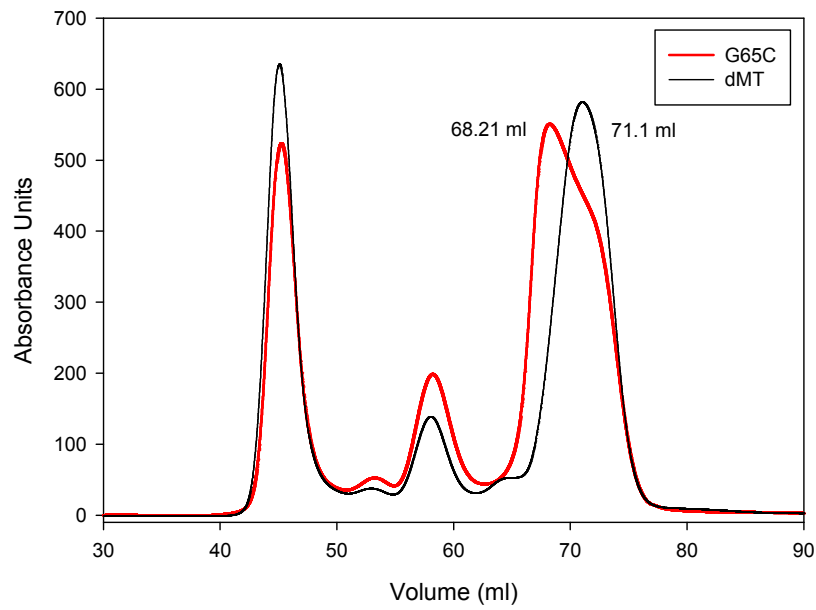
Figure 3.46: Comparison of size exclusion chromatograms of native dMT and G65C.

Elution profiles of dMT and G65C are compared, as shown in figure 3.46. Difference in elution volumes indicates size difference, 68.21 ml, corresponding to 23.5 kDa for G65C and 71.1 ml, corresponding to 19.3 kDa for dMT.

Another striking difference is that dMT peak is symmetrical, while G65C peak is asymmetrical and wider, indicating that polydispersity index is higher among G65C samples.
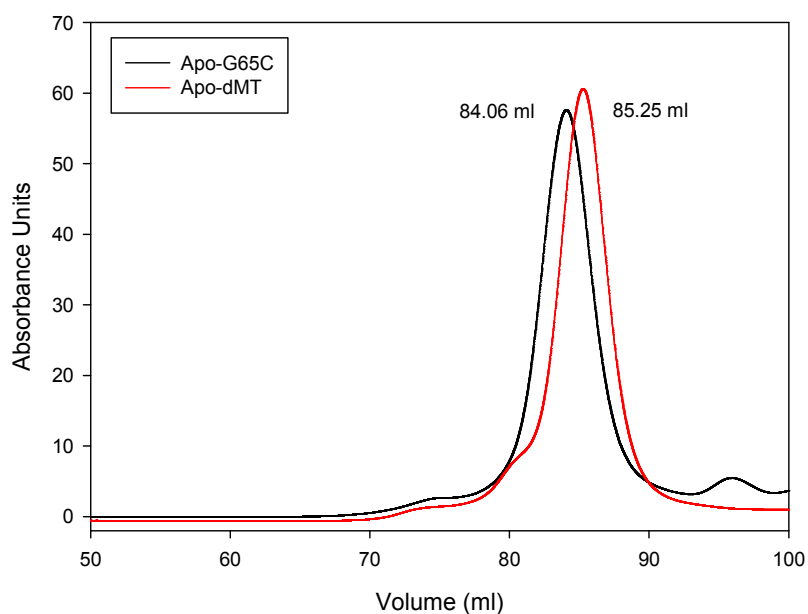
Figure 3.47: Comparison of size exclusion chromatograms of apo-dMT and apo-G65C.

The obvious difference of elution volumes that is seen in holo-protein elution cannot be seen at apo- state of both proteins (figure 3.47). Once dMT and G65C are stripped from their metals, the differences between elution volumes disappear. Both apo-proteins elute in symmetrical peaks, which indicates that there is dominant specie in protein solution. Molecular mass calculations show that apo-proteins both elute in monomeric form and calculated mass is 8 kDa for apo-G65C and 7.5 kDa for apo-dMT.

3.13.2. Comparison of CD Difference Spectra
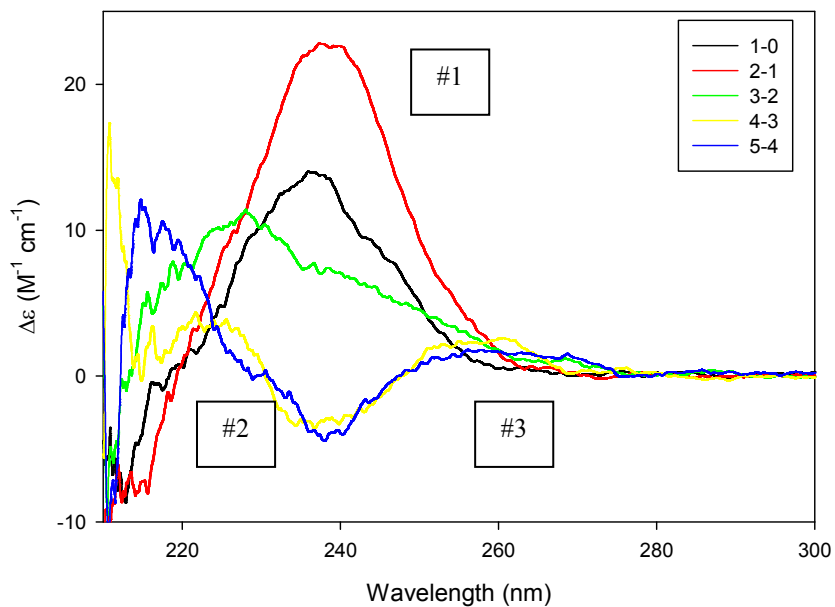
Figure 3.48: CD difference spectra of G65C for consecutive cadmium reconstitution measurements.
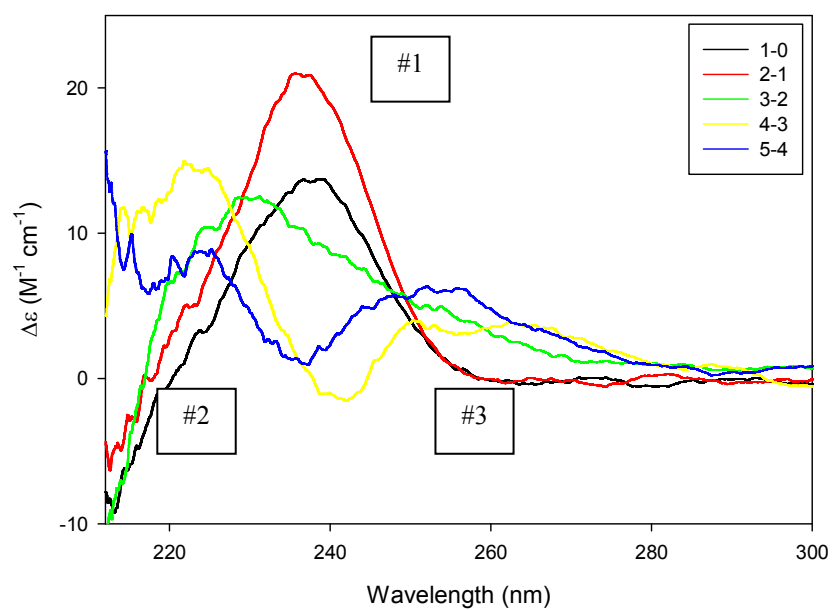
Figure 3.49: CD difference spectra of dMT for consecutive cadmium reconstitution measurements.

When figures 3.48 and 3.49 are compared, there is an obvious similarity. Largest difference is between 2 and 1 mol equivalent additions and between 3 and 2 mol equivalent additions. Upon 3 mol equivalent addition, peak #1 shifts to blue, however, G65C peak shifts broader, while dMT peak #1 begins to decrease at 220 nm. This can be caused by presence of an extra cysteine residue, which can be inducing bridging thiolates later in G65C (see discussion).

4 mol equivalent addition induces peak #2 and #3 formation in both proteins. The locations of peaks are similar for each, however, the intensity of peaks #2 and #3 for dMT are higher, which may be caused by extra bridging thiolate formation due to lack of a cysteine.

3.13.3. Comparison of Absorbance Changes During Cadmium Reconstitution

For G65C, it earlier was shown that increase in absorbance was not linear during cadmium reconstitution.
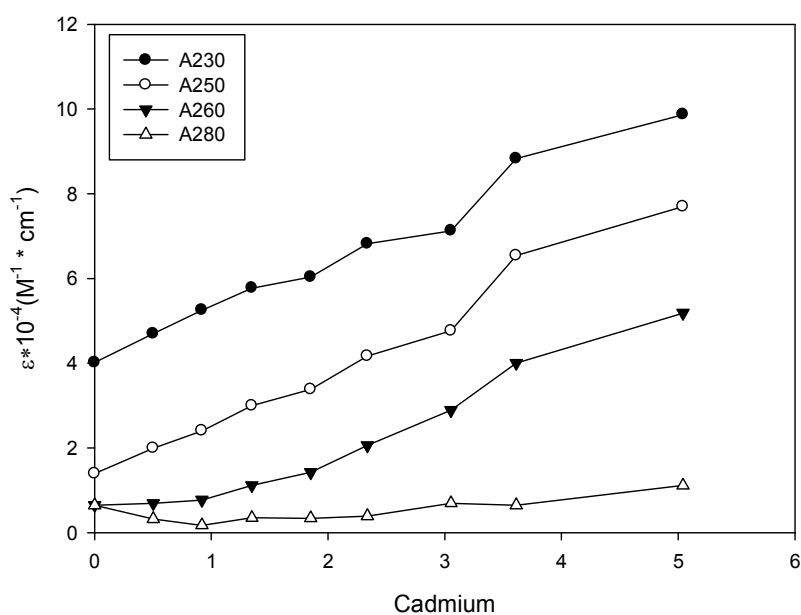
Figure 3.50: Changes in absorbance due to cadmium binding to G65C (1 mol equivalent increments). Y axis is molar absorbance and X axis is cadmium per protein, which was determined by ICP-OES after chelex treatment.
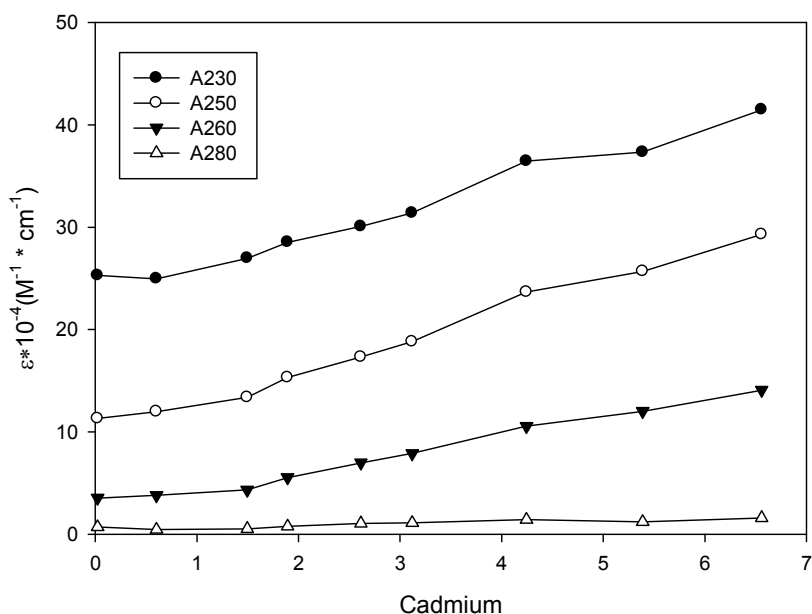
Figure 3.51: Changes in absorbance due to cadmium binding to dMT (1 mol equivalent increments). Y axis is molar absorbance and X axis is cadmium per protein, which was determined by ICP-OES after chelex treatment.

When figures 3.50 and 3.51 are observed, both G65C and dMT show nonlinear increases of absorbance during cadmium reconstitution. The steep increase between 6 and 8 mol equivalent additions seen in G65C is seen between 5 and 6 mol equivalent additions in dMT. This can be the effect of extra cysteine in G65C, while dMT starts bridging thiolates faster, G65C can use extra cysteine for terminal bonds and start bridging in later increments.

4. DISCUSSION

Since their discovery more than 50 years ago, a variety of functions have been assigned to MTs. They have been associated with heavy metal scavenging and chelating, oxidative stress response, development and senescence in plants (Freisinger 2008; Freisinger 2011) and MT3 in mammals was shown to be responsible for metal homeostasis in brain (Uchida *et al.* 1991). As explained in section 1.3.2., cys-motifs of MTs directly participate in metal binding and in type I plant MTs these are clustered in the N- and C- termini of the proteins. *Triticum durum* MT (dMT), identified in a cadmium tolerant wheat specie, is a type 1 plant MT with three domains; metal binding α (residues 1-19) and beta (residues 61-75) domains and a hinge region in between α and β domains (Bilecen *et al.* 2005).

Aims of the work presented in this thesis were (1) to modify a cysteine motif (GCSCG) of dMT in such a way that it resembles a motif found in α domain of vertebrate MTs (GCSCC) (2) to purify the mutant protein for biochemical and biophysical characterization (3) to investigate the effect of mutation in metal binding by dMT.

4.1. Expression and Purification of Holo-G65C

65th glycine of dMT was mutated to cysteine with site directed mutagenesis technique and the mutant was called G65C. cDNA sequence of G65C, confirming the mutation is given in appendix B. The same expression conditions for dMT work well for bacterial growth and overexpression of G65C. Purified recombinant protein yields are also similar, being 5 to 10 mg per 3 liter culture. Cadmium was included in growth media to facilitate folding and to stabilize expressed protein. This allows proper folding of G65C as the protein is synthesized and reduces the risk of aggregation or degradation. This is common practice in recombinant MT production and examples include, *Quercus suber* MT, for which bacterial cultures were grown with 0.5 mM CuSO$_4$ or 0.3 mM ZnCl$_2$ was used (Domenech *et al.* 2007) and *Cicer arietinum* MT for

which bacterial culture medium contained 0.4 mM CdCl2 or ZnCl2 (Freisinger 2009; Schicht *et al.* 2009).

So far all studies on biochemical and biophysical characterization of MTs were conducted on recombinant protein isolated from *E.coli* strains except for an early study on *Triticum aestivum* MT E_c-1, in which the native protein was isolated directly from the plant (Lane *et al.* 1987; Kawashima *et al.* 1992). Plant metallothioneins, especially their hinge domains, are sensitive to proteolytic degradation (Tommey, Shi et al. 1991). This problem is avoided by using *E.coli* strain BL21(DE3), that lacks proteases and by using a fusion/tag protein (Freisinger 2008). Overexpression of MTs in bacteria helps to avoid lengthy purification procedures and low yield that would be encountered if the protein was directly isolated from plants.

Tag proteins are used for detection and purification purposes and tags such as Glutathione S-Transferase (GST, GE Healthcare) or Intein (Freisinger 2009) also help stabilization of protein of interest. Histidine tags, on the other hand, are not preferred for expression of MT genes, since histidine is a metal coordinating amino acid and causes problems during both expression and purification. In this study, G65C was expressed as a GST fusion protein using pGEX4T-2 vector, in which GST is linked with G65C with a small flexible linker region (LVPRGS). GST is cleaved from protein of interest with thrombin and the target protein is readily separated using a GST affinity matrix.

G65C was purified in two principal steps which involve, affinity binding to Glutathione Sepharose matrix (GE Healthcare), followed by SEC of the cleaved G65C. Optimization studies show that 4-6 hours of binding to GST beads was sufficient, and 16 to 20 hours cleavage period increased overall G65C yield. Width and shape of G65C peak from size exclusion column shows that the recombinant protein peak contains multiple oligomeric forms. The range of molecular mass, calculated according to the elution volume, is 14.2 to 31.6 kDa. Assuming a molecular mass of 7.9 kDa, this range would include dimeric to tetrameric structures. Protein analysis on DLS data using Zetasizer software confirmed polydisperse state of holo-G65C (31% polydispersity index) and using the peak position of 2 nm for R_H a molecular mass of 17.9 kDa was calculated for the purified protein.

Taken together these results show that holo-G65C is purified in oligomeric forms. Presence of oligomeric forms of MTs have been previously observed (e.g. (Schicht and Freisinger 2009), however, their relevance to metal binding and structural studies has not been investigated. The elution profile of *Cicer arietinum* type 1 MT (Schicht and Freisinger 2009) (in exact same conditions as in this thesis) is almost the same as in figure 3.4, however, the protein is assumed to be in monomeric form and further studies are conducted without seriously considering polydispersity (Peroza and Freisinger 2007; Schicht and Freisinger 2009). A passing comment was made about possible effects of aggregates in form of protein-protein dimers and it was mentioned that this would require further studies. The polydispersity of holo-G65C preparations led us to conduct reconstitution studies only using apo-G65C which we had shown to be in monomeric form.

Holo-G65C was purified with ±5 cadmium ions. This metal content is the same observed for dMT. In earlier studies, it was seen that GSTG65C could coordinate 1 more cadmium ion than GSTdMT. Present work shows that this does not hold for the cleaved protein. It appears that the extra cysteine that is introduced in amino acid sequence has effect on bridging thiolates bonds, rather than incorporating one extra metal ion (see section 4.3.1.).

Another interesting point concerns electrophoretic behavior of recombinant G65C. Purified protein analyzed with SDS PAGE (figure 3.5) migrates above the 18.4 kDa band on molecular weight marker, while mass of a monomer is only 8 kDa. This may be due to three reasons; (1) anomalous SDS binding to the holo-protein due to the presence of metals, resulting in slow migration (Freisinger 2007; Peroza and Freisinger 2007; Schicht and Freisinger 2009) (2) oligomeric form of protein that cannot be disrupted by SDS and heat treatment (3) abundance of negatively charged residues. (pI of 4.44 and no disulfide bonds are made). Possibility (2) is unlikely to be valid, since this behavior is observed also under excessively reducing conditions and also with apo-G65C (see below). Validity of (1) or (3) are unresolved problems, but the most likely cause is insufficient SDS binding due to abundance of negatively charged residues.

4.2. Features of Apo-G65C

G65C was stripped from its metals for characterization studies, as explained in section 2.2.3.3. This is the first report in the literature where demetallated form of an MT is characterized in detail. In contrast to holo-G65C, the apo- form for which the absolute lack of metals was shown by ICP-OES, could be obtained in monomeric state (figure 3.9). This result is interpreted as metals inducing oligomerization. Metal induced dimerization of rabbit liver Cd_7MT were also observed in an early study (Palumaa *et al.* 1992). The molecular mass obtained from the elution volume of the peak (~84 ml), was 8 kDa – which corresponds to almost exactly the molecular mass calculated from the amino acid composition - while holo-G65C (~68 ml) calculations show about 23.5 kDa. Molecular mass calculations from DLS data concurred, indicating molecular mass of 9 kDa, which is a steep decrease from holo-G65Cs mass, which was 17.9 kDa. It is likely that bound metals induce oligomerization. The absolute lack of metals in apo-G65C was shown by ICP-OES.

Methods for determining concentration of MTs rely on reactivity of the sulfhydryl groups with reagents such as DTDP or DTNB. In reconstitution studies and for SAXS measurements, it was important to accurately determine the concentration of G65C. In this study, concentration of apo-G65Cs was either directly measured by DTDP assay experimentally or alternatively by an empirical method which was developed for quick estimation of concentration of holo protein. Previously, concentration was determined by another empirical method based on dMTs A_{250} values, and total S content (determined by ICP-OES) (Dede *et al.* 2007). Later this was shown to be an underestimation especially for G65C. DTDP assay has proven to be a fast and accurate way of measuring apo-G65C concentration.

Size distribution according to DLS measurements yields a peak at 2.4 nm for apo-G65C at pH 2.5. Although this is slightly larger than that for holo protein (2 nm) it is due not to the larger molecular mass, but arises from the extended shape of apo-G65C. This conclusion confirmed by the slower migration behavior of apo-G65C on native PAGE (figure 3.36).

It was aforementioned that holo-G65C has abnormal migration behavior on SDS PAGE, and same can be said for the demetallated form. SDS PAGE analyses of apo-

G65C on the other hand, a band below holo-G65C and overall smear. This behavior is no longer seen once Cd$_2$G65C complex was formed (see section 4.3.5 below).

4.2.1. Effect of Increasing pH on Apo-G65C Structural Features

Features of apo-G65C were also investigated at pH 8,3 which is the condition used for reconstitution experiments. The method generally used for reconstitution includes addition of metal ions to apoprotein and then increasing pH (e.g. (Serra-Batiste, Cols et al. 2010) (Vasák 1991)). In the work presented here, the procedure followed here is modified, and the pH is increased first and addition of metals follows. This has allowed the observation of backbone rearrangement due to pH changes.

The observation that the overall absorbance showed a significant increase upon pH increase led to studies on the effect of pH changes on a model peptide. Hexaglycine was used to study the behavior of protein backbone at pH 2.5 and 8.3. It was shown that increasing pH results in an increase of absorbance in general and in particular a peak at forms at 225 nm. The effect is also seen in CD spectra, the envelope between 225 and 232 nm is shifted to lower values and better defined peak is formed at 225 nm. Features of the absorption spectra below 230 nm are mainly due to the transitions in the peptide bond (Cantor *et al.* 1980). Under normal conditions (neutral pH), the amide electron in the polypeptide chain can be delocalized resulting in the -trans or -cis conformations. The changes in hexaglycine spectra show that when the pH is lowered, protonation of the amide groups result in a more rigid structure locking the conformation to the all-trans form. The protonated atoms are held as far away from each other as possible. When the pH is raised, the flexible structure allows for transitions and the absorption is increased. This effect already observed in the six amino acid long peptide is more pronounced in G65C, which is 81 amino acids long (figure 3.14 and 3.15).

In DLS measurements, decreasing pH (to pH 2.5 from 8.3) results in a more narrow intensity size distribution peak This also can be interpreted as a decrease in polydispersity, and establishment of a more rigid structure.

Conformational change of apo-G65C at pH 8.3 was detected also with native PAGE. At higher pH apo-G65C migrates slower and was visualized as smear, while pH 2.5 sample migrated as a more homogeneous band. These results are consistent with

DLS measurements, and show that pH 8.3 apo-G65C is more polydisperse than at pH 2.5.

4.3. Cadmium and Zinc Complexes of G65C

Spectroscopic studies on reconstitution of apo-G65c and release of metals with pH decrease provide insights on the mechanisms of metal binding and possible functions of these proteins. Although MTs lack strong secondary structure elements, spectral features change due to alterations in the conformation of peptide backbone and establishment of S-Me bonds.

4.3.1. Cadmium Reconstitution of G65C

Lack of secondary structure elements observed in other plant MTs (Domenech, Orihuela et al. 2007; Freisinger 2007; Peroza and Freisinger 2007; Schicht and Freisinger 2009) is also the case with G65C.

In most of the cadmium reconstitution work on plant MTs reported in the literature, the process is monitored by following absorbance changes (Domenech, Orihuela et al. 2007; Freisinger 2007; Peroza and Freisinger 2007; Peroza, Kaabi et al. 2009; Peroza, Schmucki et al. 2009; Schicht and Freisinger 2009; Wan *et al.* 2009; Loebus *et al.* 2011). It is reported in these studies that a monotone increase in absorbance profile and the 250 nm Cd-S bonds are observed until the saturation at 5 mol cadmium equivalents.

In reconstitution studies on mammalian MTs on the other hand, the process is followed by CD as well as absorbance measurements. Difference spectra plots allow the monitoring of nature of coordination for metal ions and interpreted in terms of formation of terminal and bridging thiolate bonds. The Me_3Cys_9 and Me_5Cys_{12} stoichiometries for mammalian MT beta and alpha domains, respectively were later confirmed by NMR (Schultze *et al.* 1988) and X-Ray crystallography (Robbins *et al.* 1991) structures and the metal clusters were shown to have tetrahedral-tetrathiolate coordination. The 3D structures and the overall stoichiometry of 2.6 S/Cd ion are indicators for the presence of bridging cysteins as well as those that are involved in terminal coordination and that the folding process may not take place in a linear fashion.

Rat liver MTs α domain which has Me_5Cys_{12} stoichiometry is similar to G65C, in which the stoichiometry is Me_5Cys_{13} (Stillman *et al.* 1987). During cadmium titration of apo-α-rMT, it was seen that the difference spectra shows a single band intensity profile increasing at 246 nm until Cd_3-rMT is obtained. Further cadmium addition resulted in development of new bands between 228 and 240 nm and at 260 nm, which resulted in biphasic difference CD spectra. A biphasic CD difference spectrum was also reported for rabbit liver MT, where new bands developed upon addition of cadmium ions beyond 3.3 mol equivalent (Willner *et al.* 1987). Both of the described studies report biphasic CD spectra occurring after thiol:metal ratio falls below 4. This feature is explained as arising from terminal thiolates being converted to bridging thiolates to accommodate more metals.

Reconstitution studies of MTs are generally monitored by absorbance and CD measurements. Although the protein lacks secondary structure elements, spectral features change due to alterations in the conformation of peptide backbone and establishment of Cd-S bonds. CD analyses showed that apo-G65C lacked any secondary structure elements and had a similar spectrum to native dMT. During reconstitution studies, apo-G65C was stepwise titrated with cadmium up to 10 mol equivalents. Biggest spectroscopic change occurred when 2 mol equivalents cadmium were added. This observation was confirmed in reconstitution studies with half mol equivalents. Changes during reconstitution are better detected when difference ellipticity spectra are examined (figures 3.21, 3.22 and 3.23).

In G65C CD difference spectra, biggest spectroscopic change occurs when 2 mol equivalent cadmium is added (figures 3.21 – 3.23). The biphasic behavior is observed when the thiol:metal ratio is below 4, showing the formation of bridging thiolates similar to rat liver MT. Studies where reconstitution was continued beyond this point, CD profiles changed very little or at higher ratios significant intensity loss occurred. This indicates that beyond the ratio of 2,6 for S:Cd either structural features (e.g. separate α and β domains) are lost or nonspecific aggregation occurs.

CD profile was almost unaffected by the binding of 5th and 6th cadmiums (6 to 10 mol equivalent additions), which can be partially explained by supermetallation. Mammalian MTs have been shown to have supermetallation ability, in which MT binds

1 or 2 extra metal ions, for the price of losing secondary structure elements (Sutherland, Willans et al. 2010; Sutherland and Stillman 2011). Even though there is no significant change in G65C CD spectra at excessive cadmium addition, bound metal quantity increases up to 5.6.

Monitoring of reconstitution by following changes in absorbance at 250 nm against bound cadmium shows that binding of metals do not follow a linear fashion. Between 3 – 4 mol equivalent additions and 6 – 8 mol additions, the increase in absorbances were not as much as the rest, which can be interpreted as formation of bridging thiolates, since double peak formation in CD difference spectra started between 3 and 4 mol equivalent addition and formation of two separate clusters. 6 and 8 mol equivalent additions also are another point of "turn" in ellipticity, which may be the spot where secondary structure is lost or no longer changes.

4.3.2. Zinc Reconstitution of G65C and Replacement of Zinc by Cadmium

Zn-S interactions are not easy to detect because zinc is a d^{10} metal with no outer shell unpaired electrons. The changes can be observed through A_{230} at absorbance spectra and with increase in ellipticity envelope at 235 nm. This is in accordance with results of (Serra-Batiste, Cols et al. 2010). Lower affinity of thiols for zinc was also demonstrated by ICP-OES measurements. Even when an excess amount − 5 mol equivalents - of zinc was added, the specie that resulted was Zn_2G65C (after chelex treatment).

Zn_2G65C was used to inspect metal preferences of G65C. As expected, thiols had more affinity for cadmium than zinc and occupied all available cysteines that zinc could not was occupied by cadmium. However, even at excess cadmium concentrations, G65C kept one zinc atom and the species obtained was Cd_3Zn_1G65C. This was also seen at recombinant *Caenorhabditis elegans* MT, at excess concentrations, they report they found Cd_6Zn_1-CeMT (Bofill *et al.* 2009).

4.3.3. pH Stability of Cd$_{3.5}$G65C Cluster

Cadmium reconstituted G65C was subjected to pH titration experiments, to gain further insight about metal binding/releasing process. As pH was gradually decreased, intensity at 230 nm and 250 nm decreased and at pH 2.5, it completely disappeared, recreating in apo-G65C spectra. Judging by changes at ellipticity, it can be speculated that Cd$_{3.5}$-G65C loses a metal between pH 8 and 7, then loses one (or more) between pH 7 and 6, whereas remaining metals are removed in the narrow range between pH 5 to 2.5. Previously, it was speculated that Cd-S interactions require backbone rearrangement, and the intensity decrease in the envelope between 210 to 230 nm indicate the change is taking place. Taken together with all previous results, it is proven that metal-thiol interactions are reversible and rely on peptide backbone alterations.

Previous reports also indicate that release of multiple cadmiums in a narrow range, generally between pH 4.5 and pH 2 (Peroza and Freisinger 2007; Schicht and Freisinger 2009). The results presented here are in alignment with literature.

4.3.4. PAGE Analyses of Reconstituted G65C

As mentioned above, the only PAGE analyses for MTs that are reported in the literature are conducted under denaturing and highly reducing conditions. In addition to that, no results for apo-MTs are available. In this thesis G65C is analyzed by both native and SDS PAGE.

Behavior of protein on native PAGE is expected to be a reflection of their conformation and for G65C changes in conformation during reconstitution are easily seen in native PAGE analysis. It can be speculated that the unfolded structure of apo-G65C changes significantly by addition of 5 mol equivalent cadmium – that corresponds to 3.6 Cd/G65C or 3.61 thiol:metal ratio. This result indicates that migration behavior of G65C is dependent on metal. The main evidence behind this claim is migration behavior of apo-G65C, which can only be visualized as smear. Reconstituted samples were visualized by native PAGE as smear and slight double bands until 5 mol equivalent addition – which corresponds to ~3.6 Cd/G65C, so it can be speculated that migration behavior of G65C is dependent on metal. The main

evidence behind this claim is migration behavior of apo-G65C, where it can only be visualized as smear - or slight double bands – on native PAGE.

4.4. SAXS Based Shape Models of Holo- and Apo-G65C

Structural studies on MTs are hindered by difficulties in crystallization of the proteins and the lack of secondary structure elements. Lack of access to NMR machines led investigation of the shape envelope of G65C by SAXS. However it has to be mentioned that SAXS is not an ideal technique for structural investigations on G65C due to low molecular mass of the protein and its propensity to aggregation at high levels of protein concentration. Another complication is due to the excess scattering from cadmium ion; methods for data reduction and calculation of *ab initio* shape models do not take into account a structure that lacks secondary structure elements and metal clusters whose structures are not well established. The contribution of cadmium to scattering was confirmed when apo- data was subtracted from holo-G65C data, resulting in a peak in s range from 0.1 to 1.5. Therefore, it can be concluded that results and models reported in this thesis on apo-G65C are more reliable than those obtained for holo-G65C. The structural parameters (tables 3.8 and 3.9) and models obtained (figures 3.44 and 3.45) support the conclusion that apo-G65C has an extended asymmetric structure and this structure is compacted upon binding metals.

It can be speculated that the shape model obtained for holo-G65C is consistent with a two-metal cluster shape, in which clusters are expected to be asymmetric.

This is in contrast with a model of single cluster proposed by (Wan and Freisinger 2009), in which the model is based on limited proteolytic digestion. It was shown that cleaved CicMT eluted as a single peak in SEC, which led to the single cluster model.

4.5. Comparison of Mutant G65C and Native dMT

Introduction of a cysteine residue for a glycine might cause problems during protein expression and folding, because of chemical differences between these residues. However results reported in this thesis show that, no problems were encountered during expression, purification and according to ICP-OES measurements, during folding.

On the other hand, biochemical and biophysical features of dMT differ from G65C. Looking at SEC profiles, it can be said that G65C elutes in a more polydisperse fashion. G65C peak is asymmetrical and wider than dMT peak, which confirms this suggestion (figure 3.46). Molecular mass calculated for top of the peaks indicate difference, 23.5 kDa for G65C and 19.4 kDa for dMT. The 4 kDa difference between G65C and dMT is caused by the introduced cysteine, which can be causing folding differences and /or inducing oligomerization. This difference is eliminated on SDS PAGE, where G65C migrates as dMT, right above 18.4 kDa marker. Molecular mass calculated from elution profiles are same when both proteins are demetallated, dropping to ~8 kDa. Monomerization upon demetallation is a common feature for both species.

The CD difference spectra show another striking difference between G65C and dMT. Both proteins show biphasic CD difference profiles upon binding of cadmium beyond Cd_3-MT species. However, the intensity of spectrum are higher for dMT, which is caused by higher bridging / terminal thiolate ratio compared to G65C. Due to its increased cysteine quantity, G65C can start bridging thiolate formation later on from dMT and this reflects on difference CD spectra as lower intensity biphasic profile.

Finally, it is interesting to note that the fusion protein GSTG65C was found to bind 1 more cadmium ion than GSTdMT. When GST tag was cleaved, this attribute has perished, equalizing Cd/protein ratio at ~5.5. Cadmium binding properties of G65C was compared with dMT during cadmium reconstitution, in which they both do not follow a linear fashion. Surprisingly G65C reaches a saturation point at ~5.6 Cd/G65C, while it appears that there is no clear point of saturation for dMT. However, it should be remembered that these values have been obtained with ICP-OES after Chelex 100 resin treatment, so any loosely bound cadmium ions can be taken away. Chelex 100 treatment can have different effect on G65C and dMT, since it was shown with difference spectra that G65C starts coordinating cadmium ions with bridging thiolates later than dMT.

5. CONCLUSION and FUTURE WORKS

In this thesis, it was shown that the mutant G65C can be stably synthesized in *E. coli* and the recombinant protein can be purified as a complex with 5 Cd^{2+} ions.

The purified Cd_5G65C solutions are polydisperse with multiple oligomeric forms (dimers to tetramers according to MW calculations) co-exist.

It is shown that apo-G65C has a more elongated / extended structure than holo-G65C, which is linked to unwinding of peptide backbone due to loss of metal ions.

Demetallated G65C can be obtained in monomeric state for reconstitution studies for structural changes upon metallation. Conversion of terminal thiolates to bridging thiolates was shown with cadmium reconstitution studies. Lower affinity for zinc than cadmium was confirmed during loading of apo-G65C with zinc and ICP-OES. Even at excess zinc concentration, the specie obtained was Zn_2G65C. Interestingly, titration of Zn_2G65C species with Cd^{2+} resulted in $Cd_{3.5}Zn_1G65C$, retention of a zinc ion is a previously reported issue and the most likely cause is that the zinc ion is kinetically trapped. Cd5G65C metal-thiol is a stable core, which was seen during pH titration. Release of metals occurs in a rather narrow pH range (4.5 to 2.5) and it was confirmed that metallation and demetallation is a reversible process.

By a combination of biophysical techniques (UV-Vis absorbance, CD, DLS, SAXS and native PAGE), it was shown that the folding process takes place in a nonlinear fashion with transitions at 3 and 5 metals per G65C.

Experimental evidence shows that transitions occur with the formation of bridging thiolates to coordinate metal ions. It is possible to speculate that this evidence supports the formation of two metal clusters, which was seen at low resolution molecular shape envelopes.

SAXS data is in agreement with DLS and native PAGE results, concluding that apo-G65C is a more extended molecule than holo-G65C.

Comparison of metal-binding features of G65C with native dMT indicates that the introduced mutation does not affect metal-binding properties. However, the oligomerization behavior and structural features of the mutant are changed. The

introduced cysteine delays the formation of bridging thiolates, due to one extra terminal bond available.

Future Works

The double cluster formation seen in models generated with SAXS data can be checked with limited digestion by proteinase K, as done in (Wan and Freisinger 2009). Further evidence towards cluster can be gained.

Properties of hinge region can be further characterized. The changes occurring in hinge region during metal binding is inevitable and needs to be studied.

Elaboration of zinc and other metal binding, as well as affinity studies towards different metals would provide a broader perspective in metal-binding mechanism of G65C. Zinc binding mechanism can be further studied to free the kinetically trapped zinc ion.

Metal-binding of previously produced other single mutants (G8C, G12C and G61C) can be studied. By this, the importance of positioning of the introduced cysteine can be determined. It is a known fact that both quantity and placement of motifs are important in metal coordination.

Andreini, C., L. Banci, I. Bertini and A. Rosato (2006). "Zinc through the three domains of life." J Proteome Res 5(11): 3173-3178.

Andrews, G. K. (2000). "Regulation of metallothionein gene expression by oxidative stress and metal ions." Biochem Pharmacol 59(1): 95-104.

Bilecen, K., U. H. Ozturk, A. D. Duru, T. Sutlu, M. V. Petoukhov, D. I. Svergun, M. H. Koch, U. O. Sezerman, I. Cakmak and Z. Sayers (2005). "Triticum durum metallothionein. Isolation of the gene and structural characterization of the protein using solution scattering and molecular modeling." J Biol Chem 280(14): 13701-13711.

Bilecen, K., U. H. Ozturk, A. D. Duru, T. Sutlu, M. V. Petoukhov, D. I. Svergun, M. H. J. Koch, U. O. Sezerman, I. Cakmak and Z. Sayers (2005). "Triticum durum Metallothionein." Journal of Biological Chemistry 280(14): 13701-13711.

Blindauer, C. A., M. D. Harrison, J. A. Parkinson, A. K. Robinson, J. S. Cavet, N. J. Robinson and P. J. Sadler (2001). "A metallothionein containing a zinc finger within a four-metal cluster protects a bacterium from zinc toxicity." Proc Natl Acad Sci U S A 98(17): 9593-9598.

Bofill, R., R. Orihuela, M. Romagosa, J. Domenech, S. Atrian and M. Capdevila (2009). "Caenorhabditis elegans metallothionein isoform specificity--metal binding abilities and the role of histidine in CeMT1 and CeMT2." FEBS J 276(23): 7040-7056.

Brahms, S. and J. Brahms (1980). "Determination of protein secondary structure in solution by vacuum ultraviolet circular dichroism." J Mol Biol 138(2): 149-178.

Brouwer, M., R. Syring and T. Hoexum Brouwer (2002). "Role of a copper-specific metallothionein of the blue crab, Callinectes sapidus, in copper metabolism associated with degradation and synthesis of hemocyanin." J Inorg Biochem 88(2): 228-239.

Calderone, V., B. Dolderer, H.-J. Hartmann, H. Echner, C. Luchinat, C. Del Bianco, S. Mangani and U. Weser (2005). "The crystal structure of yeast copper thionein: The solution of a long-lasting enigma." Proceedings of the National Academy of Sciences of the United States of America 102(1): 51-56.

Cantor, C. R. and P. R. Schimmel (1980). Biophysical Chemistry, San Francisco, W. H. Freeman.

Chan, J., Z. Huang, M. E. Merrifield, M. T. Salgado and M. J. Stillman (2002). "Studies of metal binding reactions in metallothioneins by spectroscopic, molecular biology, and molecular modeling techniques." Coordination Chemistry Reviews 233-234: 319-339.

Curdel, A. and M. Iwatsubo (1968). "Biosynthetic incorporation of cobalt into yeast alcohol dehydrogenase." FEBS Lett 1(3): 133-136.

Dede, F., G. Dinler and Z. Sayers (2007). 3D Macromolecular Structure Analyses: Applications in Plant Proteins. Brilliant Light in Life and Material Sciences. Dordrecht, The Netherlands, Springer.

Dmitri, I. S. and H. J. K. Michel (2003). "Small-angle scattering studies of biological macromolecules in solution." Reports on Progress in Physics 66(10): 1735.

Domenech, J., R. Orihuela, G. Mir, M. Molinas, S. Atrian and M. Capdevila (2007). "The Cd(II)-binding abilities of recombinant Quercus suber metallothionein: bridging the gap between phytochelatins and metallothioneins." J Biol Inorg Chem 12(6): 867-882.

Ebadi, M., M. P. Leuschen, H. el Refaey, F. M. Hamada and P. Rojas (1996). "The antioxidant properties of zinc and metallothionein." Neurochem Int 29(2): 159-166.

Ellman, G. L. (1959). "Tissue sulfhydryl groups." Archives of Biochemistry and Biophysics 82(1): 70-77.

Finney, L. A. and T. V. O'Halloran (2003). "Transition metal speciation in the cell: insights from the chemistry of metal ion receptors." Science 300(5621): 931-936.

Freisinger, E. (2007). "Spectroscopic characterization of a fruit-specific metallothionein: M. acuminata MT3." Inorganica Chimica Acta 360(1): 369-380.

Freisinger, E. (2008). "Plant MTs-long neglected members of the metallothionein superfamily." Dalton Trans(47): 6663-6675.

Freisinger, E. (2009). Metallothioneins in Plants, Royal Society of Chemistry.

Freisinger, E. (2011). "Structural features specific to plant metallothioneins." J Biol Inorg Chem.

Furey, W. F., A. H. Robbins, L. L. Clancy, D. R. Winge, B. C. Wang and C. D. Stout (1987). "Crystal structure of Cd,Zn metallothionein." Experientia Suppl 52: 139-148.

Grassetti, D. R. and J. F. Murray, Jr. (1967). "The use of 2,2'-dithiodipyridine in the determination of glutathione and of triphosphopyridine nucleotide by enzymatic cycling." Anal Biochem 21(3): 427-434.

Guinier, A. (1955). Small-angle scattering of X-rays, New York, Wiley.

Irving, H. and R. J. P. Williams (1948). "Order of Stability of Metal Complexes." Nature 162: 746-747.

Iyengar, G. V., W. E. Kollmer and H. J. M. Bowen (1978). The Elemental Composition of Human Tissues and Body Fluids, Verlag Chemie, Weinheim.

Kagi, J. H. and A. Schaffer (1988). "Biochemistry of metallothionein." Biochemistry 27(23): 8509-8515.

Kawashima, I., T. D. Kennedy, M. Chino and B. G. Lane (1992). "Wheat Ec metallothionein genes." European Journal of Biochemistry 209(3): 971-976.

Koch, M. H. J. and J. Bordas (1983). "X-ray diffraction and scattering on disordered systems using synchrotron radiation." Nuclear Instruments and Methods in Physics Research 208(1-3): 461-469.

Koch, M. H. J., P. Vachette and D. I. Svergun (2003). "Small-angle scattering: a view on the properties, structures and structural changes of biological macromolecules in solution." Quarterly Reviews of Biophysics 36(02): 147-227.

Kojima, Y. (1991). "Definitions and nomenclature of metallothioneins." Methods Enzymol 205: 8-10.

Kojima, Y., J. H. Kagi and P. A. Binz (1999). Nomenclature of metallothionein: proposal for a revision.

Konarev, P. V., V. V. Volkov, A. V. Sokolova, M. H. J. Koch and D. I. Svergun (2003). "PRIMUS: a Windows PC-based system for small-angle scattering data analysis." Journal of Applied Crystallography 36(5): 1277-1282.

Krezel, A. and W. Maret (2007). "Different redox states of metallothionein/thionein in biological tissue." Biochem J 402(3): 551-558.

Kryukov, G. V., S. Castellano, S. V. Novoselov, A. V. Lobanov, O. Zehtab, R. Guigo and V. N. Gladyshev (2003). "Characterization of mammalian selenoproteomes." Science 300(5624): 1439-1443.

Laemmli, U. K. (1970). "Cleavage of Structural Proteins during the Assembly of the Head of Bacteriophage T4." Nature 227(5259): 680-685.

Lane, B., R. Kajioka and T. Kennedy (1987). "The wheat-germ Ec protein is a zinc-containing metallothionein." Biochemistry and Cell Biology 65(11): 1001-1005.

Li, Y. and W. Maret (2009). "Transient fluctuations of intracellular zinc ions in cell proliferation." Exp Cell Res 315(14): 2463-2470.

Loebus, J., E. A. Peroza, N. Bluthgen, T. Fox, W. Meyer-Klaucke, O. Zerbe and E. Freisinger (2011). "Protein and metal cluster structure of the wheat metallothionein domain gamma-E(c)-1: the second part of the puzzle." J Biol Inorg Chem 16(5): 683-694.

Maret, W. (2010). "Metalloproteomics, metalloproteomes, and the annotation of metalloproteins." Metallomics 2(2): 117-125.

Maret, W. and M. Zeppezauer (1986). "Influence of anions and pH on the conformational change of horse liver alcohol dehydrogenase induced by binding of oxidized nicotinamide adenine dinucleotide: binding of chloride to the catalytic metal ion." Biochemistry 25(7): 1584-1588.

Margoshes, M. and B. L. Vallee (1957). "A CADMIUM PROTEIN FROM EQUINE KIDNEY CORTEX." Journal of the American Chemical Society 79(17): 4813-4814.

Martin, S. R. and M. J. Schilstra (2008). "Circular dichroism and its application to the study of biomolecules." Methods Cell Biol 84: 263-293.

McCall, K. A. and C. A. Fierke (2004). "Probing determinants of the metal ion selectivity in carbonic anhydrase using mutagenesis." Biochemistry 43(13): 3979-3986.

Melis, K. A., D. C. Carter, C. D. Stout and D. R. Winge (1983). "Single crystals of cadmium, zinc metallothionein." J Biol Chem 258(10): 6255-6257.

Meloni, G., T. Polanski, O. Braun and M. Vasak (2009). "Effects of Zn(2+), Ca(2+), and Mg(2+) on the structure of Zn(7)metallothionein-3: evidence for an additional zinc binding site." Biochemistry 48(24): 5700-5707.

Nar, H., R. Huber, A. Messerschmidt, A. C. Filippou, M. Barth, M. Jaquinod, M. van de Kamp and G. W. Canters (1992). "Characterization and crystal structure of zinc azurin, a by-product of heterologous expression in Escherichia coli of Pseudomonas aeruginosa copper azurin." Eur J Biochem 205(3): 1123-1129.

Nielsen, F. H. (1987). Trace Elements in Human and Animal Nutrition. W. M., Academic Press. 1: 245-273.

Palumaa, P., E. Eriste, O. Njunkova, L. Pokras, H. Jörnvall and R. Sillard (2002). "Brain-Specific Metallothionein-3 Has Higher Metal-Binding Capacity than Ubiquitous Metallothioneins and Binds Metals Noncooperatively†." Biochemistry 41(19): 6158-6163.

Palumaa, P., E. A. Mackay and M. Vasak (1992). "Nonoxidative cadmium-dependent dimerization of Cd7-metallothionein from rabbit liver." Biochemistry 31(7): 2181-2186.

Peroza, E. A. and E. Freisinger (2007). "Metal ion binding properties of Triticum [corrected] aestivum Ec-1 metallothionein: evidence supporting two separate metal thiolate clusters." J Biol Inorg Chem 12(3): 377-391.

Peroza, E. A., A. A. Kaabi, W. Meyer-Klaucke, G. Wellenreuther and E. Freisinger (2009). "The two distinctive metal ion binding domains of the wheat metallothionein Ec-1." J Inorg Biochem 103(3): 342-353.

Peroza, E. A., R. Schmucki, P. Guntert, E. Freisinger and O. Zerbe (2009). "The beta(E)-domain of wheat E(c)-1 metallothionein: a metal-binding domain with a distinctive structure." J Mol Biol 387(1): 207-218.

Petoukhov, M. V., P. V. Konarev, A. G. Kikhney and D. I. Svergun (2007). "ATSAS 2.1 - towards automated and web-supported small-angle scattering data analysis." Journal of Applied Crystallography 40(s1): s223-s228.

Porod, G. (1982). Small Angle X-ray Scattering, Academic Press, New York.

Putnam, C. D., M. Hammel, G. L. Hura and J. A. Tainer (2007). "X-ray solution scattering (SAXS) combined with crystallography and computation: defining accurate macromolecular structures, conformations and assemblies in solution." Q Rev Biophys 40(3): 191-285.

Riener, C. K., G. Kada and H. J. Gruber (2002). "Quick measurement of protein sulfhydryls with Ellman's reagent and with 4,4'-dithiodipyridine." Anal. Bioanal. Chem. 373(4-5): 266-276.

Robbins, A. H., D. E. McRee, M. Williamson, S. A. Collett, N. H. Xuong, W. F. Furey, B. C. Wang and C. D. Stout (1991). "Refined crystal structure of Cd, Zn metallothionein at 2.0Åresolution." Journal of Molecular Biology 221(4): 1269-1293.

Roessle, M. W., R. Klaering, U. Ristau, B. Robrahn, D. Jahn, T. Gehrmann, P. Konarev, A. Round, S. Fiedler, C. Hermes and D. Svergun (2007). "Upgrade of the small-angle X-ray scattering beamline X33 at the European Molecular Biology Laboratory, Hamburg." Journal of Applied Crystallography 40(s1): s190-s194.

Romero-Isart, N. and M. Vasak (2002). "Advances in the structure and chemistry of metallothioneins." J Inorg Biochem 88(3-4): 388-396.

Rosen, B. (2006). Metals in biology: past, present, and future. Molecular Biology of Metal Homeostasis and Detoxification. M. Tamas and E. Martinoia, Springer Berlin / Heidelberg. 14: 496-496.

Rosenzweig, A. C. (2002). "Metallochaperones: bind and deliver." Chem Biol 9(6): 673-677.

Round, A. R., D. Franke, S. Moritz, R. Huchler, M. Fritsche, D. Malthan, R. Klaering, D. I. Svergun and M. Roessle (2008). "Automated sample-changing robot for solution scattering experiments at the EMBL Hamburg SAXS station X33." Journal of Applied Crystallography 41(5): 913-917.

Sambrook, J., T. Manniatis and E. F. Fritsh (1989). Molecular Cloning: A Laboratory Manual, Cold Spring Harbor Laboratory Press.

Schicht, O. and E. Freisinger (2009). "Spectroscopic characterization of Cicer arietinum metallothionein 1." Inorganica Chimica Acta 362(3): 714-724.

Schultze, P., E. Wörgötter, W. Braun, G. Wagner, M. Vasák, J. H. R. Kägi and K. Wüthrich (1988). "Conformation of [Cd7]-metallothionein-2 from rat liver in aqueous solution determined by nuclear magnetic resonance spectroscopy." Journal of Molecular Biology 203(1): 251-268.

Schwarz, G., R. R. Mendel and M. W. Ribbe (2009). "Molybdenum cofactors, enzymes and pathways." Nature 460(7257): 839-847.

Serra-Batiste, M., N. Cols, L. A. Alcaraz, A. Donaire, P. Gonzalez-Duarte and M. Vasak (2010). "The metal-binding properties of the blue crab copper specific CuMT-2: a crustacean metallothionein with two cysteine triplets." J Biol Inorg Chem 15(5): 759-776.

Stillman, M. J., W. Cai and A. J. Zelazowski (1987). "Cadmium binding to metallothioneins. Domain specificity in reactions of alpha and beta fragments, apometallothionein, and zinc metallothionein with Cd2+." J Biol Chem 262(10): 4538-4548.

Stillman, M. J., A. Presta, Z. Gui and D. T. Jiang (1994). "Spectroscopic studies of copper, silver and gold-metallothioneins." Met Based Drugs 1(5-6): 375-394.

Stuhrmann, H. (1970). "Ein neues Verfahren zur Bestimmung der Oberflaechenform und der inneren Struktur von geloesten globularen Proteinen aus Roentgenkleinwinkelmessungen." Zeitschrift fur Physikaliche Chemie(72): 177-198.

Stuhrmann, H. (1970). "Interpretation of small-angle scattering functions of dilute solutions and gases. A representation of the structures related to a one-particle scattering function." Acta Crystallographica Section A 26(3): 297-306.

Sutherland, D. E. and M. J. Stillman (2011). "The "magic numbers" of metallothionein." Metallomics 3(5): 444-463.

Sutherland, D. E., M. J. Willans and M. J. Stillman (2010). "Supermetalation of the beta domain of human metallothionein 1a." Biochemistry 49(17): 3593-3601.

Svergun, D. (1992). "Determination of the regularization parameter in indirect-transform methods using perceptual criteria." Journal of Applied Crystallography 25(4): 495-503.

Svergun, D. I. (1999). "Restoring low resolution structure of biological macromolecules from solution scattering using simulated annealing." Biophys J 76(6): 2879-2886.

Svergun, D. I. and M. H. J. Koch (2003). "Small-angle scattering studies of biological macromolecules in solution." Reports on Progress in Physics 66(10): 1735.

Svergun, D. I., M. V. Petoukhov and M. H. Koch (2001). "Determination of domain structure of proteins from X-ray solution scattering." Biophys J 80(6): 2946-2953.

Tainer, J. A., V. A. Roberts and E. D. Getzoff (1991). "Metal-binding sites in proteins." Curr Opin Biotechnol 2(4): 582-591.

Tommey, A. M., J. Shi, W. P. Lindsay, P. E. Urwin and N. J. Robinson (1991). "Expression of the pea gene PSMTA in E. coli. Metal-binding properties of the expressed protein." FEBS Lett 292(1-2): 48-52.

Uchida, Y., K. Takio, K. Titani, Y. Ihara and M. Tomonaga (1991). "The growth inhibitory factor that is deficient in the Alzheimer's disease brain is a 68 amino acid metallothionein-like protein." Neuron 7(2): 337-347.

Vallee, B. L. and D. S. Auld (1990). "Zinc coordination, function, and structure of zinc enzymes and other proteins." Biochemistry 29(24): 5647-5659.

Vallee, B. L., J. A. Rupley, T. L. Coombs and H. Neurath (1958). "THE RELEASE OF ZINC FROM CARBOXYPEPTIDASE AND ITS REPLACEMENT." Journal of the American Chemical Society 80(17): 4750-4751.

Vallee, B. L. and W. E. C. Wacker (1970). The Proteins, Academic Press. 5.

Vasak, M. (2005). "Advances in metallothionein structure and functions." J Trace Elem Med Biol 19(1): 13-17.

Vasák, M. (1991). Metal removal and substitution in vertebrate and invertebrate metallothioneins. Methods in Enzymology. B. L. V. James F. Riordan, Academic Press. Volume 205: 452-458.

Vasak, M. and D. W. Hasler (2000). "Metallothioneins: new functional and structural insights." Curr Opin Chem Biol 4(2): 177-183.

Volkov, V. V. and D. I. Svergun (2003). "Uniqueness of ab initio shape determination in small-angle scattering." Journal of Applied Crystallography 36(3 Part 1): 860-864.

Wan, X. and E. Freisinger (2009). "The plant metallothionein 2 from Cicer arietinum forms a single metal-thiolate cluster." Metallomics 1(6): 489-500.

Willner, H., M. Vasak and J. H. Kagi (1987). "Cadmium-thiolate clusters in metallothionein: spectrophotometric and spectropolarimetric features." Biochemistry 26(19): 6287-6292.

APPENDIX A

CHEMICALS

Acetic acid (glacial)	Riedel-de Haen, Germany	27225
30 % Acrylamide-0.8 % Bisacrylamide	Sigma, Germany	A3699
Bromophenol blue	Applichem, Germany	A3640
Cadmium (II) sulphate	Fluka, Switzerland	20920
Chelex 100	Sigma, Germany	C7901
Coomassie Brillant Blue R-250	Fluka, Switzerland	27816
L-Cysteine	Sigma, Germany	A7250
EDTA- Free Complete Protease Inhibitor Cocktail Tablets	Roche	11873580001
dNTP mix	Fermentas, Germany	R0241
1,4-Dithiothreitol	Fluka, Switzerland	43815
*Dpn*I	Fermentas, Germany	ER1701
4,4-Dithiodipyridine	Sigma, Germany	143057
*Eco*RI	Fermentas, Germany	ER0271
Ethanol	Riedel-de Haen, Germany	32221
Ethylenediaminetetraaceticacid	Riedel-de Haen, Germany	27248
Formic Acid (98%)	Merck, Germany	1002641000
Glycerol (87 %)	Riedel-de Haen, Germany	15523
Glycine	Amresco, USA	0167
HEPES	Fluka, Switzerland	54461
Hexaglycine	Sigma, Germany	G6530
Hydrochloric acid (37 %)	Merck, Germany	100314

IPTG	Fermentas, Germany	R0392
MassRuler DNA Ladder Mix	Fermentas, Germany	SM0403
2-Mercaptoethanol	Aldrich, Germany	M370-1
Methanol	Riedel-de Haen, Germany	24229
PageRuler protein ladder	Fermentas, Germany	SM0661
Phenylmethylsulphonylfluoride	Amresco, USA	0754
2-Propanol	Merck, Germany	100996
Protein Molecular Weight Marker	Fermentas, Germany	SM0431
Reduced Glutathione	Merck, Germany	104090
Silver staining plus kit	BioRad	161-0449
Site-Directed Mutagenesis Kit	Stratagene	200518
Sodium Chloride	Riedel-de Haen, Germany	13423
Sodium dodecyl sulphate	Sigma, Germany	L-4390
Taq polymerase	Fermentas, Germany	EP0401
Thrombin	GE-Healthcare, Sweden	27-0846-01
Tris	Fluka, Switzerland	93349
Triton X-100	Applichem, Germany	A1388
Unstained protein MW marker	Fermentas, Germany	SM0431
*Xho*I	Fermentas, Germany	ER0691
Zinc Sulfate	Merck, Germany	108883

MOLECULAR WEIGHT MARKERS

Fermentas Unstained Protein Molecular Weight Marker

MW, kDa	Protein
116.0	β-galactosidase
66.2	Bovine serum albumin
45.0	Ovalbumin
35.0	Lactate dehydrogenase
25.0	REase Bsp98I
18.4	β-lactoglobulin
14.4	Lysozyme

12% Tris-glycine SDS-PAGE

Fermentas Unstained Protein Ladder

kDa
200
150
120
100
85
70
60
50
40
30
25
20
15
10
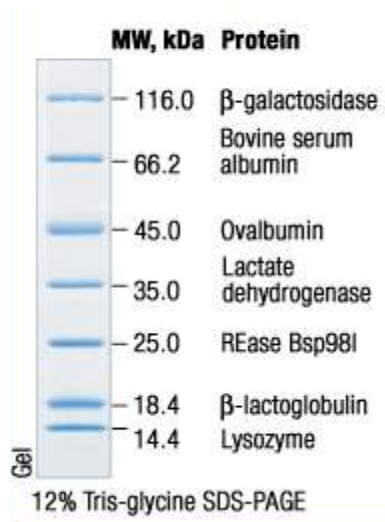
APPENDIX B

pGEX-4T-2 vector map and multicloning site with available restriction enzyme sites
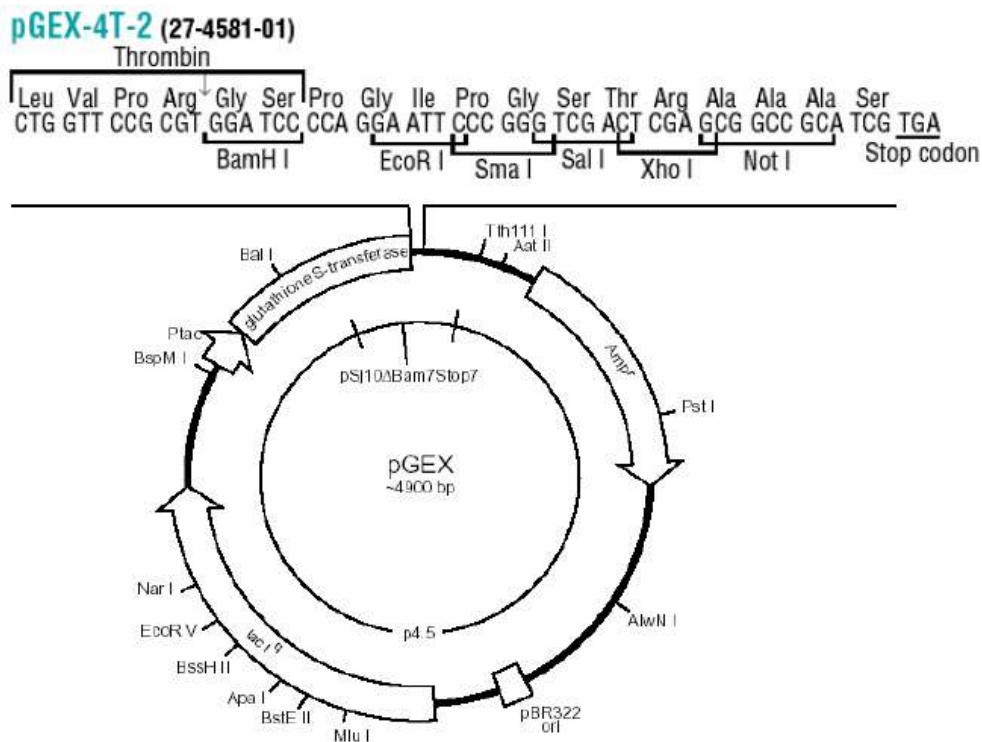
Sequencing Results of GSTdMT Mutants

```
                  190          200          210
dMTgene   GGCTGCAGCTGCGGCGACAACTGCAAGTGCAA
          :::::::::::: :::::::::::::::::::
G65C      GGCTGCAGCTGCTGCGACAACTGCAAGTGCAA
          240          250          260          270
```

BUFFERS AND SOLUTIONS

Tris Acetate EDTA Buffer (TAE) (50X): 121.1 g Tris Base, 28.55 ml Glacial Acetic acid, 7.3 g EDTA, completed to 500 ml.

Native-PAGE:

8% Separating Gel:

	for 2 gels	for 1 gel	[final]
dH$_2$O	6 ml	3 ml	
3 M Tris, pH 8.9	1.25 ml	625 μl	3.75 mM
30 % Acryl-0.8 % Bisacryl	2.67 ml	1.335 ml	8 %
10 % APS	75 μl	37.5 μl	0.075 %
TEMED	5 μl	2.5 μl	0.05 %

3 % Stacking Gel:

	for 2 gels	for 1 gel	[final]
dH$_2$O	4.2 ml	2.1 ml	
1 M Tris, pH 6.8	250 μl	125 μl	50 mM
30 % Acryl-0.8 % Bisacryl	510 μl	255 μl	3 %
10 % APS	37.5 μl	18.75 μl	0.075 %
TEMED	2.5 μl	1.25 μl	0.05 %

2X Native Sample Buffer: 200 mM Tris-HCl pH 7.5, 20 % (v/v) Glycerol, 0.05 % (w/v) Bromophenol Blue in ddH$_2$O.

Native-PAGE Running Buffer: 25 mM Tris, 192 mM Glycine in ddH$_2$O.

SDS-PAGE:

12 % Separating Gel:

	for 2 gels	for 1 gel	[final]
dH$_2$O	4.62 ml	2.31 ml	
3 M Tris, pH 8.9	1.25 ml	625μl	3.75 mM
30 % Acryl-0.8 % Bisacryl	4 ml	2 ml	12 %
20 % SDS	50 μl	25 μl	0.1 %
10 % APS	75 μl	37.5μl	0.075 %
TEMED	5 μl	2.5 μl	0.05 %

5 % Stacking Gel:

	for 2 gels	for 1 gel	[final]
dH$_2$O	3.850 ml	1.925 ml	
3 M Tris, pH 8.9	250 μl	125 μl	50 mM
30 % Acryl-0.8 % Bisacryl	850 μl	425μl	5 %
20 % SDS	10 μl	5 μl	0.1 %
10 % APS	37.5 μl	18.75 μl	0.075 %
TEMED	2.5 μl	1.25μl	0.05 %

2X SDS Sample Buffer: 4 % (w/v) SDS, 20 % (v/v) Glycerol, 0.004 % (w/v) Bromophenol blue, 10 % (v/v) 2-mercaptoethanol, 0.125 M Tris-HCl, pH 6.8 in ddH$_2$O.

SDS-PAGE Running Buffer: 25 mM Tris, 192 mM Glycine, 0.1 % (w/v) SDS in ddH$_2$O.

Tris-Tricine Gel:

	16 % Resolving Gel	3 % Stacking Gel
29:1 Acrylamide/bisacrylamide	2.5 ml	400 μl
Tris-Cl/SDS, pH 8.45	2.5 ml	1.24 ml
Glycerol	1 ml	-
TEMED	5 μl	4 μl
10 % APS	60 μl	40 μl
dH$_2$O	1.4 ml	3.3 ml

Tris-Tricine Gel Running Buffers:

1X Cathode Buffer (Load on top into wells): 0.1 M Tris, 0.1 M Tricine, and 0.1 % SDS in ddH$_2$O.

1X Anode Buffer (Load on gel apparatus tray): 0.2 M Tris-Cl, pH 8.9 in ddH$_2$O.

Coomassie Staining Solution: 0.1 % (w/v) Coomassie Brillant Blue R-250, 40 % (v/v) Methanol, 10 % (v/v) Glacial Acetic acid in ddH$_2$O.

Destaining Solution: 4 % (v/v) Methanol, 7.5 % (v/v) Glacial Acetic acid, completed to 1 L.

APPENDIX D

EQUIPMENTS

AKTA FPLC: GE-Healthcare, SWEDEN

Autoclave: Hirayama, Hiclave HV-110, JAPAN

Certoclav, Table Top Autoclave CV-EL-12L, AUSTRIA

Cenrifuge: Eppendorf, 5415C, GERMANY

Eppendorf, 5415D, GERMANY

Eppendorf, 5415R, GERMANY

Hitachi, Sorvall RC5C Plus, USA

Hitachi, Sorvall Discovery 100 SE, USA

Dynamic Light Scattering: Malvern, Zetasizer Nano-ZS, UK

Deepfreeze: -80 ^{o}C, Kendro Lab. Prod., Heraeus Hfu486, GERMANY

-20 ^{o}C, Bosch, TURKEY

Distilled water: Millipore, Elix-S, FRANCE

Millipore, MilliQ Academic, FRANCE

Electrophoresis: Biogen Inc., USA

Biorad Inc., USA

Ice Machine:	Scotsman Inc., AF20, USA
ICP-OES:	Varian, Vista-Pro CCD, AUSTRALIA
Incubator:	Memmert, Modell 300, GERMANY
	Memmert, Modell 600, GERMANY
Laminar Flow:	Kendro Lab. Prod., Heraeus, HeraSafe HS12, GERMANY
Magnetic Stirrer:	VELP Scientifica, ARE Heating Magnetic Stirrer, ITALY
	VELP Scientifica, Microstirrer, ITALY
Microliter Pipette:	Gilson, Pipetman, FRANCE
Microwave Oven:	Bosch, TURKEY
pH Meter:	WTW, pH540 GLP MultiCal, GERMANY
Power Supply:	Biorad, PowerPac 300, USA
	Wealtec, Elite 300, USA
Refrigerator:	+4 ^{o}C, Bosch, TURKEY
Shaker:	Forma Scientific, Orbital Shaker 4520, USA
	GFL, Shaker 3011, USA
	New Brunswick Sci., Innova 4330, USA
Sonicator:	BioBlock Scientific, Vibracell 7504, FRANCE
Spectrophotometer:	Nanodrop, ND-1000, USA
Speed Vacuum:	Savant, Speed Vac Plus Sc100A, USA
	Savant, Refrigerated Vapor Trap RVT 400, USA
Thermocycler:	Eppendorf, Mastercycler Gradient, GERMANY